Université catholique de Louvain

Faculté des Sciences
Département de Physique
Institut d'astronomie et de géophysique
Georges Lemaître

ON THE ASSIMILATION OF ICE VELOCITY AND CONCENTRATION DATA INTO LARGE-SCALE SEA ICE MODELS

Doctoral dissertation presented by

Valérie Dulière

in fulfillment of the requirements for the degree of Doctor in Sciences

Prof. Thierry Fichefet, Supervisor	ASTR, UCL
Prof. Pierre Defrance	PAMO, UCL
Prof. Eric Deleersnijder	ASTR, UCL
Dr. Gilles Garric	Mercator-Ocean, Toulouse
Prof. Hugues Goosse	ASTR, UCL
Prof. René Prieels, Chair	FYNU, UCL
Dr. Ralph Timmermann	AWI, Bremerhaven
Prof. Jean-Pascal van Ypersele	ASTR, UCL

à Jérémy et Marie-Lou,

Remerciements

A l'issue de ces années passées à l'Institut d'astronomie et de géophysique Georges Lemaître, j'aimerais remercier toutes celles et ceux qui, de près ou de loin, ont participé à la réalisation de cette thèse de doctorat. Que ceux que j'oublierais de citer veuillent bien m'en excuser et soient assurés de toute ma reconnaissance.

Mes tous premiers remerciements vont à mon promoteur, le Professeur Thierry Fichefet. Grâce à Thierry, j'ai eu l'opportunité de travailler sur un sujet aussi passionnant qu'innovant : le rapprochement du monde de l'assimilation de données avec celui de la modélisation de la glace de mer. Un tout grand merci à toi, Thierry, de m'avoir guidée tout en m'accordant ta confiance quand je prenais des initiatives. Merci pour tes nombreux et judicieux conseils, et surtout pour ton soutien au cours de ces années! Merci encore pour tes lectures très minutieuses de ce manuscrit.

Je remercie également le Professeur Hugues Goosse pour ses remarques perspicaces et ses conseils en tout genre, toujours pleins de bon sens.

Merci au Docteur Ralph Timmermann de m'avoir initiée avec son incroyable bonne humeur à la modélisation de la glace de mer et à IDL, outil qui m'a été très précieux tout au long de ce travail. Merci aussi pour tes nombreuses suggestions qui m'ont permis de compléter et d'améliorer ce texte.

Je tiens également à remercier le Professeur René Prieels, Président du Département de Physique et Président du Jury, ainsi que les aux autres membres du Jury: le Dr. Gilles Garric, le Prof. Pierre Defrance, le Prof. Eric Deleersnijder et le Prof. Jean-Pascal van Ypersele. Je les remercie pour leurs questions témoignant de leur intérêt pour mon travail.

Merci à Martin Vancopenolle, collègue de bureau hors pair, à l'écoute et attentif, jamais avare de commentaires sensés ou surréalistes et capable de transformer une simple journée de travail en délire le plus complet!

I would also like to thank deeply Ron Lindsay, Walt Meier, Cecilia Bitz and Mark Drinkwater for considering my work with interest and for the great benefits I took from discussing with them.

Merci aussi à chacun des membres de l'Institut pour avoir contribué directement ou indirectement à l'aboutissement de cette thèse. Je pense tout particulièrement à Xavier Fettweis, le Mac Gyver de l'informatique ainsi qu'à Liliane, Nicole et Céline, les dévouées secrétaires d'ASTR. Il est malheureusement impossible de citer toutes les personnes avec lesquelles j'ai passé de bons moments en ASTR durant cette thèse. Merci, entre autres, à la bande des plus "jeunes" : Martin, Emilie, Xavier, Manu, Aurore, Wouter, Sylvain, Anne, Marie-France, Sébastien, Manu H., Frank, Rafic, Chantal, Michel, Chris, Didier et tous les autres pour les soirées en tout genre, escalade, beach volley et matchs de badminton, sans oublier les nombreux temps de midi passés à la *cafet* ou ailleurs!

Merci à toute l'équipe des assistants du Professeur Lega, avec qui j'ai eu beaucoup de plaisir à donner les séances de laboratoire et d'exercices de physique.

Merci à l'équipe de Science Infuse de l'UCL de m'avoir permis d'animer des groupes d'enfants sur le thème de l'effet de serre et des changements climatiques. Cette activité a réellement donné une autre dimension à ce travail de recherche.

Merci à Delphine, Laurence, Anne-Françoise, Bérengère, Marie, Caro D et Caro W, mes "vieilles" copines qui n'ont pas fini d'entendre parler de moi! Merci à Anne-So pour ces petits dîners réparateurs et pour tout le reste!

Merci au *Physician Power*, Marjo, Estelle, Yan, Christophe et Nico pour leur amitié très *physique* et pour tous les excellents moments passés ensemble!

Je tiens également à remercier le FRIA (Fonds pour la formation à la Recherche dans l'Industrie et dans l'Agriculture), ainsi que l'Université catholique de Louvain pour avoir mis à ma disposition les moyens logistiques nécessaires à la réalisation de cette thèse. Merci aussi à toute l'équipe du calcul intensif pour le support technique.

Un immense merci à Maman, Papa, Muriel, Ombeline et Arnoud de m'avoir guidée et appuyée dans mes choix. Sans eux, je n'aurais certainement pas pu arriver là où j'en suis aujourd'hui. Merci à Suzanne, ma tante, pour les petits dîners en tête-à-tête, moyen idéal pour se changer les idées et revenir plein d'entrain l'après-midi au boulot!

Finalement, j'aimerais dédier cette thèse à Jérémy et Marie-Lou en qui j'ai pu trouver le soutien, l'énergie et le courage quand ils faisaient défaut. Rien que de penser à eux m'a souvent aidée à relativiser certaines petites mésaventures. Merci à toi Jérémy de t'être coupé en quatre pour régler tous les petits soucis du quotidien au cours des ces derniers mois. Le fait que tu aies cru en moi jusqu'au bout et que tu m'aies soutenue 24h/24h compte énormément pour moi! Merci à ma petite puce, Marie-Lou d'être ce petit bonheur sur pattes dont je ne peux plus me passer!

Contents

Chapter 1

Introduction

1.1 General context

Sea ice is defined as *any form of ice found at sea which has originated from the freezing of seawater* (WMO, 1970). It covers about 7% of the global ocean and 4.5% of the Earth surface, on an annual average. In polar regions, the presence of sea ice significantly modifies the interactions between atmosphere and ocean. Because of its high albedo[1] (e.g. Perovich *et al.*, 2002; Eicken *et al.*, 2004; Brandt *et al.*, 2005) and insulating behavior (e.g. Pringle *et al.*, 2006), sea ice largely affects the surface radiative balance and the oceanic heat budget. In addition, the melting of weakly saline ice or the brine[2] rejection occurring during ice formation induces variations in the sea surface salinity that affect the mixed layer[3] dynamics and the ocean circulation (e.g. Goosse and Fichefet, 1999). On the other hand, the ice dynamics play an important part in modulating the momentum transfer from the atmosphere to the ocean.

Sea ice extent[4] varies spectacularly through the year. It reaches its minimum ($9.3 \times 10^6 km^2$) in September, at the end of the summer melt season, while March usually marks its maximum ($15.7 \times 10^6 km^2$). The high sensitivity of

[1] The *albedo* is defined by the fraction of the incident sunlight that is reflected.

[2] *Brine* is water saturated or nearly saturated with salt (NaCl).

[3] The *oceanic surface mixed layer* is a layer in which active turbulence has homogenized some range of depths. This turbulence is generated by winds, cooling, or processes such as evaporation or sea ice formation which result in an increase in salinity.

[4] The sea ice *extent* is the area of the ocean that is covered by at least 15% of ice.

the sea ice characteristics mainly derives from an important feedback called the *albedo-temperature feedback* (Ebert and Curry, 1993). A small positive perturbation in the surface energy budget triggers a decrease in ice coverage. This enhances the surface absorption of solar radiation and further decreases the ice cover. Therefore, a small climate warming perturbation may be amplified by the melting of the sea ice cover. This explains why the Intergovernmental Panel on Climate Change considers sea ice as a major indicator of short-term climate change (Houghton *et al.*, 2001). The understanding of the sea ice mass balance (therefore of ice extent, thickness and velocity) and its interannual variations is crucial for the assessment of ongoing climate changes in polar regions and at the global scale (Bamber and Payne, 2004).

During the past 35 years, Arctic sea ice concentration and motion have been widely observed with the aid of passive microwave sensors aboard satellites (e.g. Bjørgo *et al.*, 1997; Cavalieri *et al.*, 1997; Emery *et al.*, 1997; Parkinson *et al.*, 1999; Comiso and Steffen, 2001; Cavalieri *et al.*, 2003). Analysis of these records indicate that the Arctic sea ice extent has shrunk at an annual mean rate of about $0.30 \times 10^6 km^2$ with strong interannual variability since the early 1970s (Cavalieri *et al.*, 2003). Lately, the September ice extents of years 2002 to 2005 have been 20 % below the mean September sea ice extent for 1979-2000 (Lindsay and Zhang, 2005; Comiso, 2006) and the summer sea ice area of year 2006 was abnormally small. In addition to this, the Northern Hemisphere sea ice area of this present year broke by far the record of the lowest ice area in observed history.

Our knowledge of sea ice thickness in the Northern Hemisphere comes mainly from upward-looking sonar (ULS) profiling by submarines. Rothrock *et al.* (1999) compared ice draft[5] data acquired by the Scientific Ice Expeditions (SCICEX) program in 1993, 1996 and 1997 with data from six cruises during the period 1958-1976. They found a decrease in the mean ice draft at the end of the melt season of about 1.3 m (i.e. 40%) in most of the deep-water areas of the Arctic Ocean. Comparing data from single cruises in 1996 and 1976 from Fram Strait to the North Pole, Wadhams and Davis (2000) reported a strikingly similar reduction in ice draft. In contrast, ice draft data collected during six submarine cruises from Alaska to the North Pole in 1991-1997 exhibit almost no change (Winsor, 2001). From nine cruises from 1976 through 1994 on the Alaska-to-North Pole section, Tucker *et al.* (2001) found an abrupt thinning between the mid-1980s and early 1990s. No similar trend was however observed near the North Pole. Recently, a detailed analysis of submarine and modeled ice thicknesses (Holloway and Sou, 2002) has demonstrated that ice motion and high interannual variability make inference of trends from sonar transect data ambiguous, suggesting that

[5]The ice *draft* is the distance between the bottom of the ice and the sea surface. About 89% of the ice thickness is under water and seen as draft.

the available sonar data are insufficient to resolve the variability of the Arctic ice thickness. Later, the thinning of the Arctic ice cover has been reconfirmed. Comparing 8 cruises spanning the years 1987-1997 in the Arctic Ocean, Rothrock *et al.* (2003) found a decrease in draft data of about 1 m over the 11-year span. Several other studies point towards a thinning of the Arctic ice cover (e.g. Yu *et al.*, 2004; Perovich *et al.*, 2003; Rigor and Wallace, 2004; Fowler *et al.*, 2004; Comiso, 2002). New techniques to measure the sea ice thickness from space are now being developed (e.g. Laxon *et al.*, 2003; Yu and Lindsay, 2003; Kwok *et al.*, 2004). Nevertheless, an accurate knowledge of past ice thickness variations remains necessary in order to assess human-induced climate changes in the Arctic.

A number of regional or global ice-ocean general circulation models driven by atmospheric reanalysis data fields have been used to document the variability of the Arctic sea ice over the last few decades (e.g. Maslowski *et al.*, 2000; Holloway and Sou, 2002; Fichefet *et al.*, 2003; Köberle and Gerdes, 2003; Rothrock and Zhang, 2005; Timmermann *et al.*, 2005). These models provide very useful information regarding the behavior of the ice pack. However, their ability to simulate the shorter-term variability as well as summer features of the ice cover remains rather limited. Consequently, hindcast simulations of Arctic sea ice often deviate from reality. One way to improve the estimation of the ice cover might be to assimilate the available ice concentration and/or velocity observations into the models. Assimilating data into numerical models has proven very useful in the atmospheric and oceanic modeling communities for many years (e.g. Ghil and Malanotte-Rizzoli, 1991). For instance, the assimilation of sea level anomaly, wind stress, ocean current, sea surface salinity and temperature as well as profiles of salinity and temperature, with the help of optimal interpolation scheme, simplified Kalman filter and variational approaches, was found very helpfull in support of operational oceanography and oceanographic research (e.g. Ferry *et al.*, 2007; Drecourt *et al.*, 2006; Foreman *et al.*, 1996). It is however a less common practice in large-scale sea ice modeling.

Data assimilation into sea ice models designed for climate studies started about 15 years ago. In most of the studies conducted so far, it is assumed that the improvement brought by the assimilation is straightforward. However, some studies suggest this might not be true. In order to elucidate this question we analyze here results from a number of twin experiments (i.e. experiments in which the data to be assimilated are model outputs) carried out first with a simplified model of the Arctic sea ice pack and then with NEMO-LIM2, an ice-ocean global general circulation model. Our objective is to determine to what degree the assimilation of ice velocity and/or concentration data improves the overall performance of the models and, more specifically, reduces the error in the computed ice thickness. A simple optimal interpolation scheme is used, and outputs from control runs and from perturbed experiments without and with data assimilation are thoroughly compared.

1.2 Structure of this thesis

First of all, the literature for data assimilation and more specifically for data assimilation into sea ice modeling will be reviewed in Chapter 2 for a good understanding of the main issue. This chapter motivates the powerful and singular experimental design used throughout this thesis.

Chapter 3 presents the dynamic-thermodynamic sea ice toy model that we built and a detailed study of the impact of assimilating velocity and/or concentration observations on the toy model general behavior. In order to circumvent the limited knowledge of both modeling and observational errors, we address this issue in a very different way than previously done. Here, we build an idealized observational dataset from model outputs and perform so-called *twin experiments* (see Sections 3.3 and 4.3). Twin experiments are common practice in atmospheric and oceanic modeling (e.g. Lin *et al.*, 2001; Fox *et al.*, 2000). However, to our knowledge, it is the very first time that simulations of this kind are performed with a sea ice model. A simple optimal interpolation scheme is used, and outputs from a control run and from perturbed experiments without and with data assimilation are thoroughly compared. In this chapter, we present a detailed analysis of a representative sample of these experiments in order to give a first idea of the data assimilation effects on the major sea ice physical processes with no concern on ocean feedback and complex physical parameterizations.

In Chapter 4, we test the robustness of the conclusions of Chapter 3. We first give a brief description of NEMO-LIM2, a primitive equation ocean general circulation model coupled to LIM2 (the second generation of the Louvain-la-Neuve sea ice model) and the chosen experimental design which is similar but more realistic than the one in the previous chapter. We then give a detailed analysis of the results of the twin experiments carried out with NEMO-LIM2.

Finally, Chapter 5 discusses a couple of more specific issues brought by the assimilation of sea ice data. First, we study the influence of rejecting salt and conserving the snow volume and heat contents in ice and brine pockets on the model results when concentration data are assimilated. Then we discuss the issue of errors in the observations of sea ice concentration and velocity and assess their effects on the data assimilation results. Finally, we consider the impact of the resolution of the observed velocities on the data assimilation results.

Concluding remarks and perspectives are given in Chapter 6.

Chapter 2

Data assimilation

2.1 Introduction to data assimilation systems

All models give only estimates of the real state. Even the best models which account for complex physical processes are stained with biases and errors. Errors are, for example, due to initial conditions, imperfect physical parameterizations or inaccurate forcing. Also, the nature of chaotic nonlinear systems can rapidly move the model estimate away from the real state. It is then essential to take benefit from information derived from actual observations to restore the model state close to the real one. This process is called *data assimilation*. Data assimilation has been the subject of considerable research in the atmospheric community over the past few decades, driven by the need for accurate weather forecasts, and more recently by the need for information in the oceanic community. Many assimilation techniques have therefore been developed. They differ in their numerical cost, their optimality and in their suitability for real-time data assimilation.

There are two basic approaches to data assimilation: *sequential* and *non-sequential* (or *retrospective*) assimilations. The first approach considers only observations made before the time of analysis (like for real-time assimilation systems), while the second one also uses observations after the time of analysis (mostly for reanalysis exercises). Another distinction can be made between methods that are *intermittent* or *continuous* in time. In an intermittent method, observations are used punctually in time, which is usually technically convenient. In a continuous method, observations are considered over longer periods of time. The correction is then smoother in time, which is physically more realistic. Compromises between these approaches are possible.

One of the simplest methods which is still widely used is called the *Cressman analysis* (Bergthorsson and Döös, 1955; Cressman, 1959). This nonstatistical method sets the model state equal to the observed values in the vicinity of available observations and to an arbitrary state otherwise:

$$\mathbf{x}_a(j) = \mathbf{x}_b(j) + \frac{\Sigma_{i=1}^{n}\ w(i,j)\ [\ \mathbf{y}(i) - H(\mathbf{x}_b(i))\ ]}{\Sigma_{i=1}^{n}\ w(i,j)} \tag{2.1}$$

$$w(i,j) = max\left(0, \frac{R^2 - d_{i,j}^2}{R^2 + d_{i,j}^2}\right) \tag{2.2}$$

where $\mathbf{x}_a(j)$ and $\mathbf{x}_b(j)$ are the analysis state provided by a Cressman analysis and the previous estimate (or *background*) of the model state, respectively, at each model grid point *j*, $\mathbf{x}_b(i)$ is the background state interpolated to observation grid point i, $\mathbf{y}(i)$ represents the set of observations of the same parameter with $i \in [1, ..., n]$ and *H* is the observation operator that calculates the model equivalent of the observations. The weight function, $w(i,j)$, is a decreasing function of distance which is equal to one for co-located observations and grid point and goes to zero if $d_{i,j} > R$. $d_{i,j}$ is a measure of the distance between grid points i and j and R is a user-defined constant distance beyond which observations have no influence.

A more general variation of the Cressman analysis is the *successive correction method* where the maximum weight is less than one. Therefore, a weighted average of background and observation states is applied instead of replacing the background state with observations. With enough sophistication, such a method can be as good as any other assimilation method. However, there is no direct method for specifying the optimal weights.

Other data assimilation methods attempt to assign weights to the observations and model values based on their error characteristics in order to minimize the analysis error (the difference between the true value and the assimilation result) in a statistical sense. Those statistical assimilation methods include simple schemes such as *optimal interpolation* (OI) as well as more sophisticated methods like the *Kalman Filter*. We can illustrate this with a simple scalar example of least-squares estimation. Let us say that we want to estimate the temperature T_t in a room. A thermometer measures T_1 with a known accuracy σ_1 (the standard deviation of measurement error). T_1 is one estimation we can get from T_t. Let us say that we have another estimation T_2 (for example, from a model or from an independent thermometer) of accuracy σ_2. Intuitively, T_1 and T_2 can be combined to provide a better estimation (T_a where the subscript *a* stands for the *analysis*) of T_t than any of these taken alone. We can look for a linear weighted average of the form:

$$T_a = kT_1 + (1-k)T_2 \tag{2.3}$$

This can be rewritten as:

$$T_a = T_2 + k(T_1 - T_2) \tag{2.4}$$

If we assume that the two errors are uncorrelated, the error variance of the estimate is:

$$\sigma_a^2 = k^2\sigma_1^2 + (1-k)^2\sigma_2^2 \tag{2.5}$$

Therefore, the optimal value of k that minimizes the analysis error variance is:

$$k = \frac{\sigma_2^2}{\sigma_2^2 + \sigma_1^2} \tag{2.6}$$

For such a k value, the variance of the analysis error then becomes:

$$\frac{1}{\sigma_a^2} = \frac{1}{\sigma_1^2} + \frac{1}{\sigma_2^2} \tag{2.7}$$

It is therefore clear that the analysis error variance is always smaller than both the background and observation error variances. We can extend this procedure to the OI analysis (Lorenc, 1981; Hollingsworth and Lönnberg, 1986):

$$\mathbf{x}_a = \mathbf{x}_b + \mathbf{K}[\mathbf{y} - H(\mathbf{x}_b)] \tag{2.8}$$

$$\mathbf{K} = \mathbf{B}\mathbf{H}^T(\mathbf{H}\mathbf{B}\mathbf{H}^T + \mathbf{R})^{-1} \tag{2.9}$$

where $\mathbf{x}$ is the state vector. $\mathbf{K}$ is an operator called *the gain* or *weight* and is determined through the least-squares minimization of the error covariance of the assimilated value compared with a statistical *true* value. H and $\mathbf{H}$ refer to the observation operator that calculates the model equivalent of the observations and to its corresponding linear operator, respectively. $\mathbf{H}(\mathbf{x} - \mathbf{x}_b) = H(\mathbf{x}) - H(\mathbf{x}_b)$ for any $\mathbf{x}$ close enough to $\mathbf{x}_b$. $\mathbf{B}$ and $\mathbf{R}$ stand for the covariance matrices of the background and observation errors, respectively. Therefore, $\mathbf{HBH}^T$ is just the background error covariance expressed in observation state.

In OI, Equation 2.8 is solved directly by inversion. It is possible to reduce the size and the time it takes to solve the analysis problem numerically by assuming that only the closest observations determine the analysis at a certain grid cell. This divides the global analysis problem into local optimal analysis. The observation errors are also assumed to be unbiased and random, and are uncorrelated with each other and with model errors. Their variance is considered to be constant over the interpolated area. We finally assume that the model errors are unbiased and that the model error covariance matrix **B** is known. According to Meier *et al.* (2000), these assumptions are probably not completely true; this will lead to less optimal assimilation results. However, these errors are expected to be reasonably small relative to other error sources and they are therefore most of the time ignored.

In the framework of this study, we prefer an OI scheme to other schemes for its low computational cost and for its easy implementation. There are other more complex assimilation algorithms that we will only briefly describe here.

A method to overcome the least-squares approach, and therefore the local data selection of the OI technique, is to look for the analysis as an approximate solution to the minimization problem defined by a cost function J, where J is a measurement of the misfit between a model state **x** and the data input into the assimilation scheme. The solution is sought iteratively. This algorithm is know as *3D-VAR* (where 3D refers to the 3 spatial dimensions) or *4D-VAR* (when observations are also distributed in time), and has the strong constraint that the model equations must solve the sequence of model states from the initial time forwards. This assumes a *perfect* model and requires the implementation of an adjoint model to integrate the so-called tangent linear time-stepping operator. This makes it difficult to realize.

The Kalman Filter is used to assimilate sequentially the observations in a way that it minimizes the least-squares error of the analysis (like for the OI). This procedure updates the forecast error covariance misfit at each time step based on the knowledge of system noise and observational error statistics, as well as the entire past history of the model state. It is the *most optimum least-squares error fitter*. However, it requires prohibitively large resources for practical applications. Many approximations of the Kalman filter exist. For example, the Ensemble Kalman Filter (EnKF; Evensen (2003)) is a simplification of the Kalman filter which uses an ensemble of model states to estimate the model error statistics.

2.2 Assimilating data into sea-ice models

Assimilating data into sea ice models has only started a few years ago. Here is a short review of the state of the art.

Thomas and Rothrock (1989, 1993) have applied Kalman smoothing to passive microwave ice concentration data. They utilized a simple sea ice model, driven by velocities optimally interpolated from buoy motions, to form independent model-derived concentration estimates that were optimally blended with the concentration data. They then analyzed seven years of first-year and multiyear ice concentration data for the Arctic Ocean, which they divided into seven regions. They showed that the regions along the coasts of Alaska and Siberia and the area just north of Fram Strait are source of first-year ice with the rest of the Arctic Ocean acting as a sink for first-year ice through rigding and aging and that all the Arctic Ocean is a source of multiyear ice except for the Beaufort and the Chukchi seas. Later, Thomas *et al.* (1996) extended this work to the calculation of ice thickness. They used observed ice motions, winds and ice concentrations plus a thermodynamic sea ice model to produce a spatially and temporally varying ice thickness distribution in the Arctic. By comparing their results with submarine ice thickness data, they found that, for the whole Arctic Ocean, their estimates agree with the observational data but show less spatial and temporal variability. More recently, Lisaeter *et al.* (2003) demonstrated the assimilation of passive microwave ice concentration data into a comprehensive ice-ocean general circulation model of the Arctic Ocean using an ensemble Kalman filter. They concluded that the assimilation of ice concentration data is a viable way of controlling the simulated ice cover, but does not correct the generally underestimated model ice thickness.

The study of Meier *et al.* (2000) was the first attempt to assimilate observed ice motion data into a large-scale model of the Arctic sea ice cover in order to maximize the model accuracy. These authors employed an optimal interpolation scheme to assimilate ice velocity data derived from passive microwave imagery. They found that the assimilation substantially reduces the error standard deviation and improves the correlation of the simulated motions relative to buoy observations. Nevertheless, they noticed that the assimilation induces unrealistic changes in ice thickness near the Greenland coast and the Canadian Archipelago as well as in the outflow of ice mass through Fram Strait. In other studies, Meier and Maslanik (2001a,b) demonstrated the utility of a data assimilation approach for improving the model estimation of buoy trajectories and for investigating synoptic events in the Arctic sea ice drift. Later, Arbetter *et al.* (2002) combined satellite-derived and modeled ice velocities in a large-scale Arctic sea ice model to simulate the anomalous summer ice retreats observed in 1990 and 1998. For both years, the computed ice extent appears in better agreement with observational estimates when ice velocity data are assimilated, but excessive ice melt occurs in the central pack. Meier and Maslanik (2003) further investigated the effects of local conditions (namely, the proximity to the coast, the ice thickness and the wind forcing) on Arctic remotely sensed, modeled and assimilated ice velocities. They showed that the optimal interpolation assimilation technique improves the quality of the ice motion throughout most ranges of wind speed and ice thickness both in coastal and non-coastal regions. Their results also suggest that the use of assimilation weights optimized for typical environmental conditions would further reduce errors and yield greater benefits from assimilation. Very recently, Dai *et al.* (2006) showed that efforts to adjust a sea ice model by altering the frictional loss parameter[1] have limited effects in cases where observed ice motions are assimilated because the assimilation essentially bypasses the model dynamics. In parallel, Zhang *et al.* (2003) conducted a hindcast simulation of the Arctic sea ice variations over the period 1992-1997 with a regional ice-ocean general circulation model in which buoy and passive microwave ice motion data were assimilated by means of an optimal interpolation scheme. Assimilation was found to significantly improve the modeled ice motion, with substantially reduced stoppage, which in turn leads to strengthened ice outflow at Fram Strait, enhanced ice deformation and ice drafts that are slightly closer to those derived from submarine measurements. Lindsay *et al.* (2003) extended this work for a 10-month period in 1997 and 1998. Comparisons of ice velocity Radarsat Geophysical Processor System (RGPS) measurements to the modeled velocities showed excellent agreement for the model with data assimilation but poorer agreement for the model-only run. However, the deformation from the data assimilation run was in only modest agreement with observations, suggesting that some model aspects need improvement.

Very recently, Lindsay and Zhang (2006) extended the work of Zhang *et al.* (2003) by incorporating in their model of the Arctic ice-ocean system a nudging scheme with a non-linear weighting function to assimilate passive microwave ice concentration data. They observed that the assimilation of ice concentration alone increases the ice draft bias, especially in the marginal seas, but improves the correlation with ice draft measurements made by upward looking sonars on submarines and moorings. When both ice concentration and velocity data are assimilated, an improvement in the ice draft comparison is obtained, but a significant bias still exists in the large-scale ice thickness pattern. It should be noted that Lindsay and Zhang (2005) used this experimental set-up to investigate the causes of the recent changes of the Arctic ice pack.

The studies mentioned above indicate that data assimilation generally improves the model estimate of the assimilated variable(s) but can deteriorate the simulation of other variables. So far, no detailed assessment of the impact of data assimilation on the global performance of a large-scale sea ice model has been performed. This is mainly due to our very limited knowledge of both modeling and observational errors (Weaver *et al.*, 2000).

[1]The *frictional loss parameter* is used in the ice-strength parameterization. It is defined as the ratio of the total energy loss to potential energy change and is the parameter that controls the comprehensive strength of the ice cover.

Chapter 3

Assimilation of data into a toy model of Arctic sea ice

3.1 Introduction

First of all, this chapter presents the sea ice toy model that we built, the experimental design and the data assimilation scheme that we used. For two major reasons, building a simplified sea ice model to test the impact of data assimilation scheme on the model behavior was an excellent first step towards data assimilation into NEMO-LIM2, a more complex global sea ice-ocean model (see Chapter 4). Firstly, the toy model computational time is much lower. Secondly, the toy model is not coupled to an ocean model. Hence, the data assimilation scheme may be implemented with no concern about ocean feedback.

This chapter is further devoted to a detailed analysis of results from a series of twin experiments (i.e. experiments in which the data to be assimilated are model outputs). We choose to assimilate sea ice concentration and motion because they have been widely observed during the last 35 years with the aid of passive microwave sensors aboard satellites (e.g. Bjørgo *et al.*, 1997; Cavalieri *et al.*, 1997; Emery *et al.*, 1997; Parkinson *et al.*, 1999; Comiso and Steffen, 2001; Cavalieri *et al.*, 2003). A simple optimal interpolation scheme is used, and outputs from control runs and from perturbed experiments without and with data assimilation are thoroughly compared.

3.2 Toy model formulation and forcing

The model used in this first part of the work is a simplified two-level, thermodynamic-dynamic sea ice model. This model takes into account the most relevant sea ice processes while being inexpensive in CPU (Central Processing Unit) time. As mentioned above, this model is used to have a first estimate on assimilation of data into a sea ice model. Therefore, it is not meant to reproduce exactly the sea ice features and should be taken as a toy model.

The main model variables are the ice thickness, h_i, the ice concentration (relative area of ocean covered by ice), A_i, and the ice velocity, $\overrightarrow{u_i}$. The presence of snow on top of sea ice is neglected. However, a prescribed, monthly varying surface albedo that takes into account the presence of snow is used (Semtner, 1976). Local changes in ice thickness and concentration are calculated from the following conservation laws:

$$\frac{\partial A_i h_i}{\partial t} = -\nabla \cdot (\overrightarrow{u_i} A_i h_i) + S_h \qquad (3.1)$$

$$\frac{\partial A_i}{\partial t} = -\nabla \cdot (\overrightarrow{u_i} A_i) + S_A \qquad (3.2)$$

where t is the time and S_h and S_A are thermodynamic source or sink terms computed as in Hibler (1979). The vertical growth/decay rate of the ice is determined by the zero-layer model proposed by Semtner (1976). When ice is present in a grid cell and the heat budget of the open-water area becomes negative, ice of thickness h_o = 0.5 m (Hibler, 1979) is accumulated onto the side of the existing ice. The thickness of the newly formed ice is then averaged with that of the older ice to obtain a single value. Furthermore, a minimum open-water fraction of 0.5% (hence a maximum ice fraction, A_{max}) is prescribed to simulate the fact that cracks or leads are always present inside the pack due to unresolved dynamical effects.

Ice dynamics is computed by assuming that sea ice behaves as a two-dimensional continuum in dynamical interaction with atmosphere and ocean. A first estimate of the sea ice velocity is obtained from the so-called *free-drift* equation:

$$-mf\overrightarrow{k} \times \overrightarrow{u_i} + \overrightarrow{\tau_a} + \overrightarrow{\tau_w} = 0 \qquad (3.3)$$

where m is the ice mass per unit area, f is the Coriolis parameter, $\overrightarrow{k}$ is a vertical unit vector and $\overrightarrow{\tau_a}$ and $\overrightarrow{\tau_w}$ are the forces due to air and water drags, respectively. Note that the force associated with the tilt of the sea surface is neglected. The computed velocity is then corrected to avoid excessive ice build-up in regions of convergent ice motion due to the neglect of internal ice forces. Following Kreyscher *et al.* (2000), the ice velocity is set equal to zero where (1) the ice thickness exceeds 3 *m* and (2) the ice would be transported into an area with thicker ice. Applied as it is, this correction causes a velocity gradient that is too steep and leads to problems when assimilating data into the model. To prevent these troubles, it is necessary to smooth the transition by applying a hyperbolic tangent reduction factor to the ice velocity as a function of h_i.

An upstream scheme with anti-diffusion is used for advection (Smolarkiewicz, 1983). First the thermodynamical equations then the dynamical ones are solved on a Cartesian grid covering the Arctic Ocean and adjacent seas, with a spatial resolution of about 100 *km* (Figure 3.1). A time step of one day is employed.

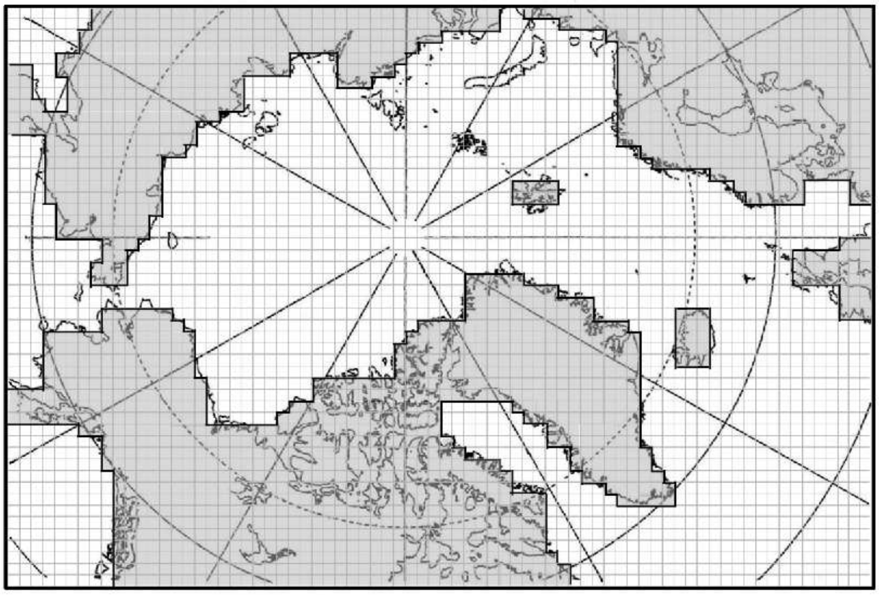

Figure 3.1: Model domain and grid.

Daily 2-*m* air temperatures and 10-*m* winds from the National Centers for Environmental Prediction/National Center for Atmospheric Research (NCEP/NCAR) (Kalnay *et al.*, 1996) are utilized to drive the model. The other atmospheric input fields consist of climatological monthly surface relative humidities (Trenberth *et al.*, 1989) and cloud fractions (Parkinson and Washington, 1979). The surface fluxes of heat are determined from these data using empirical parameterizations described by Goosse (1997). The oceanic heat flux at the base of the ice layer, F_b, is given by:

$$F_b = \rho_w c_{pw} h_{ml} \gamma_t (T_{obs} - T_{ml}) \tag{3.4}$$

where ρ_w is the density of seawater, c_{pw} is the specific heat of seawater, h_{ml} is the mixed-layer depth (30 *m*), γ_t is a time constant ($6 \times 10^{-8} s^{-1}$), T_{ml} is the model mixed-layer temperature and T_{obs} is the monthly mean observed mixed-layer temperature given by the Polar Science Center Hydrographic Climatology (PHC, Steele *et al.* (2001). When sea ice is present in a grid cell, T_{ml} is set equal to the freezing point of seawater (271.2 *K* according to Semtner (1976)). Ice is not allowed in grid cells where T_{ml} is greater than the freezing point of seawater. In ice-free grid cells, T_{ml} is determined from the heat budget of the mixed layer. It is worth mentioning that F_b is included in this heat budget to implicitly account for the advection of heat by oceanic currents. If T_{ml} reaches the freezing point, then a new ice layer of thickness h_o forms at the ocean surface. The momentum fluxes at the various interfaces are obtained from standard bulk formulas described by Goosse (1997). For the quadratic drag coefficients between air and ice and between ice and water, we use constant values of 1.2×10^{-3} (McPhee, 1980) and 5×10^{-3} (Timmermann *et al.*, 2005), respectively. The ocean is assumed to be motionless.

3.3 Experimental design

As mentioned in Section 2.2, the major problem when assimilating data into large-scale sea ice models comes from our rather poor knowledge of both model and observation errors. To overcome this problem, we build an idealized observational dataset with the model and perform so-called *twin experiments* (Figure 3.2).

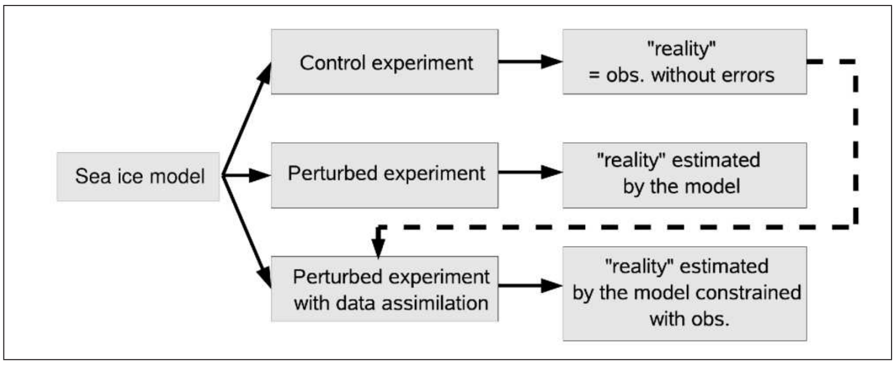

Figure 3.2: Schematic representation of the experimental design.

A control run from 1977 to 2000 is first conducted. The model is initialized with a 3 *m*-thick and 99.5%-compact ice cover over the entire domain. Outputs for years 1995 and 1996 are regarded as the *reality* or *true state* (hereafter referred to as TS) for those years (i.e. as observations without any error). Then, to account for model errors in estimating the TS, the model is perturbed and new experiments are carried out over the years 1995 and 1996. In order to introduce errors that remain consistent with the model physics, perturbations are applied to the model forcing. Three types of disturbance are considered:

1. We use the surface air temperatures of years 1992 and 1993 instead of those of years 1995 and 1996. In this case, the dynamic component of the model is regarded as perfect and the thermodynamic component as a direct source of errors. Such experiments are referred to as WA_T, VA_T_XX, CA_T_YY and VCA_T_XX_YY in Table 3.1. *WA* stands for the experiment without assimilation and *VA*, *CA* and *VCA* for experiments with assimilation of velocities, concentrations and velocities and concentrations, respectively. XX and YY are the gains to assimilate, respectively, velocity and concentration data.
2. The surface winds employed to compute the air-ice stress are replaced by these of years 1992 and 1993. This time, it is the thermodynamic component of the model which is considered as perfect and the dynamic component as a direct source of errors. Those experiments are referred to as WA_D, VA_D_XX, CA_D_YY and VCA_D_XX_YY in Table 3.1.
3. Initial conditions (IC) of year 1995 are replaced with IC of year 1992. Those experiments are referred to as WA_IC, VA_IC_XX, CA_IC_YY and VCA_IC_XX_YY in Table 3.1.

The chosen perturbations are fairly strong. However, we also forced the model with weighted mixes of forcings from two different years. We ran several tests combining different years (not only 1992-1993 and 1995-1996). We also tested several weights. Nevertheless, all experiments pointed towards the same type of conclusion. In this study, we focus on the 1995-1996 period because it gives a good summary of all the experiments we have run. For the different types of perturbation, we assess how the assimilation of ice velocities and/or concentrations from the TS improves the model behavior.

Twin experiments are common practice in atmospheric and oceanic modeling (e.g. Lin *et al.*, 2001; Fox *et al.*, 2000). However, to our knowledge, it is the first time that simulations of this kind are performed with a sea ice model. Usually, twin experiments are carried out in a forecasting perspective, and thus the model is perturbed by changing initial conditions. Here, as the purpose is rather oriented toward reanalysis, we also find it appropriate to alter the thermal and dynamical forcings.

The observational data sets are compiled from control experiment outputs. No noise is added. The impact of the data set quality on the assimilated results is not studied here, yet this work will be carried out with NEMO-LIM2 in Chapter 5.

3.4 Assimilation scheme

At each time step, an optimal interpolation scheme is used to assimilate ice concentration and ice velocity data into the model according to :

$$A_{ass} = A + k_A(A_{obs} - A) \tag{3.5}$$

$$\overrightarrow{u}_{ass} = \overrightarrow{u} + k_u(\overrightarrow{u}_{obs} - \overrightarrow{u}) \tag{3.6}$$

where A and $\overrightarrow{u}$ are the ice concentration and velocity. The subscripts *ass* and *obs* stand for assimilated and observed data. While the ice velocity is updated at the end of the model velocity computation (before the computation of ice transport), the ice concentration update is done at the end of the model time step. k_A and k_u are the *weights* or *gains* for ice concentration and ice velocity data assimilation, respectively, and are usually determined through a least-squares minimization of the error variance of the assimilated value compared to a statistical true value (Meier *et al.*, 2000; Lindsay and Zhang, 2006). If we assume uncorrelated and biasless errors:

$$k_{th,A} = \frac{\sigma^2_{\epsilon A}}{\sigma^2_{\epsilon A_{obs}} + \sigma^2_{\epsilon A}} \tag{3.7}$$

$$k_{th,u} = \frac{\sigma^2_{\epsilon u}}{\sigma^2_{\epsilon u_{obs}} + \sigma^2_{\epsilon u}} \tag{3.8}$$

where the subscripts A and u stand for the ice concentration and velocity. k_{th} is the gain computed by the least-squares method, $\sigma^2_{\epsilon A/u}$ and $\sigma^2_{\epsilon A/u_{obs}}$ are the variances of modeled and observed errors respectively. Because the present experimental design provides one observation per model grid cell with zero error, the weights should then be set to one, and observed data would directly be inserted into the model. Indeed, such weights give the best estimation for the assimilated values but often on the detriment of other variables. In this study, we gave the preference to a global improvement of the sea ice estimation rather than improving one single sea ice variable at a time. In this way, we found that the choice of the weights is determinant. We also found that choosing the weights on a physical basis was more efficient than to choose them on a statistical basis. However, all along this work we will still call this scheme an *optimal interpolation* scheme for convenience.

	Thermodynamical perturbation	Dynamical perturbation	Initial conditions perturbation
Without data assimilation	WA_T	WA_D	WA_IC
Assimilation of ice velocity data	VA_T_XX	VA_D_XX	VA_IC_XX
Assimilation of ice concentration data	CA_T_YY	CA_D_YY	CA_IC_YY
Assimilation of ice velocity and concentration data	VCA_T_XX_YY	VCA_D_XX_YY	VCA_IC_XX_YY

Table 3.1: Acronyms of the twin experiments performed with the toy-model. XX and YY represent the values of the weight for ice velocity and concentration assimilation, respectively.

The model may estimate the presence of sea ice where observations do not. No velocity observations are then available to improve the model estimations. Moreover, velocity data assimilation brings about discontinuities in the assimilated velocity field at the edge between areas where ice velocity observations exist and areas where they don't. To circumvent this problem, the data assimilation scheme considers observations from the 9 contiguous grid cells to each cell close to this edge. If velocity observations exist, they are linearly interpolated with an inverse distance weighting function. The resulting velocity is then assimilated into the model, using half of the gain. This procedure, which is essential when velocity data are assimilated, is of minor importance for concentration data assimilation. Actually, the transition between areas with sea ice and areas with no sea ice is smoother for concentrations than for velocities. Furthermore, velocity data vary quickly over time and therefore need a strong gain. However, for instabilities reasons, the concentration data assimilation gain must be taken much lower. In turn, this attenuates the possible discontinuities. Finally, if observations do not estimate sea ice in a grid cell when the model does, the assimilation scheme should decrease the ice concentration estimation without considering the neighboring grid cells.

In cases where the model estimates no ice where observations do, concentration data assimilation brings an ice block of thickness h_o = 0.5 *m* into the grid cell. If the ocean mixed layer temperature T_{ml} is equal to the freezing point of seawater, the ice remains. Otherwise, the ice block melts and T_{ml} decreases according to :

$$T'_{ml} = T_{ml} - \frac{Ah_oQ_{ice}}{\rho_w c_{pw} h_{ml}} \tag{3.9}$$

where A is the concentration of the newly formed ice, Q_{ice} is the volumetric latent heat of fusion of sea ice, ρ_w is the density of seawater, c_{pw} is the specific heat of seawater and h_{ml} is the mixed-layer depth.

The assimilation technique used in this thesis is fairly simple but accurate enough for the purpose of our study. In particular, as shown in Section 3.5, it allows to underline a number of problems posed by the assimilation of ice concentration and/or velocity data into large-scale sea ice models.

3.5 Results

3.5.1 Control run

The model ice circulation averaged over 1979-1999 (Figure 3.3a) exhibits many of the recurrent or permanent features of the observed ice motion (e.g. Emery *et al.*, 1997). In particular, the clockwise Beaufort Gyre, the Transpolar Drift Stream and the East Greenland Drift Stream are all reproduced. Note that the model has a motionless ocean. The magnitude of the ice velocity appears globally underestimated. On average, the simulated ice drift tends to thin the ice off the Alaskan and Siberian coasts while increasing the ice thickness by convergence and ridging off the Canadian Archipelago and the north coast of Greenland (Figure 3.3b). The shape and magnitude of the simulated ice thickness contours are in general agreement with those derived from submarine sonar measurements (e.g. Bourke and Garrett, 1987). The most significant departure from current estimates is observed along the Canadian Archipelago and the north coast of Greenland, where the model generates too thin an ice cover. This feature together with the generally too weak ice velocities mainly result from the simplistic treatment of the effect of internal ice forces in the model.

Figure 3.4 compares the March and September mean ice concentrations computed by the model to the corresponding observations of Comiso (1999). In March, the modeled location of the ice edge agrees relatively well with the observed one. One notes, however, that the ice cover protrudes slightly too far southward in the Barents, Greenland and Labrador Seas. In September, the simulated ice edge is somewhat south of the observed one in the Barents and Kara Seas, and ice persists in Baffin Bay, whereas observations show that this area is totally free of ice during that month. A detailed inspection of Figure 3.4 also reveals that the percentage of open water within the summer pack is somewhat overestimated.

Although we have identified a certain number of shortcomings in the results of the control run conducted with the model, the discussion above demonstrates that the model shows acceptably good agreement with enough aspects of the seasonal behavior of the Arctic sea ice cover to permit a reliable study of the effect of the assimilation of ice velocity and/or concentration data through twin experiments.

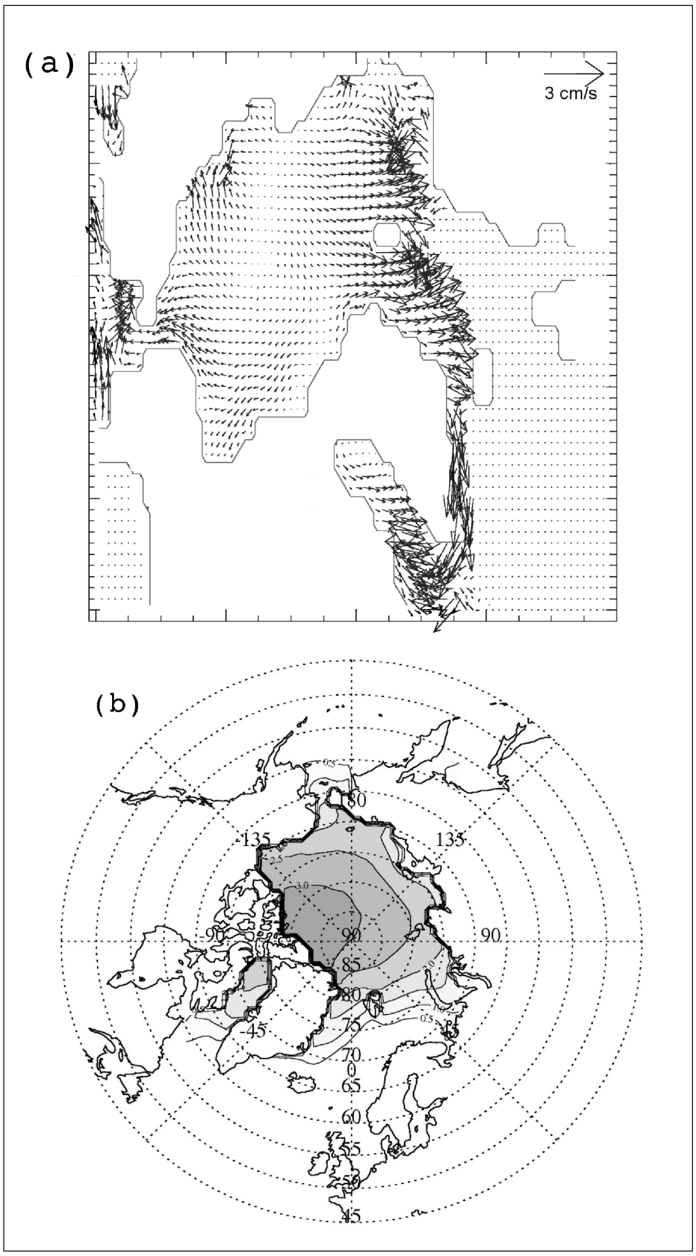

Figure 3.3: Annual mean ice velocities (a) and March ice thicknesses (b) from the control run averaged over the period 1979-1999. Scale vector for ice velocity is 3 $cm \times s^{-1}$. Selected contours for ice thickness are 0.5, 1, 1.5, 2, 2.5 and 3 m.

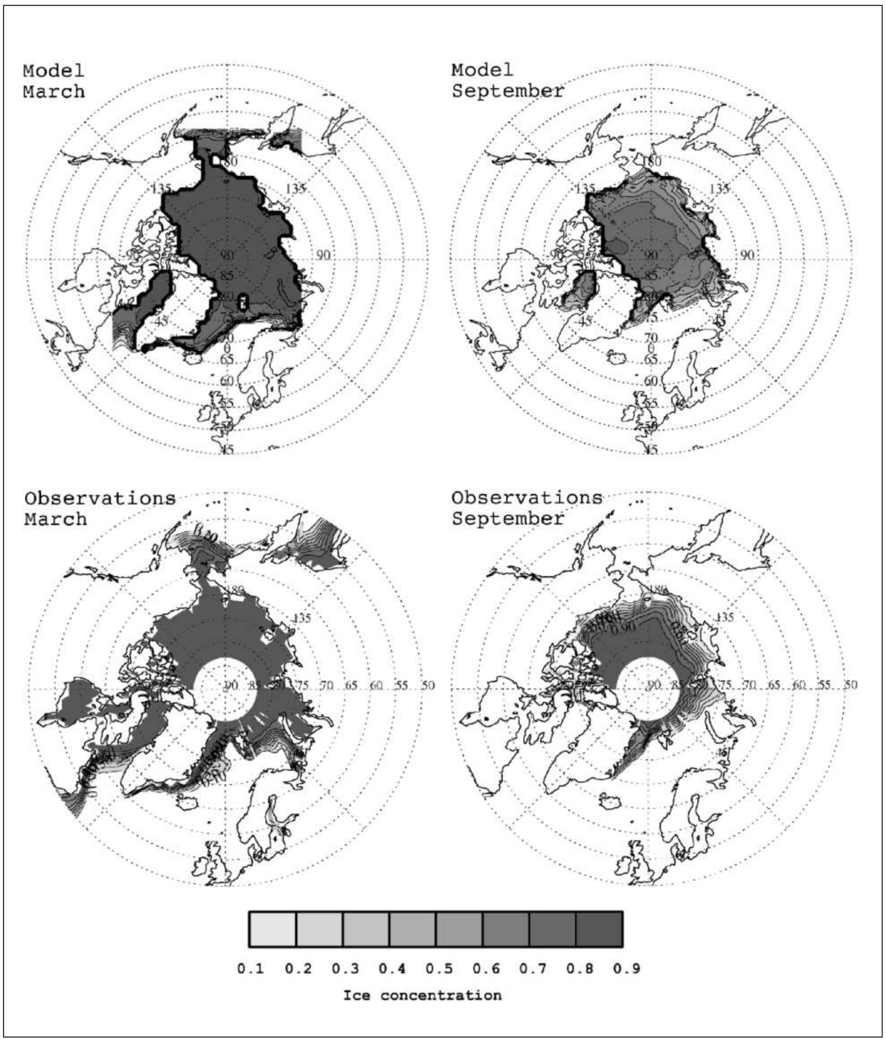

Figure 3.4: March (left) and September (right) ice concentrations averaged over the period 1979-1999 from the control run (top) and as observed (Comiso (1999); bottom). The pole hole in the observations is due to lack of satellite coverage in that area. Contour interval is 0.10.

3.5.2 Thermodynamical perturbation

3.5.2.1 Assimilation of ice velocity data

In this section, we examine the impact of assimilating ice velocities from the TS on the model behavior when the model is thermodynamically perturbed (see Section 3.3). U and V are the 2 components of the ice velocity defined on grid of Arakawa type B.

Tables 3.2 and 3.3 compare the annual mean results obtained without and with assimilation for year 1995 to the TS for different values of the weight k_u (0.3, 0.5 and 0.9). Clearly, the assimilation of ice velocity data is a good way to improve the simulation of the ice motion. In addition, the correlations between the perturbed ice concentrations and thicknesses and the TS fields are also enhanced when assimilation is performed and when k_u increases. As expected, the higher k_u, the better the assimilated ice velocities. However, taken together, the error in ice thickness averaged over the entire area occupied by the pack and the standard deviation of this error are minimum for k_u = 0.5. As can be seen from Figure 3.5, the standard deviation of the ice thickness error is slightly weaker for k_u = 0.9 than for k_u = 0.5 during the first five months of 1995 and becomes significantly larger afterwards. The reason for this is that when the thermodynamic perturbation is applied to the model, thermodynamics seek an anomalous extreme in ice thickness. The model ice dynamics then act to reduce this anomaly, but data assimilation defeats this process. For instance, if the ice is too thick in a region because of too low an air temperature, convergence will weaken in this area via the Kreyscher *et al.* (2000) correction. When higher ice velocities are assimilated, convergence becomes larger and ice thickens, thus defeating to lower the ice thickness error. This is especially true during summer melt and autumn freeze up. In conclusion, a large gain might be usefull to improve the ice thickness on small time scales, when the thermodynamic error remains quite low. As error increases with time, a smaller gain (around 0.5) is more appropriate since it less heavily weights the TS velocities which are not fully suitable to reduce the ice distribution errors.

Figure 3.5 suggests to take k_u equal to 0.5 in experiments longer than five months also, such a gain leads to another problem. Table 3.3 indicates that for k_u = 0.5 the area-averaged, annual mean ice concentration bias is enhanced compared to the no-assimilation case. By contrast, the error in ice thickness is reduced, but not due to the enhancement of the ice transport. When velocity data are assimilated with k_u = 0.5, the velocity field after assimilation is the arithmetic

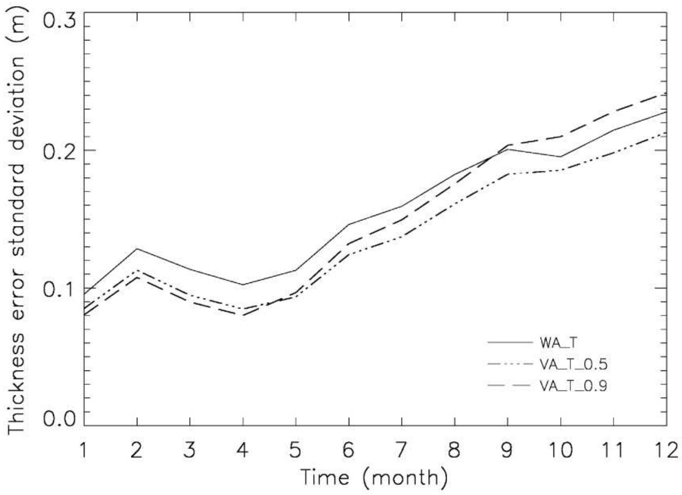

Figure 3.5: Temporal evolutions over year 1995 of the standard deviation of the ice thickness error for experiments WA_T (solid line), VA_T_0.9 (dashed line) and VA_T_0.5 (dashed-dotted line).

average of the model and TS velocity fields. This average globally smoothes the ice advection. Therefore, the ice cover experiences less divergence, which yields an enhanced ice compactness and less convergence, resulting in less ice build-up. This problem fades away as k_u increases.

As *perfect* data are assimilated into our model, one was expecting to obtain the best results with the highest weight. Our results show that this is not necessarily the case. Eventhough the assimilation of sea ice velocity data generally improves the estimation of the velocity, it sometimes deteriorates other sea ice variables, namely here, the ice thickness and ice concentration. Therefore, on time scales less than five months, it seems preferable to use a large k_u, while over longer time scales, a smaller k_u must be used, which generates too smooth an ice transport.

3.5.2.2 Assimilation of ice concentration data

Here, we evaluate the effects of the assimilation of ice concentrations from the TS when a thermodynamic perturbation is applied to the model.

	Correlation		Bias ($10^{-4}m/s$)		Error std (m/s)	
	U	V	U	V	U	V
WA_T	0.38	0.36	2.48	-2.15	0.028	0.023
VA_T_0.3	0.69	0.68	1.12	-1.09	0.018	0.015
VA_T_0.5	0.84	0.83	1.25	-0.91	0.012	0.010
VA_T_0.9	0.98	0.98	0.39	-0.22	0.002	0.002
CA_T_0.15	0.43	0.41	-0.41	-1.76	0.026	0.022
VCA_T_0.9_0.15	0.98	0.98	0.10	-0.14	0.002	0.003

Table 3.2: Area-averaged, annual mean correlations between the ice velocity components from experiments WA_T, VA_T_0.3, VA_T_0.5, VA_T_0.9, CA_T_0.15 and VCA_T_0.9_0.15 and the TS, and area-averaged, annual mean errors in the ice velocity components and standard deviations of these errors. In experiments CA_T_0.15 and VCA_T_0.9_0.15, ice thickness conservation is imposed near the ice margin and where the thermodynamic error is larger than the indirect dynamic one, and ice volume conservation is imposed everywhere else (for detail, see Section 3.5.2.2).

	Correlation		Bias		Error std	
	h_i	A_i	h_i ($10^{-2}m$)	A_i (10^{-2})	h_i (m)	A_i
WA_T	0.75	0.32	8.77	1.81	0.142	0.078
VA_T_0.3	0.79	0.56	6.23	2.27	0.125	0.072
VA_T_0.5	0.82	0.73	6.48	2.22	0.121	0.067
VA_T_0.9	0.87	0.93	8.82	1.82	0.132	0.062
CA_T_0.15	0.56	0.78	4.44	0.36	0.120	0.041
VCA_T_0.5_0.15	0.85	0.87	-2.94	0.41	0.114	0.029
VCA_T_0.9_0.15	0.90	0.97	2.82	0.38	0.100	0.023

Table 3.3: Area-averaged, annual mean correlations between the ice thickness and concentration from experiments WA_T, VA_T_0.3, VA_T_0.5, VA_T_0.9, CA_T_0.15, VCA_T_0.5_0.15 and VCA_T_0.9_0.15 and the TS, and area-averaged, annual mean errors in the ice thickness and concentration and standard deviations of these errors. In experiments CA_T_0.15, VCA_T_0.5_0.15 and VCA_T_0.9_0.15, ice thickness conservation is imposed near the ice margin and where the thermodynamic error is larger than the indirect dynamic one, and ice volume conservation is imposed everywhere else (for detail, see Section 3.5.2.2).

In each grid cell, the sea ice volume V_i can be diagnosed from:

$$V_i = A_i h_i S \tag{3.10}$$

where S is the grid cell area (constant). When the ice concentration varies owing to assimilation, one may either conserve ice volume or ice thickness. The first solution appears more appropriate given the huge effort put in recent years into developing energy-conserving sea ice models (e.g. Bitz and Lipscomb, 1999).

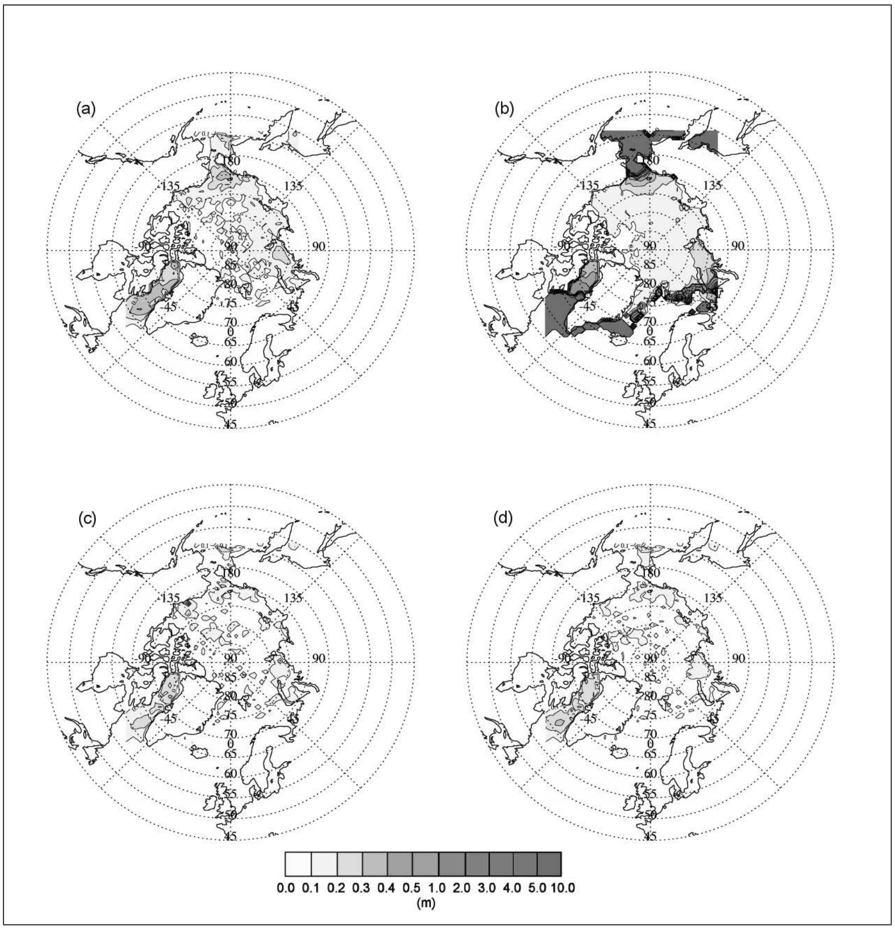

Figure 3.6: Differences (in absolute value) in annual mean ice thickness for year 1996 between experiment WA_T and the TS (a), and between experiment CA_T_0.15 and the TS when we impose ice volume conservation everywhere (b), ice thickness conservation everywhere (c) and ice thickness conservation near the ice margin and where the thermodynamic error is larger than the indirect dynamic one, and ice volume conservation everywhere else (d). For detail, see Section 3.5.2.2

Nonetheless, it can create serious problems. Indeed, if the ice concentration in a grid cell is too large (small) due to the use of an erroneously low (high) surface air temperature, there is every chance that the ice thickness is also overestimated (underestimated)[1]. The assimilation will then tend to reduce (increase) the ice concentration. If the conservation of ice volume is imposed, this will lead to an increase (decrease) in ice thickness, thus enhancing the initial thickness bias. Figures 3.6a and 3.6b display the changes (in absolute value) in annual mean ice thickness between the experiments without and with assimilation of ice concentration data and the TS for year 1996. In the case with assimilation, ice volume conservation is imposed and $k_A = 0.15$. It can be seen from these figures that the assimilation deteriorates in many places the simulation of the sea ice thickness, especially near the ice edge where the thermodynamic error can be quite large due to the high interannual variability of the air temperature.

The second solution is to conserve ice thickness. Overall, this solution improves the ice thickness estimate compared to the no-assimilation case (Figure 3.6 c). However, the thickness bias increases along the north coast of Alaska. In several grid cells there, the applied thermodynamic perturbation produces so large ice accumulations that there is no longer ice convergence (because of Kreyscher *et al.* (2000) correction) into the grid cells. Only ice divergence is allowed, which tends to decrease the ice compactness. At this stage, the dynamic error has become larger than the thermodynamic one. The assimilation of ice concentration data corrects the too low concentration by adding an ice block of thickness equal to that of the pre-existing ice. Furthermore, as ice volume is not conserved in the assimilation process, during ice divergence episodes, the grid cells affected by this problem act as a source of ice volume for the neighboring ones. Clearly, in those specific cases, it would be better to impose ice volume conservation.

Given these results, we propose to combine the two solutions. Basically, the thermodynamic perturbation introduces direct thermodynamic errors into the model as well as indirect dynamic and thermodynamic ones, due to ice thickness and concentration biases and their effect on sea ice rheology. Near the ice edge and in areas where thermodynamic errors are greater than dynamic ones, ice thickness conservation is imperative. Elsewhere, it seems more appropriate to conserve ice volume. The problem now is to draw a distinction between thermodynamic and dynamic errors. We observed that, when ice concentration in a grid cell has been corrected during the previous time step through data assimilation, the next time step modeled concentration remains close to (strongly deviates from) the TS one if the error is of thermodynamic (dynamic) nature. Therefore, we assume that the magnitude of the ice concentration error is an indicator of the model

[1] This is at least true during the winter and during summer melt. The autumn freeze-up case would probably be different.

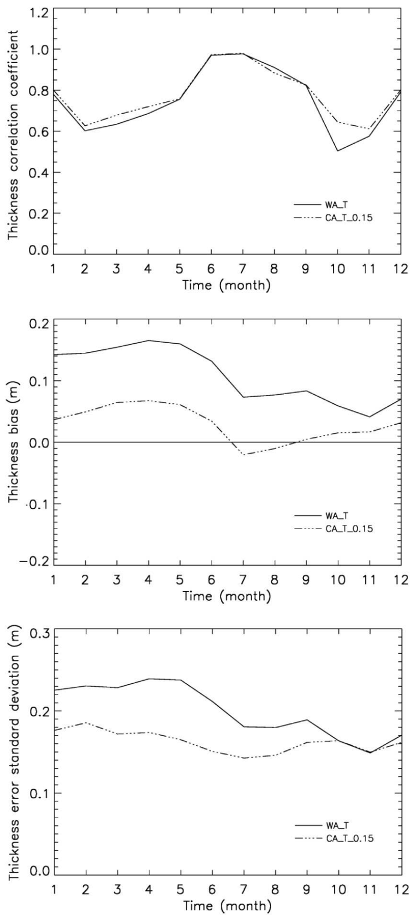

Figure 3.7: Temporal evolutions over year 1996 of the area-averaged correlations between ice thicknesses from experiments WA_T and CA_T_0.15 and the TS ones (a), the area-averaged ice thickness errors for experiments WA_T and CA_T_0.15 (b), and the standard deviations of the ice thickness errors for experiments WA_T and CA_T_0.15 (c). In the experiment with assimilation, ice thickness conservation is imposed near the ice margin and where the thermodynamic error is larger than the indirect dynamic one, and ice volume conservation is imposed everywhere else.

error type. When the difference between modeled and TS concentrations before assimilation is smaller (greater) than a certain threshold, the error is assumed to be thermodynamic (dynamic) so that the ice thickness (volume) is enforced to be conserved. Figure 3.6d reveals that this technique further improves the simulation of the annual mean ice thickness pattern for year 1996 compared to the case where ice thickness conservation is applied everywhere. On the other hand, Figure 3.7 shows that the monthly values of the area-averaged ice thickness bias and thickness error standard deviation are significantly reduced in comparison with the no-assimilation case and that the correlation between the modeled and TS ice thicknesses is slightly improved.

Figure 3.6d indicates that, in some places, the assimilation slightly deteriorates the ice thickness estimate. This feature is mostly due to the use of thresholds in the model, such as the thickness of newly formed ice in leads, the maximum allowable ice concentration or the Kreyscher *et al.* (2000) correction threshold. Owing to those thresholds, small differences in the sea ice state can have noticeable effects. These effects are particularly visible during the first couple of years of simulation. Afterwards, when the ice thickness error caused by the perturbed forcing grows, they become negligible and the improvement brought by data assimilation to the model becomes clearer.

In this subsection, we presented results of year 1996 (instead of year 1995) because they gave a clearer representation of the major problems that we have encountered when we assimilated concentrations in the toy model. To be consistent with the rest of this section, 1995 annual statistical values compared to the TS and averaged over the model domain are shown in Tables 3.2 and 3.3 (see CA_T_0.15 experiment). Those values bear out the improvement of the ice velocity, concentration and thickness estimations with concentration data assimilation.

All the experiments we conducted with the model point to the fact that choosing k_A equal to 0.15 gives the best model improvement while preventing the appearance of model instabilities. They also suggest that, because of the strong connection between ice concentration and ice thickness, assimilation of concentration data has to be handled with care. The best solution we found is to conserve ice thickness after assimilation near the ice margin and where the thermodynamic error is larger than the indirect dynamic one, and to conserve ice volume everywhere else. To be complete, the ice thickness correction should depend on the physical mechanisms involved. However, such mechanisms are somewhat very inter-dependent and it is not realistic to actually determine the nature of the ice thickness error at each time step and for each grid cell. According to our results, the correction suggested in this study is one possible correction to be applied. This solution is therefore retained in the experiments discussed in the following section.

3.5.2.3 Assimilation of ice velocity and concentration data

The model performance can be further enhanced by assimilating simultaneously ice velocities and concentrations from the TS. But, here again, the choice of the weights appears crucial.

In Table 3.3, we compare the annual mean results obtained without and with assimilation for year 1995 to the TS for two sets of weights: k_u = 0.5 and k_A = 0.15; k_u = 0.9 and k_A = 0.15. For k_u = 0.5 and k_A = 0.15, the correlations between the estimated ice concentrations and thicknesses and the TS are significantly increased, and the standard deviations of the errors in ice concentration and thickness are markedly reduced. Nevertheless, as a result of the assimilation-induced smoothing of the ice velocity field discussed in Section 3.5.2.1, the simulated ice pack is slightly too thin and too compact. When k_u = 0.9 and k_A = 0.15, the model results seem further improved. However, for the same reason as the one given in Section 3.5.2.1, when time goes by, the simulation of ice thickness progressively deteriorates.

In summary, the assimilation of ice velocity and/or concentration data is able to weaken the effect of the thermodynamic perturbation applied to the model. Nonetheless, given the sensitivity of the improvement brought by assimilation to the weights, their value must be selected carefully as a function of the characteristic time scale of the assimilated variable, the type of model error and the model integration length.

3.5.3 Dynamical perturbation

3.5.3.1 Assimilation of ice velocity data

Here, we assess the impact of the assimilation of ice velocities from the TS on the model performance when the model is dynamically perturbed (see Section 3.3). Several values of k_u have been tested. In Tables 3.4 and 3.5, we compare the annual mean results obtained without and with assimilation for year 1995 to the TS. As presupposed, the larger k_u, the better the ice velocity estimation (see Table 3.4). In addition, for k_u = 0.5, Table 3.5 shows that the correlations between the simulated ice concentrations and thicknesses and the TS increase notably compared to the no-assimilation case, and that the standard deviations of the errors in ice concentration and thickness decrease significantly. However, once again, because of the ice velocity smoothing caused by assimilation, the model ice field becomes somewhat too thin and too compact. The situation is much improved when k_u = 0.9. Actually, the best way to get rid of this problem would be to use a weight equal to 1. This means that with wrong model dynamics, directly inserting observed sea ice velocities in the model might be a good solution to improve the model.

	Correlation		Bias ($10^{-5} m/s$)		Error std (m/s)	
	U	V	U	V	U	V
WA_D	0.04	0.01	-1.85	-0.06	0.035	0.028
VA_D_0.5	0.72	0.70	-0.90	-0.06	0.016	0.013
VA_D_0.9	0.98	0.98	-0.18	-0.03	0.003	0.003
CA_D_0.3	0.04	0.01	-1.78	-0.07	0.035	0.028
VCA_D_0.9_0.3	0.98	0.98	-0.18	-0.02	0.003	0.003

Table 3.4: Area-averaged, annual mean correlations between the ice velocity components from experiments WA_D, VA_D_0.5, VA_D_0.9, CA_D_0.3 and VCA_D_0.9_0.3 and the TS, and area-averaged, annual mean errors in the ice velocity components and standard deviations of these errors. In experiments CA_D_0.3 and VCA_D_0.9_0.3, we impose ice volume conservation within the ice pack and ice thickness conservation close to the ice edge.

	Correlation		Bias		Error std	
	h_i	A_i	h_i $(10^{-2}m)$	A_i (10^{-2})	h_i (m)	A_i
WA_D	0.78	0.29	0.21	0.05	0.106	0.066
VA_D_0.5	0.90	0.72	-3.18	0.63	0.079	0.043
VA_D_0.9	0.98	0.98	-0.80	0.14	0.027	0.014
CA_D_0.3	0.55	0.68	1.17	0.05	0.119	0.029
VCA_D_0.9_0.3	0.92	1.00	-0.01	0.02	0.055	0.006

Table 3.5: Area-averaged, annual mean correlations between the ice thickness and concentration from experiments WA_D, VA_D_0.5, VA_D_0.9, CA_D_0.3 and VCA_D_0.9_0.3 and the TS, and area-averaged, annual mean errors in the ice thickness and concentration and standard deviations of these errors. In experiments CA_D_0.3 and VCA_D_0.9_0.3, we impose ice volume conservation within the ice pack and ice thickness conservation close to the ice edge.

3.5.3.2 Assimilation of ice concentration data

In this section, we try to find the best way to assimilate ice concentrations from the TS into the model in order to improve the ice thickness estimate when a dynamic perturbation is applied to the model.

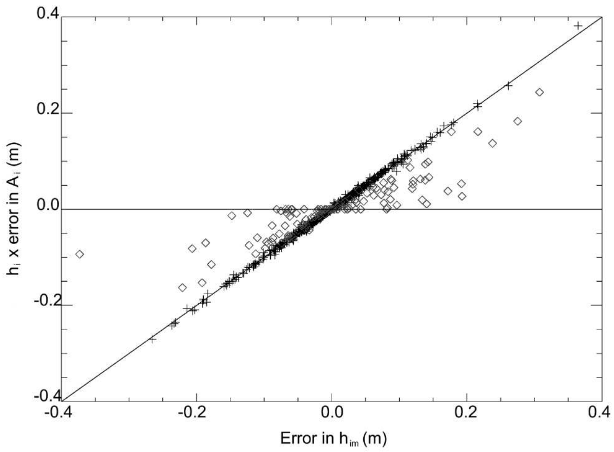

Figure 3.8: Error in h_{im} versus error in A_i times h_i at the end of the first time step of experiment WA_D. The diamonds correspond to the grid cells where either the modeled or TS ice concentration is equal to A_{max} and the crosses correspond to the other grid cells. The 1:1 line is also plotted.

As already mentioned, the ice concentration is tightly linked to the ice thickness and volume. To avoid error feedbacks, we analyze ice concentration and thickness errors just after the first time step of the experiment without assimilation. We define the mean ice thickness in a given grid cell as $h_{im} = A_i h_i$. Figure 3.8 reveals that, for most grid cells, the error in h_{im} is quasi-equal to the product of h_i and the error in A_i. As $V_i = h_{im} S$ (where V_i is the ice volume and S the grid cell area) this suggests that the ice volume should be corrected by adding or removing an ice block of thickness h_i and of concentration equal to the error in A_i. In other words, the in-situ ice thickness should be conserved after assimilation of ice concentration data. This also suggests that k_A should be taken equal to 1. If this technique is used, the error in h_{im} is reduced to almost zero in the majority of grid cells (crosses in Figure 3.9a). Nonetheless, in grid cells where either the modeled or TS concentration is equal to the maximum allowable value A_{max} (diamonds in Figure 3.9a), the bias remains large. During the second time step, the assimilation of ice concentration data lowers the error in h_{im} in most grid cells (crosses in Figure 3.9b). By contrast, the mean ice thickness worsens in grid cells where a significant bias was observed during the first time step (triangles in Figure 3.9b). This behavior is mainly due to ice piling. The model piles the ice to prevent $A_i > A_{max}$. If ice piling occurs in the perturbed experiment but not in the TS, assimilation of ice concentration data is only able to partly correct the simulated ice concentration. On the other hand, as we suppose that h_i is conserved after assimilation, the error in h_i remains, as well as part of the error in h_{im}. Later, this error weakly perturbs the thermodynamic component of the model and strongly affects the dynamic one, which leads to error amplification. Note that this is also true for grid cells where $A_i < A_{max}$ while TS shows $A_i = A_{max}$. The proposed solution therefore seems to work on short time scales, with initial conditions very close to reality. However, on longer time scales, it is inappropriate because, in problematic grid cells, it leaves errors which grow afterwards. It is worth noting that a smaller k_A lowers the error amplification process without erasing it.

Another possible solution might be to impose, after assimilation, ice volume conservation within the ice pack and ice thickness conservation close to the ice edge, where the mean ice thickness is less than say 0.5 m. This solution would be consistent with the best solution found for the thermodynamically perturbed model. However, as shown in Table 3.5 for $k_A = 0.30$, it deteriorates the ice thickness simulation compared to the no-assimilation case. This is caused by the fact that, during a particular time step, the perturbed wind forcing greatly modifies the ice circulation and the geographical distribution of ice thickness. Consequently, the next time step, the ice melt/growth rate and transport can be very different from the TS.

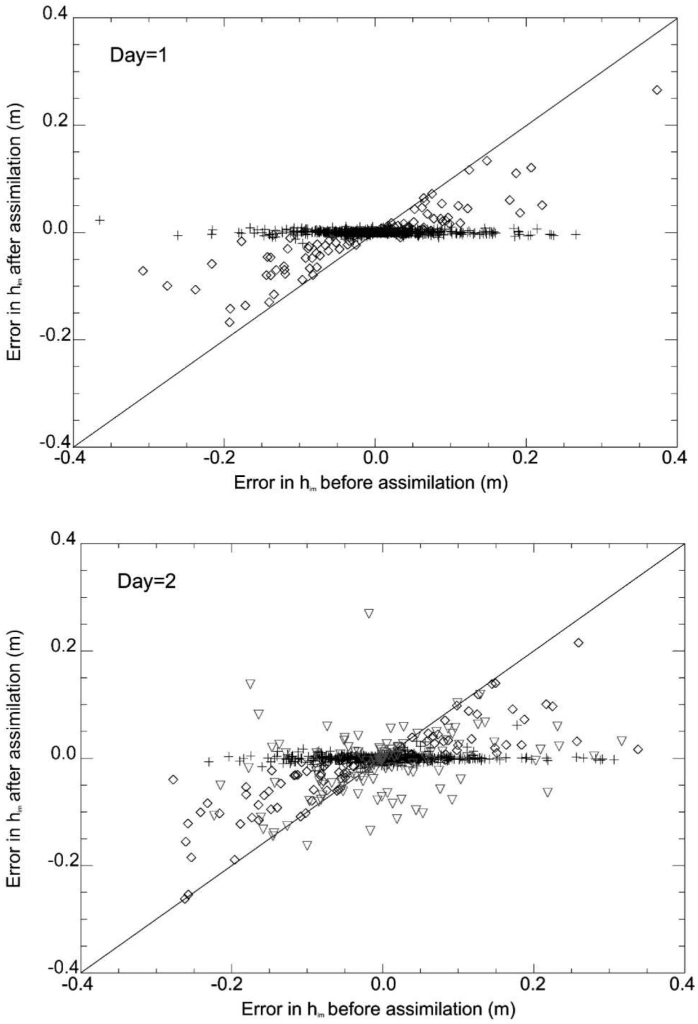

Figure 3.9: (a) Error in h_{im} before assimilation versus error in h_{im} after assimilation for the first time step of experiment CA_D_0.3. The ice thickness is supposed to be conserved during the assimilation process. (b) Same as (a), but for the second time step of experiment CA_D_0.3. The diamonds correspond to the grid cells where either the modeled or TS ice concentration is equal to A_{max}. The triangles correspond to the grid cells where, during the previous time step, either the modeled or TS ice concentrations were equal to A_{max}. The crosses correspond to the other grid cells. The 1:1 line is also plotted.

In conclusion, when the model is dynamically perturbed, assimilation of ice concentrations is one way to improve the estimated ice concentrations but not always the estimate of ice thickness. As a matter of fact, for short-term studies (a few days), the best model improvement is observed when in-situ ice thickness is conserved. For longer-term studies, one should rather conserve the ice volume than the in-situ ice thickness, unless the mean ice thickness is lower than 0.5 *m*.

3.5.3.3 Assimilation of ice velocity and concentration data

When both ice velocities and concentrations from the TS are assimilated into the model, the problems mentioned above remain and the model improvement is not always straightforward. The best results are obtained with k_u = 0.9 and k_A = 0.3 (a k_u equal to 1 would correct most of the errors without giving the chance to the concentration assimilation to operate) and when the ice volume is forced to be conserved everywhere except near the ice margin. Results for year 1995 of this experiment are summarized in Tables 3.4 and 3.5. The model performance is overall enhanced compared to the velocity- or the concentration-only assimilation case. Even if the average correlation between the computed ice thicknesses and the TS ones is slightly reduced in comparison with the velocity-only assimilation experiment, the average ice thickness bias and the standard deviation of this error are drastically diminished.

We concluded that the combined assimilation of sea ice concentration and velocity data is the most powerful approach to improve the model results in a dynamically perturbed model.

3.5.4 Initial conditions perturbation

In this section, we analyse results of experiments carried out with initial conditions from control experiment (referred to as CE hereafter) outputs for year 1992 instead of year 1995. Figure 3.10a shows ice concentration initial conditions

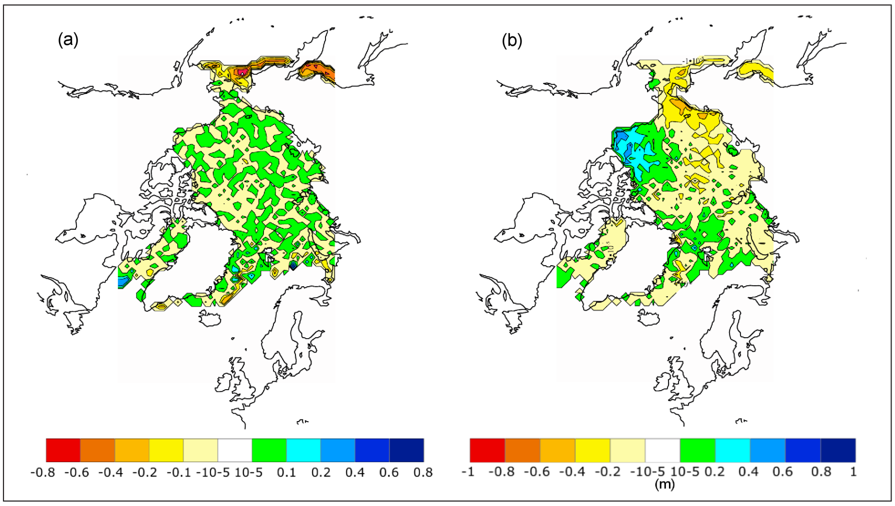

Figure 3.10: Initial conditions of ice concentration (a) and ice thickness (b) from control experiment outputs for year 1992 minus initial conditions for year 1995.

discrepancies between years 1992 and 1995. Differences remain globally under 0.05 value in the central Arctic. Larger discrepancies arise along the ice edge like in the Bering and Okhotsk Seas where the ice extent is larger in 1995 than in 1992. In Davis Strait as well as in the Greenland, Iceland, and Norwegian Seas (GIN Seas), the ice is sometimes sparser, sometimes more compact. This results from slightly but different ice edge patterns.

Figure 3.10b presents ice thickness differences between 1995 initial conditions and 1992. The ice is up to 0.5 *m* thicker along the Siberian coasts, in the East Siberian Sea, the Chukchi Sea and in the Bering Sea. Yet, in other regions like in the Beaufort Sea and near the Svalbard Islands, 1995 ice is thinner by about 0.1 to 0.5 *m*.

3.5.4.1 Assimilation of ice velocity data

Here, we assess model estimation improvement brought by velocity data assimilation when the perturbation arises from spurious initial conditions.

As expected, data assimilation of ice velocity clearly improves the velocity model estimation (see the statistical values presented in Table 3.6). Area-averaged, annual mean correlation coefficients are strongly increased for both velocity components. Errors standard deviations and biases are reduced. Furthermore, the

	Correlation		**Bias** ($10^{-4} m/s$)		**Error std** (m/s)	
	U	V	U	V	U	V
WA_IC	0.39	0.38	-0.44	2.52	0.028	0.023
VA_IC_0.1	0.50	0.50	-0.85	1.89	0.024	0.020
VA_IC_0.5	0.86	0.85	-1.15	0.99	0.012	0.010
VA_IC_0.9	0.99	0.99	-0.35	0.37	0.003	0.002
VA_IC_1.0	1.00	1.00	-0.00	0.00	0.000	0.000

Table 3.6: Area-averaged, 1995 annual mean correlations between the ice velocity components from experiments WA_IC, VA_IC_0.1, VA_IC_0.5 VA_IC_0.9 and VA_IC_1.0 and the TS, and area-averaged, 1995 annual mean errors in the ice velocity components and standard deviations of these errors.

	Correlation		**Bias**		**Error std**	
	h_i	A_i	h_i ($10^{-2}m$)	A_i (10^{-2})	h_i (m)	A_i
WA_IC	0.81	0.36	-2.01	-0.28	0.098	0.060
VA_IC_0.1	0.83	0.44	-3.35	-0.03	0.099	0.058
VA_IC_0.5	0.90	0.78	-4.45	0.10	0.102	0.047
VA_IC_0.9	0.97	0.98	-2.50	-0.21	0.101	0.038
VA_IC_1.0	0.99	0.99	-1.98	-0.28	0.116	0.039

Table 3.7: Area-averaged, 1995 annual mean correlations between the ice thickness and concentration from experiments WA_IC, VA_IC_0.1, VA_IC_0.5 VA_IC_0.9 and VA_IC_1.0 and the TS, and area-averaged, 1995 annual mean errors in the ice thickness and concentration and standard deviations of these errors.

larger the gain, the better the improvement. Nevertheless, for k_u $= 0.1$ and k_u $= 0.5$, the biases of the velocity U-component increase.

As seen in Table 3.7, the improvement of the ice concentration estimation is not as clear as it is for the ice velocity estimation (cfr. Table 3.6). Although annual concentration correlation coefficients are increased and error standard deviations are globally lowered, biases improvements are mitigated. On one side, the mean concentration increases in VA_IC_0.1 and VA_IC_0.5 experiments, in comparison with the WA_IC experiment where concentrations are in average too small. On the other side, the gain k_u = 1.0 has no significant effect on the concentration bias.

According to the statistical values presented in Table 3.7, the ice thickness estimation is barely enhanced through velocity data assimilation. Correlation coefficients are improved, but thickness biases and error standard deviations outline degradation of the thickness estimation. Actually, the WA_IC ice thickness is globally too thin in comparison with the TS one. In the VA_IC_0.1 and VA_IC_0.5 experiments, the ice is even thinner. The greatest errors occur when k_u = 0.5, i.e. when observed velocities are arithmetically averaged with modeled ones. The resulting motion field is then smoothed and the advection lowered. Less advection leads to less ridged ice, and therefore to thinner ice (see Table 3.7). Less advection also involves less divergence which brings less ice openings hence larger ice concentration (see Table 3.7). Figure 3.11a displays the difference (in absolute value) in the ice thickness changes due to advection processes between the experiment without data assimilation and the TS during January 1995. The

	Correlation		**Bias**		**Error std**	
	h_i	A_i	h_i $(10^{-2}m)$	A_i (10^{-2})	h_i (m)	A_i
WA_IC	0.82	0.37	-0.07	-0.29	0.069	0.053
VA_IC_0.1	0.83	0.44	-1.88	0.14	0.069	0.048
VA_IC_0.5	0.90	0.78	-3.75	0.35	0.067	0.037
VA_IC_0.9	0.99	0.99	-0.70	0.04	0.043	0.011
VA_IC_1.0	1.00	1.00	-0.04	0.00	0.052	0.013

Table 3.8: Area-averaged, 1996 annual mean correlations between the ice thickness and concentration from experiments WA_IC, VA_IC_0.1, VA_IC_0.5 VA_IC_0.9 and VA_IC_1.0 and the TS, and area-averaged, 1996 annual mean errors in the ice thickness and concentration and standard deviations of these errors.

dark (light) areas point out that less (more) ice is ridged in the WA_IC experiment than in the TS. As Figure 3.11a is rather patchy (with a mild dominance of the darker color), the ice ridging during the WA_IC experiment is sometimes stronger, sometimes lighter than in the TS. There is no clear trend. However, for VA_IC_0.1 (see Figure 3.11b), the pattern darkens, meaning that the ice is less ridged when velocity data are assimilated. This is also true with $k_u = 0.9$ (not shown here). As presented in Figure 3.11c, this phenomenon is further intensified for $k_u = 0.5$.

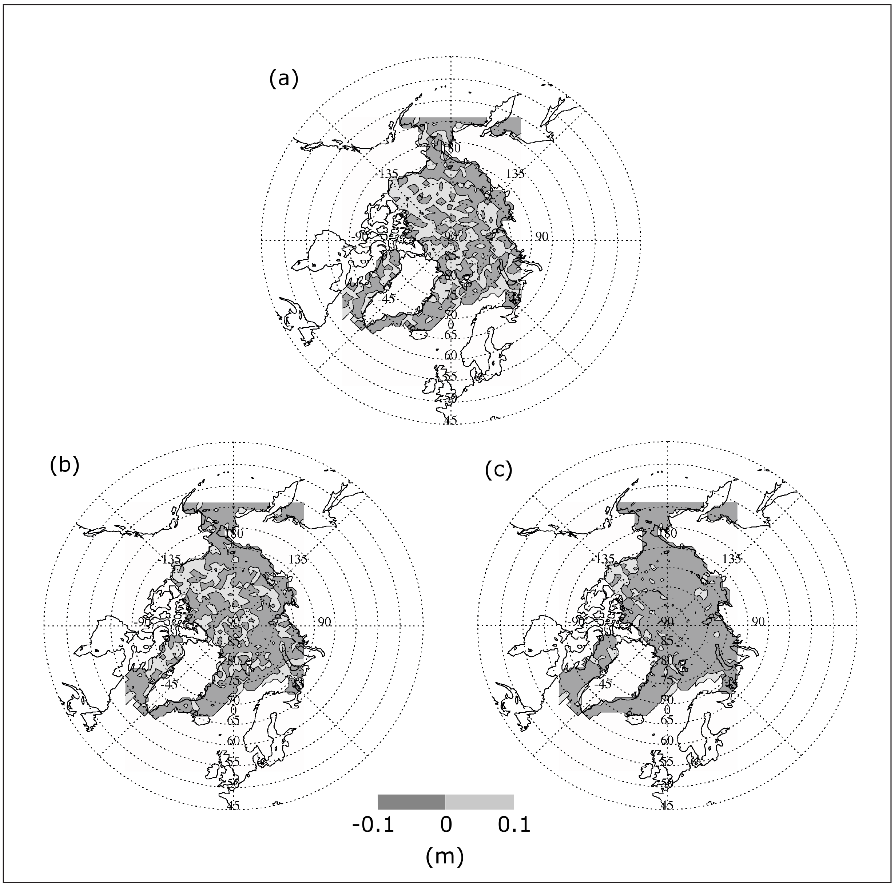

Figure 3.11: Differences (in absolute value) in the ice thickness growth through advection between the experiment without data assimilation and the control experiment (a) and between the experiment with data assimilation (for $k_u = 0.1$ and 0.5 respectively) and the control experiment (b and c respectively). Those values are averaged over January 1995.

Hence, motion data assimilation induces a smoothing of the estimated motion field and therefore a thinner but denser ice. In turn, the next model motion estimation will be different and, most of the time, will be worse than for the WA_IC experiment compared to the TS. If velocity data are assimilated into the model, the estimations will be partly corrected. Some errors remain however, especially when the gain is small. This comes out in Table 3.6 through the U-velocity component biases. For all those reasons, one should avoid smoothing the velocity field and a large weight should be chosen.

Unfortunately, for $k_u = 1.0$, yearly ice concentration bias is not actually improved (cfr. Table 3.7). Indeed, its value remains very close to the WA_IC experiment. Moreover, the ice thickness error standard deviation is deteriorated. This may be explained by the fact that when TS velocities are combined with the TS ice distribution (i.e. ice thicknesses and ice concentrations), the model leads to the next time step TS ice distribution. Since initial conditions are changed, the ice velocities and distribution are different and the model will lead to another ice distribution. Now, if the model starts with the wrong ice distribution but the TS velocities, there is no guarantee that the next time step estimated ice distribution will be better that the WA_IC one. This is the reason why restoring the estimated velocities towards the observed ones can sometimes amplify the ice distribution errors. Nevertheless, after one year of simulation (that is when the model discards from its initial conditions), velocity data assimilation with a large k_u really improves the global model ice estimation (cfr. Table 3.8).

In conclusion, velocity data assimilation in a simulation with perturbed initial conditions only partly improves the model estimation of the ice characteristic.

3.5.4.2 Assimilation of ice concentration data

In this section, we investigate how concentration data assimilation can be used to globally improve the modeled ice estimation if the model is perturbed with wrong initial conditions.

As mentioned in Section 3.5.2.2, ice concentration is strongly related to the ice thickness and volume. Therefore, the way concentration data are assimilated can strongly affect the ice thickness model estimation. In this sense, a relation between ice thickness and ice concentration errors would be very useful. However, comparison of Figures 3.10a and 3.10b indicates that no such relation exists. This is confirmed by Figure 3.12 where the ice concentration errors are plotted versus the corresponding ice thickness errors. Since no clear relation exists between these errors, the three methods described in Section 3.5.2.2 are put to the test. For reminding, the first method keeps the ice volume constant and changes the ice thickness in order to fit better concentration estimations to observations. The second method allows the ice volume to vary when concentration data are assimilated while the ice thickness is kept constant. Finally, the third method is a mix between the two previous ones : the ice thickness is kept constant everywhere unless the mean ice thickness is larger than $0.5\ m$ and the difference between modeled and observed ice concentrations is larger than a certain threshold.

Figure 3.13 displays the area-averaged monthly statistical values of the ice concentration estimation. Compared to the no-assimilation case, the three methods produce higher correlation coefficients by about 0.2. Monthly biases are also globally reduced, especially for CA_IC_0.15(2) and CA_IC_0.15(3) experiments. Likewise, concentration data assimilation lowers the concentration error standard deviations by about 0.02 compared to the no-assimilation case. Each method thus improves the model concentration estimate.

As presented in Figure 3.14, concentration data assimilation where the ice volume is conserved (CA_IC_0.15(1) experiment) deteriorates the ice thickness estimation. The monthly correlation coefficients are not only lowered but the biases and error standard deviations are also slightly increased in comparison with the no-assimilation experiment. On the contrary, CA_IC_0.15(2) and CA_IC_0.15(3) experiments show slight improvement of thickness correlation coefficients. Bi-

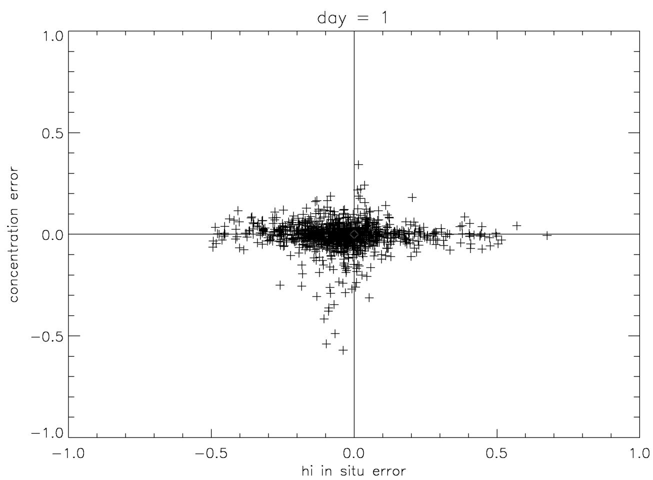

Figure 3.12: Ice concentration errors according to in-situ ice thickness errors between initial conditions of years 1992 and 1995. Ice thickness errors are given in meters.

ases are reduced (and of opposite sign after some time), while error standard deviations remain almost constant.

These results reflect the fact that erroneous initial conditions may cause ice concentration errors which are sometimes in phase with the corresponding ice thickness errors and sometimes not. When concentration data are assimilated in a manner that the ice volume is conserved, concentration and thickness correc-

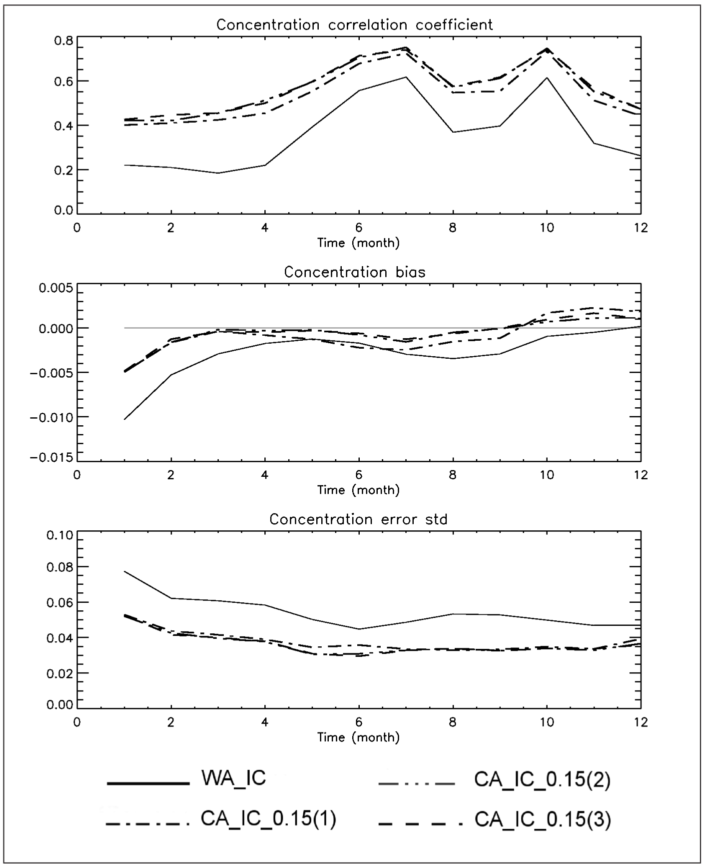

Figure 3.13: Area-averaged 1995 monthly mean correlation coefficients, biases and error standard deviations between ice concentration estimations of CA_IC_0.15-experiments compared to the TS. CA_IC_0.15(1) stands for the experiment with concentration data assimilation where the ice volume conservation is imposed. CA_IC_0.15(2) represents the experiment with data assimilation where the ice thickness conservation is imposed. Finally, in the CA_IC_0.15(3) experiment, the ice thickness is kept constant everywhere unless the mean ice thickness is lower than 0.5 m or the difference between modeled and observed ice concentration is larger than a certain threshold.

tions are of opposite signs. Hence, for cases where errors are out of phase, this method is the most appropriate one. However, for cases where errors are in phase, concentration data assimilation amplifies the ice thickness error. It is also worth mentioning that, for this specific year, monthly ice concentrations and thicknesses are both globally underestimated compared to the TS ones (mainly due to large errors in the Bering Strait region). When the data assimilation scheme conserves the ice volume, the concentration is globally increased and the ice thins as seen in Figure 3.14. After September, this process is inverted and the ice becomes globally too thick.

In the same way, conserving the in-situ ice thickness when concentration data are assimilated into the model may amplify the ice thickness errors if they are

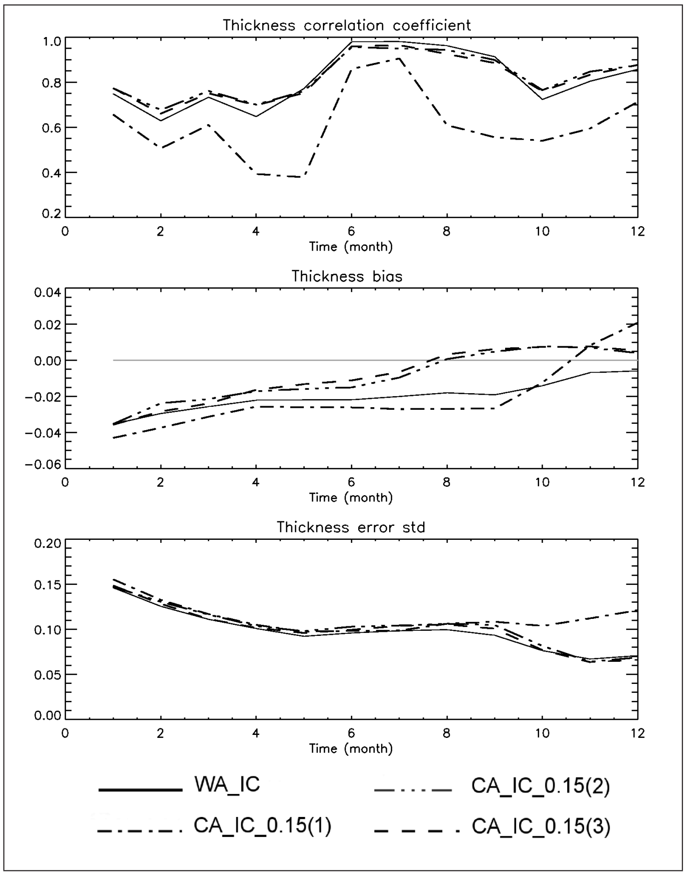

Figure 3.14: Same as Figure 3.13 but for the ice thickness. Biases and error standard deviations are given in m.

out of phase with the corresponding concentration ones. Yet, for this study, this process is not that significant and the ice thickness is globally enhanced by concentrations assimilation as seen in Figure 3.14 (cfr. CA_IC_0.15(2)). Finally, the third method gives about the same results as the concentration data assimilation experiment where the ice thickness is conserved. The model thickness estimation is no further improved.

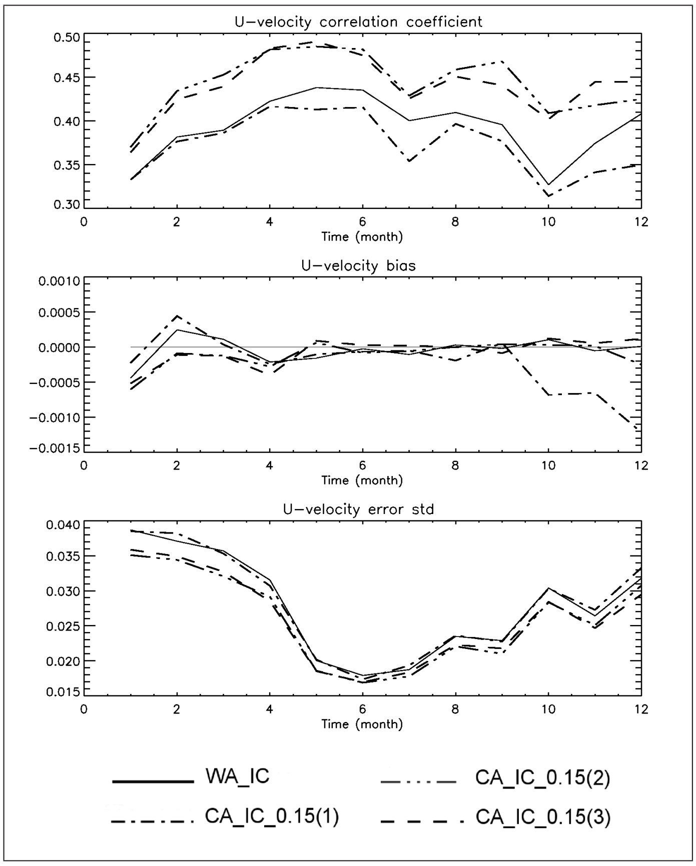

Figure 3.15: Area-averaged 1995 monthly mean correlation coefficients, biases and error standard deviations between velocity U-components of CA_IC_0.15-experiments compared to the TS. CA_IC_0.15(1) stands for the experiment with concentration data assimilation where the ice volume conservation is imposed. CA_IC_0.15(2) represents the experiment with data assimilation where the ice thickness conservation is imposed. Finally, in the CA_IC_0.15(3) experiment, the ice thickness is kept constant everywhere unless the mean ice thickness is lower than 0.5 m or the difference between modeled and observed ice concentration is larger than a certain threshold. Biases and error standard deviations are given in m/s.

Monthly statistical values of the ice U- and V-velocity components are presented in Figures 3.15 and 3.16. For CA_IC_0.15(1) experiment, the velocity estimation gets a slightly worse in comparison with the no-assimilation experiment. However, for CA_IC_0.15(2) and CA_IC_0.15(3) experiments, the velocity correlation coefficients are increased and error standard deviations are lowered. Such results were expected since those two experiments lead to the best ice distribution estimates. Nonetheless, there is no clear improvement of the monthly ice velocity biases.

To conclude, concentration data assimilation does not fully ameliorate the model simulation when perturbed initial conditions are used. Nevertheless, the ice thickness conservation scheme and the compromise scheme (which conserves the ice thickness everywhere unless the mean ice thickness is lower than 0.5 *m* or the dif-

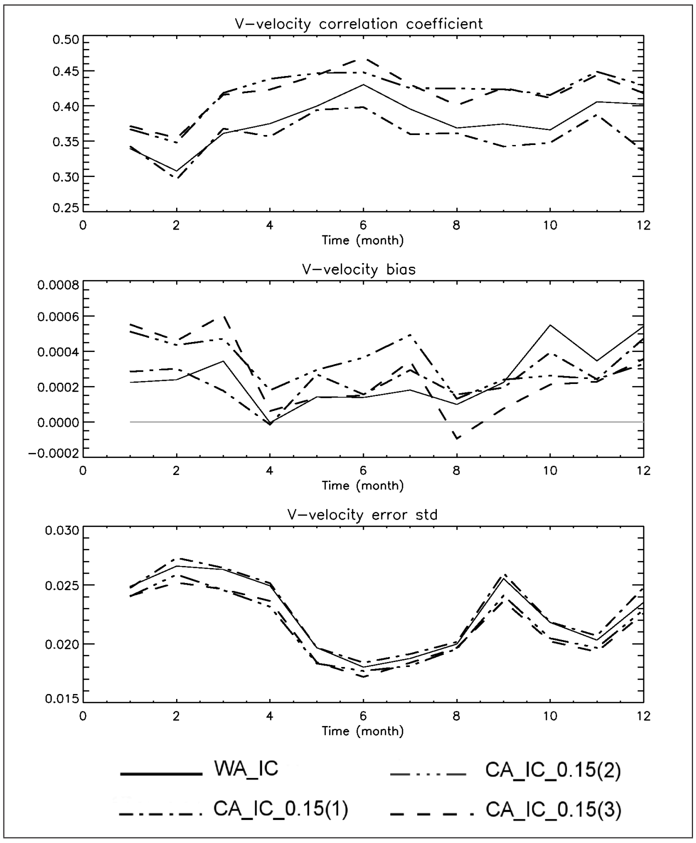

Figure 3.16: Same as Figure 3.15 but for the velocity V-component. Biases and error standard deviations are given in m/s.

ference between modeled and observed ice concentration is larger than a certain threshold) both globally improve most of the ice model estimation.

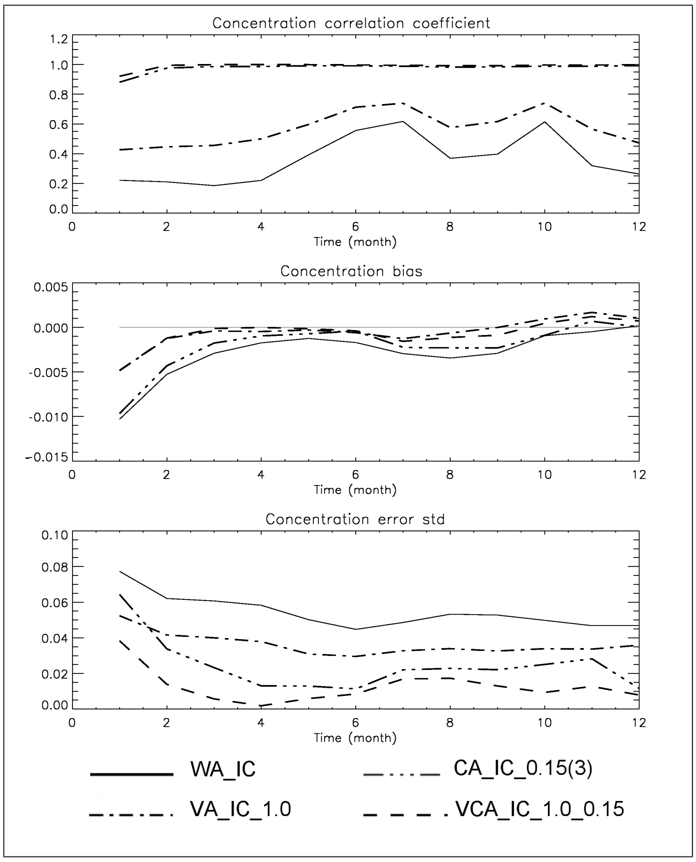

Figure 3.17: Area-averaged 1995 monthly mean correlation coefficients, biases and error standard deviations between ice concentration estimations of several experiments carried out with perturbed initial conditions compared to the TS. WA_IC stands for the perturbed experiment with no-data assimilation. VA_IC_1.0, CA_IC_0.15(3) and CVA_IC_1.0_0.15(3) stand for the perturbed experiments with respectively velocity-alone, concentration-alone and simultaneous velocity and concentration data assimilation. Where velocities are assimilated, $k_u = 1.0$. Where concentrations are assimilated, we use $k_A = 0.15$ and the ice thickness is kept constant everywhere unless the mean ice thickness is larger than 0.5 m and the difference between modeled and observed ice concentrations is larger than a certain threshold.

3.5.4.3 Assimilation of velocity and concentration data

The model performance can be further improved by assimilating simultaneously ice velocities and concentrations. However, in some cases, the problems mentioned above remain. Indeed, for $k_u = 0.9$ and $k_A = 0.15$ (not shown here), the ice thickness correction due to concentration data assimilation combined with the smoothing of the ice velocity field leads to some ice thinning. In turn, this deteriorate the model ice thickness estimation. The best results are obtained with $k_u = 1.0$ and $k_A = 0.15$ and the concentrations assimilation scheme conserves the ice thickness everywhere unless the mean ice thickness is larger than $0.5\ m$ and the difference between modeled and observed ice concentrations is larger than a certain threshold.

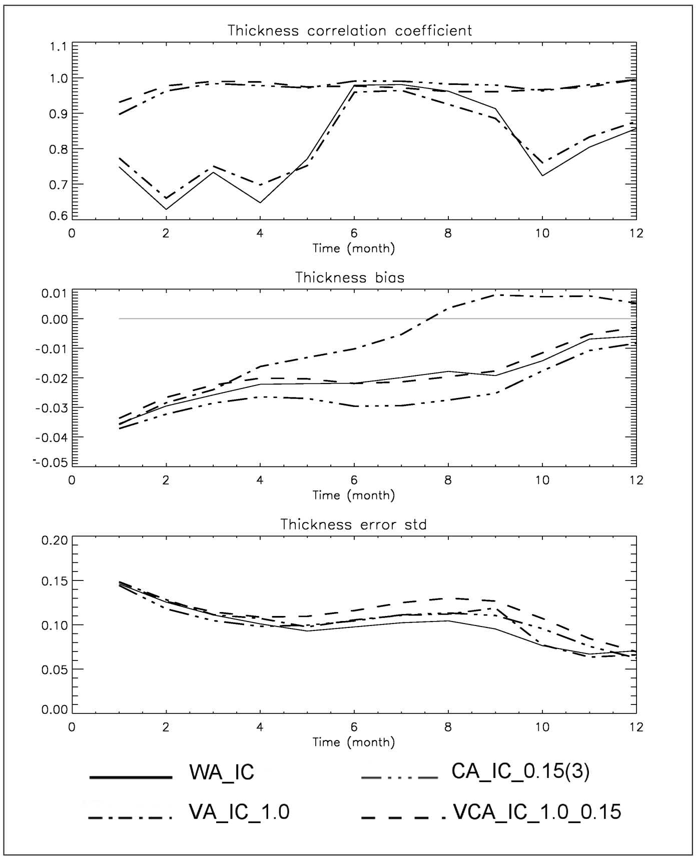

Figure 3.18: Same as Figure 3.17 but for the ice thickness. Biases and error standard deviations are given in m.

As seen in Figures 3.17 and 3.18, assimilating simultaneously ice velocities and concentrations markedly increases the correlation coefficients between the modeled ice concentrations and thicknesses and the TS. It also significantly decreases the concentration biases and error standard deviations. Nevertheless, the ice remains too thin, and the ice thickness error standard deviations are not improved compared to the no-assimilation case.

In summary, the assimilation of ice velocity and/or concentration data is able to attenuate the effect of the initial conditions perturbation applied to the model. The model estimation of ice velocities and concentrations may be significantly improved, especially if the gains are appropriately chosen. Nonetheless, since no coherent relation exists between the ice concentration and the ice thickness errors, the ice thickness model estimation is hardly improved.

3.6 Summary

Twin experiments have been conducted with a simplified model of the Arctic sea ice cover in order to determine to what extent the assimilation of ice velocity and/or concentration data improves the model behavior and, in particular, the simulation of ice thickness. Such experiments are idealized and do not allow tackling all the problems encountered when assimilating real observations into more complex models. Likewise, the data assimilation results are found to be model dependent to a certain extent and the model used here is simplified (no shear deformation, no ocean feedbacks, no explicit snow layer, ...). However, this study is a first step towards real data assimilation into NEMO-LIM2, a more complex ice-ocean model, and permits a detailed analysis of the way the model reacts to different data assimilation schemes.

Our results show that the assimilation of ice concentration data can easily lead to a deterioration of the model performance if it is not handled with care. This is mostly due to the strong but varying connection between ice concentration and ice thickness.

- When initial conditions are correct, the best way to estimate the sea ice state through concentration assimilation in the sea ice model is to make the distinction between model thermodynamic and dynamic errors. When the model error in a grid cell is mainly thermodynamic or near the ice edge, the assimilation must add or remove an ice block of thickness equal to that of the pre-existing ice to better fit the observed ice concentration, which means that ice volume must not be conserved in the process. On the contrary, when the model error is mainly dynamic, the assimilation must preserve the ice volume.
- When the initial conditions are perturbed, the link between ice concentration and ice thickness errors remain unfixed. The improvement of the ice thickness estimate through concentration data assimilation therefore remains quite uncertain. For our experimental design, the most appropriate value for the weight, k_A, is 0.15-0.3.

As expected, the assimilation of ice velocity data is found to significantly improve the overall ice model estimation if the model dynamics is wrong, especially when a high weight is utilized. Nevertheless, when the model error is thermodynamic or when it comes from initial conditions perturbation, the improvement brought by assimilation is not always as clear.

The results obtained in the present study also reveal that the assimilation of ice velocity data and the assimilation of ice concentration data are very complementary. Indeed, assimilating simultaneously ice velocity and ice concentration data into the model seems to be the best way to enhance the ability of the model to reproduce the observed features of the sea ice field.

Data assimilation is surely a suitable method for improving simulations of the sea ice pack made by sea ice models. Nevertheless, it is worth stressing that a better estimate of one model variable does not automatically yield better estimates of the other model variables. In addition, thresholds in the sea ice model can increase errors when data are assimilated. Finally, a good knowledge of model errors is also essential to apply consistent corrections.

Chapter 4

Assimilation of data into NEMO-LIM2

4.1 Introduction

In the previous chapter, we presented a series of results from experiments carried out with a sea ice toy model. However, the conclusions of Chapter 3 not only result from the experiments described in this thesis, but from numerous experiments which could not have been all presented here. For instance, we have tested many ways to correct the ice thickness due to the assimilation of ice concentration data. We have also tested many model perturbations. This huge amount of work would not have been possible with the NEMO-LIM2 model (a primitive-equation global ocean general circulation model coupled to the second version of the Louvain-la-Neuve sea ice model, LIM2), owing to its large computational time cost and to its higher degree of complexity. Nevertheless, the previous chapter gave us a good picture of what should be expected when assimilating sea ice data into models. It is now time to check its robustness, and to assess to what extent the conclusions of Chapter 3 are also applicable in a more realistic framework.

In this chapter, we first describe the NEMO-LIM2 model. We then present the experimental design, the model perturbations and the data assimilation scheme employed in this study. Finally, we analyse results of the experiments carried out with NEMO-LIM2 and check the robustness of the conclusions from Chapter 3. In comparison with the previous chapter, note that the present experimental design is more realistic and that the model takes into account ocean feedbacks and includes a more complex representation of the dynamical and thermodynamical sea ice processes.

4.2 Model formulation and forcing

NEMO-LIM2 is an updated version of ORCA2-LIM. Only a brief description of this model is given here. Further details can be found in Dulière (2002); Fichefet and Morales Maqueda (1997, 1999); Goosse and Fichefet (1999); Madec *et al.* (1999) and Timmermann *et al.* (2005).

4.2.1 NEMO, the ocean model

The ocean component of NEMO-LIM2 is based on version 8.2 of the hydrostatic, primitive equation ocean model OPA (Océan Parallélisé, Madec *et al.* (1999) see full documentation at http://www.lodyc.jussieu.fr/opa/). OPA is a finite difference global ocean general circulation model (OGCM) with a free sea surface and a non-linear equation of state in the Jackett and McDougall (1995) formulation.

In the NEMO-LIM2 configuration, lateral tracer mixing is done along isopycnals. Eddy-induced tracer advection is parameterized following Gent and McWilliams (1990). Momentum is mixed along model level surfaces using coefficients varying with latitude, longitude and depth.

The vertical eddy diffusivity and viscosity are computed by a level-1.5 turbulence closure scheme based on a prognostic equation for the turbulent kinetic energy. This parameterization has been developed for the atmosphere by Bougeault and Lacarrère (1989), adapted to the ocean by Gaspar *et al.* (1990) and embedded in OPA by Blanke and Delecluse (1993). Double diffusive mixing (i.e. salt fingering and diffusive layering) is represented following Merryfield *et al.* (1999). In locations with a statistically unstable stratification, a value of 100 m^2/s is assigned to the vertical eddy coefficients for momentum and tracers.

The Beckmann and Döscher (1997) bottom boundary layer scheme ensures an improved representation of dense water spreading over topography in this geopotential-coordinate model.

4.2.2 LIM2, the ice model

The ice component of NEMO-LIM2 is the second generation Louvain-la-Neuve sea ice model (LIM2), which is a dynamic-thermodynamic model specifically designed for climate studies. Most constants and parameters used in the model are defined in Table 4.1.

4.2.2.1 Vertical growth and decay of the ice

The formulation of the vertical growth and decay of the ice due to thermodynamic processes is essentially an improved version of the three-layer model of Semtner (1976). Within the ice-covered portion of each grid cell, sea ice is considered as a horizontally homogeneous slab of ice (divided into two layers of equal thickness) on which snow may accumulate when the surface temperature is below the melting point. The internal temperatures of snow and ice are governed by a one-dimensional heat diffusion equation:

$$\rho c_p \frac{\partial T}{\partial t} = G(h_e) k \frac{\partial^2 T}{\partial z^2} \tag{4.1}$$

where ρ, c_p and k are the density, specific heat and thermal conductivity of snow or ice, respectively. T is the temperature, t is the time and z is the vertical coordinate. $G(h_e)$ is a correction factor that accounts for the fact that the unresolved ice floes of varying thickness contribute differently to the average heat conduction (Mellor and Kantha, 1989). Assuming that the snow and ice thicknesses are uniformly distributed between zero and twice their mean value over the ice-covered part of the grid cell and ignoring the heat capacity of the system, one has (see Fichefet and Morales Maqueda (1997) for details):

$$G(h_e) = 1 + \frac{1}{2} ln\left(\frac{2h_e}{e\epsilon}\right) \tag{4.2}$$

In this expression, e is the base of the natural logarithms and ϵ is the threshold thickness which determines the limit of validity of Equation 4.2. h_e is an effective thickness for heat conduction defined as:

$$h_e = \frac{k_s k_i}{k_s + k_i}\left(\frac{h_s}{k_s} + \frac{h_i}{k_i}\right) \tag{4.3}$$

where the subscripts s and i stands for snow and ice, respectively. k and h are the thermal conductivity and the mean thickness, respectively. At the surface of the snow-ice system, a balance of fluxes is supposed to exist, so that

$$B_{su}(T_{su}) = (1 - i_0)(1 - \alpha_{su})F_{sw} + \epsilon_{su} F_{lw} - \epsilon_{su} \sigma T_{su}^4 + F_h + F_{le} + F_{cs} = 0 \tag{4.4}$$

where the subscript su refers to a property of the top surface (snow or ice), F_{sw} is the incoming shortwave radiation, α is the albedo, i_0 is the fraction of the net shortwave radiation that penetrates into the snow or bare ice and F_{lw} is the incoming longwave radiation. ϵ is the emissivity and σ is the Stephan-Boltzmann constant. F_h and F_{le} are the turbulent fluxes of sensible heat and latent heat, respectively. Finally, F_{cs} is the conductive heat flux below the surface. The convention used in Equation 4.4 is that a flux toward the surface is taken positive, while one away from the surface is negative. Following Maykut and Untersteiner (1971), i_0 is set equal to 0 in case of snow-covered ice. When ice is free of snow, i_0 is parameterized as (Ebert and Curry, 1993)

$$i_0 = 0.18(1 - c) + 0.35\ c \tag{4.5}$$

where c is the cloud fraction. According to Equation 4.5, the amount of solar radiation transmitted into the ice interior is larger for overforcast conditions than for a clear sky. This results from the combined effect of multiple reflections between the surface and the base of clouds and of the selective absorption by clouds of the less reflective longwave radiation (Grenfell and Maykut, 1977). If the heat balance (4.4) requires the surface temprature (T_{su}) to be above the melting point, T_{su} is held at this point and the excess of energy is balanced by melting snow or ice:

$$\left(\frac{\partial h_s}{\partial t}\right)_{su,abl} = -\frac{B_{su}(T_{su})}{L_s} \qquad h_s > 0 \tag{4.6}$$

$$\left(\frac{\partial h_i}{\partial t}\right)_{su,abl} = -\frac{B_{su}(T_{su})}{L_i} \qquad h_s = 0 \tag{4.7}$$

where L_s and L_i are the volumetric latent heats of fusion of snow and ice, respectively. Solid precipitation represents the only source of mass at the surface. When the load of snow is large enough so that the lower boundary of the snow is lowered under the seawater level, seawater is assumed to infiltrate the submerged snow and to freeze there. A snow ice cap is formed and changes of the snow and ice thicknesses are given by:

$$-(\triangle h_s)_{si} = (\triangle h_i)_{si} = \frac{\rho_s h_s - (\rho_w - \rho_i)h_i}{\rho_s + \rho_w - \rho_i} \tag{4.8}$$

where ρ_w is the reference density of seawater. In this parameterization, the difference of density between snow ice and ordinary ice is neglected. The latent heat and the brine released during the freezing of the seawater component are discharged into the oceanic surface. The internal temperatures of the ice cover are recomputed by a weighted formula.

The approach of Semtner (1976) was used to incorporate the mechanism of brine damping in the model. The solar energy absorbed inside the ice is stored in a heat reservoir that represents internal meltwater and is used to keep the temperature from the upper ice layer from dropping below the freezing point in autumn. Thereby, it simulates the release of latent heat through the refreezing of the internal brine pockets. We assume that the absorption of shortwave radiation within the ice is exponential (Grenfell and Maykut, 1977) therefore the energy from the reservoir Q_{st} evolves according to

$$\frac{\partial Q_{st}}{\partial t} = i_o(1-\alpha_{su})F_{sw}[1-e^{-1.5(h_i-b)}] - F_{lbp} \tag{4.9}$$

where b equals $0.1\ m$ and F_{lbp} is the heat flux necessary to prevent the upper ice layer from cooling below T_{fi}. The heat reservoir is limited to 50 % of the energy required to melt the whole ice sheet. This value for the limitation is somewhat arbitrary but is needed to prevent the model from numerically storing more heat than is needed to melt all the ice. Once this limit is reached, the shortwave radiation absorbed inside the ice contributes to the ice melting.

At the bottom of the ice layer, imbalances between the conductive flux within the ice, F_{cb}, and the heat flux from the ocean, F_w, are compensated by an accretion or ablation of ice:

$$\left(\frac{\partial h_i}{\partial t}\right)_{acc-abl} = \frac{F_{cb}-F_w}{L_i} \tag{4.10}$$

4.2.2.2 Lateral growth and decay of the ice

Inside the ice pack, the floes are separated by zones of open water which are very important, even if they are small, since they allow direct exchanges between the atmosphere and the ocean. This fraction of open water is represented into the model by the introduction of the variable A, the ice concentration, which is defined as the percentage of each grid cell that is covered by ice. The thermodynamic variations of A depend on the heat budget of the open water area B_l (see Goosse (1997) for details). If B_l is negative, ice of thickness h_o and of temperature T_{fw} is formed in the open water and A follows the law (Fichefet and Morales Maqueda, 1997):

$$\left(\frac{\partial A}{\partial t}\right)_{acc} = \sqrt{1-A^2}\frac{(1-A)B_l}{L_i h_o} \tag{4.11}$$

In order to account for the fact that cracks or leads are always present inside the pack due to unresolved dynamical effects, this parameterization retains the leads

Symbol	Definition	Value	Unit
a	Earth's radius	$6.371\ 10^6$	m
A^{vm}	Vertical eddy viscosity	$1.2\ 10^{-4}$	$m^2\ s^{-1}$
A^{vT}	Diffusivity for heat	$1.2\ 10^{-5}$	$m^2\ s^{-1}$
A^{vS}	Diffusivity for salt	$1.2\ 10^{-5}$	$m^2\ s^{-1}$
C	Ice strength parameter	20	
C_{ai}	Atmosphere-ice drag coef.	$1.2\ 10^{-3}$	
C_{aw}	Atmosphere-ocean drag coef.	$1.2\ 10^{-3}$	
C_{db}	Bottom ocean drag coef.	$4\ 10^{-4}$	
c_h	Coefficient in McPhee (1992) law	0.006	
C_{iw}	Water drag coefficient	$2.4\ 10^{-3}$	
c_{pi}	Specific heat of sea ice	2093	$J\ kg^{-1}\ K^{-1}$
c_{ps}	Specific heat of snow	2093	$J\ kg^{-1}\ K^{-1}$
c_{pw}	Specific heat of seawater	4000	$J\ kg^{-1}\ K^{-1}$
D	Horizontal diffusivity	350	$m^2\ s^{-1}$
ϵ	Threshold thick. for ice temp. eq.	0.1	m
ϵ_{su}	Emissivity of snow or ice	0.97	
ϵ_w	Emissivity of seawater	0.97	
g	Acceleration due to gravity	9.80665	$m\ s^{-2}$
h_0	Thick. of newly formed ice in leads	0.3	m
k	Von Karman Constant	0.4	
k_i	Thermal conductivity of sea ice	2.0344	$Wm^{-1}K^{-1}$
k_s	Thermal conductivity of snow	0.22	$Wm^{-1}K^{-1}$
L_i	Vol. latent heat of fusion of sea ice	$300.330\ 10^6$	$J\ m^{-3}$
L_s	Vol. latent heat of fusion of snow	$110.121\ 10^6$	$J\ m^{-3}$
P^*	Ice strength parameter	20000	$N\ m^{-2}$
ρ_i	Density of sea ice	900	$kg\ m^{-3}$
ρ_s	Density of snow	330	$kg\ m^{-3}$
ρ_0	Reference density of seawater	1020	$kg\ m^{-3}$
S_i	Salinity of sea ice	6	psu
S_w	Reference salinity of seawater	34.7	psu
σ	Stefan-Boltzmann Constant	$5.67\ 10^{-8}$	$W\ m^{-2}\ K^{-4}$
T_{fi}	Melting point of sea ice	273.05	K
T_{fs}	Melting point of snow	273.15	K
Ω	Earth's angular velocity	$7.2722\ 10^{-5}$	s^{-1}

Table 4.1: Numerical values of the constants and parameters used in NEMO-LIM2.

closure by partitioning the heat loss (B_l) between lateral and vertical ice growth. Only a percentage $\sqrt{1-A^2}$ of the ice formed in the leads contributes to increase the ice concentration. The remaining fraction is rather assumed to lead to an increase in the thickness of the preexisting ice.

If B_l is positive, we suppose that the entire heat gain in leads contributes to basal melting through F_w. Assuming that the ice is uniformly distributed in thickness between 0 and $2h_i$ over the ice-covered portion of the grid cell, and that the melting rate is independent of the local ice thickness, if ice ablation is larger than ice accumulation, A is reduced following:

$$\left(\frac{\partial A}{\partial t}\right)_{abl} = \frac{A}{2h_i}\left(\frac{\partial h_i}{\partial t}\right)_{abl-acc} \tag{4.12}$$

Otherwise,

$$\left(\frac{\partial A}{\partial t}\right)_{abl} = 0 \tag{4.13}$$

After determining the decrease in ice concentration, the ice thickness must be corrected accordingly so as to conserve ice volume. When the ice concentration decreases, the snow present at the surface of the removed ice is piled up onto the remaining ice. The internal temperatures of the ice cover are recomputed by a weighted formula.

4.2.2.3 Ice dynamics

For the momentum balance, the ice is considered as a two-dimensional continuum in dynamical interaction with the atmosphere and ocean. Following Thorndike (1986), the advection of momentum is neglected since inertial forces due to ice acceleration are small compared with other forces acting on the pack. Then, the momentum equation reduces to

$$m\frac{\partial \overrightarrow{u_i}}{\partial t} = -mf\overrightarrow{k} \times \overrightarrow{u_i} + \overrightarrow{\tau_{ai}} + \overrightarrow{\tau_{wi}} - mg\overrightarrow{\nabla}\xi + \overrightarrow{F} \tag{4.14}$$

where m is the mass of the snow-ice system per unit area, $\overrightarrow{u_i}$ is the sea ice velocity, t the time, f the Coriolis parameter, $\overrightarrow{k}$ the upward unit normal, $\overrightarrow{\tau_{ai}}$ and $\overrightarrow{\tau_{wi}}$ are the forces per unit area due to air and water drags, respectively, g is the acceleration due to gravity, and ξ is the sea surface dynamic height. F is the force per unit area due to variations in internal ice stress and can be written in terms of the divergence of the two-dimensional stress tensor, $\overrightarrow{F} = \overrightarrow{\nabla} \cdot \overrightarrow{\sigma}$. Following

Hibler (1979), sea ice is assumed to have a viscous-plastic constitutive law :

$$\overrightarrow{\sigma} = 2\mu\overrightarrow{\dot{\varepsilon}} + \left[(\zeta - \mu)T(\overrightarrow{\dot{\varepsilon}}) - \frac{P}{2}\right]\overrightarrow{I} \tag{4.15}$$

where ζ and μ are non-linear shear and bulk viscosities, respectively, $\overrightarrow{\dot{\varepsilon}}$ is the strain rate tensor, $T(\overrightarrow{\dot{\varepsilon}})$ is the trace of $\overrightarrow{\dot{\varepsilon}}$, P is the ice strength, and $\overrightarrow{I}$ is the two-dimensional unity tensor. The rheology used in NEMO-LIM2 allows sea ice to flow plastically for normal strain rates and to deform in a linear viscous manner for every small strain rates. In accordance with Hibler (1979), the ice strength is parameterized as

$$P = P^* A h_i e^{-C(1-A)} \tag{4.16}$$

where P^* and C are empirical constants. Note that the contribution of snow to P is ignored.

4.2.2.4 Continuity equations

Variables that are advected are the ice concentration, the snow volume per unit area, the ice volume per unit area, the snow enthalpy per unit area, the ice enthalpy per unit area and the latent heat contained in the brine reservoir per unit area. Local changes in these variables are computed from the following general conservation law:

$$\frac{\partial \psi}{\partial t} = -\overrightarrow{\nabla} \cdot (\overrightarrow{u_i}\psi) + D\nabla^2\psi + S_\psi \tag{4.17}$$

where ψ stands for any of the variables listed above, ∇ stands for the divergence and ∇^2 for the Laplacian. S_ψ is the rate of change of ψ due to thermodynamics, and D is a horizontal diffusivity to avoid nonlinear instabilities arising from the coupling between ice dynamics and transport. D is set constant inside the pack and equal to 0 at the ice edge.

4.2.3 Ice-ocean coupling

The ocean model is run with a time step of 5760 s (which converts to 96 minutes, or 15 time steps per day) and coupled bidirectionally to the sea ice model every five time steps. Hence, the sea ice model is called 3 times per day.

4.2.3.1 Exchange of momentum

Momentum exchange at the ice-ocean interface is derived from the difference between the ice velocity $\overrightarrow{u}_i$ and the surface ocean velocity $\overrightarrow{u}_w$, using a quadratic bulk formula. The ocean velocities of the uppermost grid are assumed to be surface velocities. Therefore, no turning angle is applied:

$$\overrightarrow{\tau}_{iw} = \rho_w C_{iw} |\overrightarrow{u}_i - \overrightarrow{u}_w| (\overrightarrow{u}_i - \overrightarrow{u}_w) \tag{4.18}$$

in which ρ_w and C_{iw} are the water density and the water drag coefficient.

4.2.3.2 Exchange of heat

Following McPhee (1992), the ice-ocean heat flux is assumed to be proportional to the difference between the surface temperature T_{ml} and the temperature at the freezing point T_{fw} (which in turn depends on the sea surface salinity), and the friction velocity u_{*iw} at the ice-ocean interface :

$$F_w = \rho_w c_{pw} c_h u_{*iw} (T_{ml} - T_{fw}) \tag{4.19}$$

c_{pw} stand for the specific heat of seawater and the coefficient c_h is set to 0.006 (McPhee, 1992).

4.2.3.3 Exchange of mass

The mass exchanges between ice and ocean are represented in terms of an equivalent salt flux :

$$F_{salt} = S_w \frac{\partial m_s}{\partial t} + (S_w - S_i) \frac{\partial m_i}{\partial t} \tag{4.20}$$

where S_i and S_w represent the sea ice and the seawater salinities, respectively, which are assumed to be constant. m_i and m_s stand for the ice and the snow masses per unit area, respectively. The first term of the right hand side represents the freshwater flux due to snow melting, and the second term the flux due to the formation and melting of ice.

4.2.4 Model grid

In the NEMO-LIM2 configuration, the model domain extends from 78^o S to 90^o N. The model uses a tripolar grid with 2^o zonal resolution and a meridional resolution varying from 0.5^o at the equator to 2^o $cos\varphi$ south of 20^o S (see Figure 4.1). The grid features two points of convergence in the Northern Hemisphere, both situated on continents. Maximum resolution in high latitudes is about 65 km in the Arctic and 50 km in the Antarctic. Local mesh refinements are applied to the Mediterranean, Red, Black and Caspian Seas. None of them appears to be of particular importance for the study of high latitude climate, but fine resolution is needed in order to correctly consider their local circulation and their role on the World Ocean's circulation. Partial cells (Pacanowski and Gnanadesikan, 1998) i.e., specifying the depth of the bottom cell variable and adjustable to the real depth of the ocean, induce a better representation of small topographic slopes and oceanic general circulation (Barnier *et al.*, 2006).

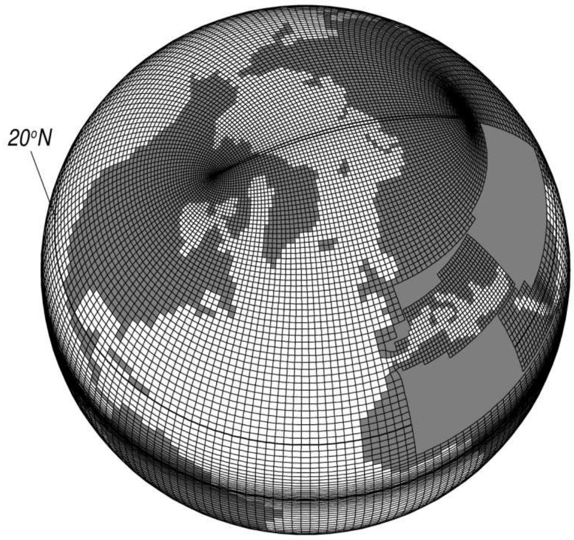

Figure 4.1: The NEMO-LIM2 model grid.

4.3 Experimental design

As already mentioned in Section 2.2, the major problem when assimilating data into large-scale sea ice models comes from our rather poor knowledge of both model and observation errors. To overcome this problem, we use the same kind of experimental design than the one described in Chapter 3. Hence, we build an idealized observational dataset with the model and perform so-called *twin experiments* (cfr. Figure 3.2). This study will focus on the Arctic region.

Firstly, a control run from 1970 to 2006 is conducted. The model is initialized using the January data from the Polar Science Center Hydrographic Climatology (PHC; Steele *et al.* (2001)). In the Arctic (Antarctic), the model is initialized with a 3 (1) m-thick and 95 (90) %-compact ice cover in regions where the sea surface temperature is below 0^oC . An initial sow cover of 0.5 (0.1) m thickness is prescribed. Daily 2-m air temperatures and 10-m winds from the National Centers for Environmental Prediction/National Center for Atmospheric Research (NCEP/NCAR) (Kalnay *et al.*, 1996) are utilized to drive the model. The other atmospheric input fields consist of climatological monthly surface relative humidities (Trenberth *et al.*, 1989), cloudiness (Berliand and Strokina, 1980) and precipitations (Large and Yeager, 2004). Reanalysis and climatologies data are interpolated from a 2^o x 2^o latitude-longitude grid to the ORCA2 grid with the 3^{rd}-order moments conserving algorithm IMOMS3 provided in the SAXO package (S. Masson and F. Pinsard, personal communication). Surface wind stress on the ice (ocean) is derived from quadratic bulk formulae assuming an atmospheric drag coefficient of $C_{ai} = 1.2 \times 10^{-3}$ ($C_{aw} = 1.2 \times 10^{-3}$). Surface fluxes of sensible and latent heat are computed using empirical parameterizations described by Goosse (1997). Evaporation/sublimation is derived from the latent heat flux. River runoff rates are prescribed using the climatological Baumgartner and Reichel (1975) dataset combined with a mean seasonal cycle derived from the Global Runoff Data Center (GRDC, 2000) data. No sea surface salinity restoring is applied. Outputs of this run are regarded as the *reality* or *true state* (i.e. as observations without any error, referred to as TS hereafter).

Secondly, the model is perturbed and new experiments are performed starting in 1984. We have chosen the year 1984 because we were seeking for a more realistic experimental design than in Chapter 3 and during the mid-80's period, NEMO-LIM2 seems to best reproduce the ice distribution and its variability.

In order to introduce errors that remain consistent with the model physics, perturbations are applied either to the model forcing or to the model initial conditions. Three types of disturbance are considered.

- For the first study, we perturb the wind forcing used in the ice motion computation within all ice-covered grid cells. A non-perturbed wind drives the thermodynamical sea ice processes as well as the atmosphere-ocean stress in ice-free grid cells. In this study, the thermodynamic component of the model is considered as perfect and the dynamic component as a

	Thermodynamical perturbation	Dynamical perturbation	Initial conditions perturbation
Without data assimilation	N_WA_T	N_WA_D	N_WA_IC
Assimilation of ice velocity data	N_VA_T_XX	N_VA_D_XX	N_VA_IC_XX
Assimilation of ice concentration data	N_CA_T_YY	N_CA_D_YY	N_CA_IC_YY
Assimilation of ice velocity and concentration data	N_VCA_T_XX_YY	N_VCA_D_XX_YY	N_VCA_IC_XX_YY

Table 4.2: Acronyms of the twin experiments performed with NEMO-LIM2. XX and YY represent the values of the weight for ice velocity and concentration assimilation, respectively.

direct source of errors. In opposition to Chapter 3 where the wind forcing was replaced by some other year wind forcing, a time- and space-coherent pseudo-random noise is here added to the wind forcing. The perturbation is chosen to be biasless in order to avoid the insertion of a bias in the model simulations (for more details, see Section 4.4).

- In the second study, a coherent pseudo-random noise (cfr. Section 4.4) is added to the air temperature forcing in all ice-covered grid cells. This time, the dynamic component of the model is regarded as perfect and the thermodynamic component as a direct source of errors.
- Finally, we start the ice model with initial conditions from another year.

Sea ice concentration and/or velocity datasets compiled from the TS simulation are assimilated into NEMO-LIM2; the effect on the model behavior is assessed for the different model perturbations. Table 4.2 summarizes the various types of experiment carried out.

4.4 Pseudo-random noise generation

As mentioned above, we need to perturb the model in order to run twin experiments and to assess how data assimilation may improve the model ice estimation (cfr. Section 4.3). One way of doing this is by adding scalar noises to the wind and air temperature forcings. First, we have tested a basic pseudo-random noise added to the wind forcings but it strongly affected the ice transport, leading to model instabilities. Moreover, a basic pseudo-random noise added to the air temperature forcing demanded a large amplitude to actually affect the thermodynamical processes, also sometimes leading to model instabilities. To avoid this, we used noises which are coherent in space and time.

One method to generate such noises is based on the Perlin Noise Function, which is commonly used to increase the impression of realism in computer graphics (Ebert *et al.*, 1998). As seen in Equation 4.21, the Perlin Noise Function ($Perlin(\overrightarrow{x})$) is simply defined as the sum of N pseudo-random noise functions ($noise^i(\overrightarrow{x})$) at a range of different amplitudes and frequencies. In our study, $\overrightarrow{x}$ is a 3-D vector which is space- and time- dependent.

$$Perlin(\overrightarrow{x}) = \sum_{i=0}^{N-1} noise^i(\overrightarrow{x}) \tag{4.21}$$

We illustrate this methodology with a simple 1-D example. To begin, pseudo-random noise needs to be created. Let's say that we generate a pseudo-random noise with dimension A (Figure 4.2). For simplicity, we will assume a model grid of dimensions $[1 \times B]$. We then stretch the pseudo-random noise matrix to fit the model grid dimensions. Finally, values are interpolated. The ratio between A and B dimensions determines the frequency (i.e. the inverse of the distance between random values) of the resulting noise. Indeed, for $A << B$, the obtained noise is smooth, and for $A \simeq B$, the noise becomes more disruptive. To illustrate this, Figures 4.3a, b and c present three noise functions with different frequencies. These functions are also weighted to give a larger amplitude to lower frequency noises. The sum of those three functions is shown in Figure 4.3d. Hence, this method ensures a resulting noise which has large, medium and small variations with temporal coherence. In our case, we generalise this method to three dimensions. We generate pseudorandom functions $random^i(\overrightarrow{y^i})$ which vary in space and time. We then apply the corresponding $\mathbf{H}^i$ operator to them (see Equation 4.22). As given by Equation 4.23, $\mathbf{H}^i$ is composed of 4 different operators. The first one, called $\mathbf{S}^i_S$, spatially stretches $random^i(\overrightarrow{y^i})$ on the model grid. The second one, $\mathbf{S}^i_I$, interpolates the ensued vector in space. Finally, $\mathbf{T}^i_S$ and $\mathbf{T}^i_I$ respectively stretch and interpolate the resulting vector in time:

$$noise^i(\overrightarrow{x}) = t^i s^i \mathbf{H}^i(random^i(\overrightarrow{y^i})) \tag{4.22}$$

$$\mathbf{H}^i = \mathbf{T}^i_I \mathbf{T}^i_S \mathbf{S}^i_I \mathbf{S}^i_S \tag{4.23}$$

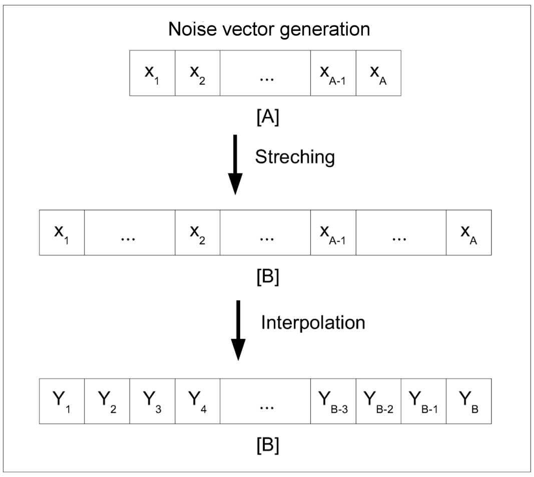

Figure 4.2: 1-D illustration of the methodology to generate pseudo-random noises at a range of different frequencies. A vector is first generated and then stretched to fit the model dimension. Finally, vector values are interpolated.

where t^i and s^i are values to weight the amplitude of the pseudo-random noise functions according to their temporal and the spatial noise frequencies, respectively. Once those pseudo-random noise functions are generated, they are summed according to Equation 4.21.

The noises added to the wind and air temperature forcings hold temporal frequencies of 2, 4, 6, 8 and 10 days and space frequencies of 2, 4, 6, 8 and 10 grid cells. The root mean square of the wind (air temperature) perturbation is about $3\ m/s$ ($1.5\ K$), meaning that 68% of the noise values remain within the interval $[-3\ m/s, 3\ m/s]$ ($[-1.5\ K, 1.5\ K]$) and 95% of the values within $[-6\ m/s, 6\ m/s]$ ($[-3\ K, 3\ K]$). Air temperature and wind perturbations are displayed on Figures 4.4 and 4.5 for the 1^{st} of January 1984.

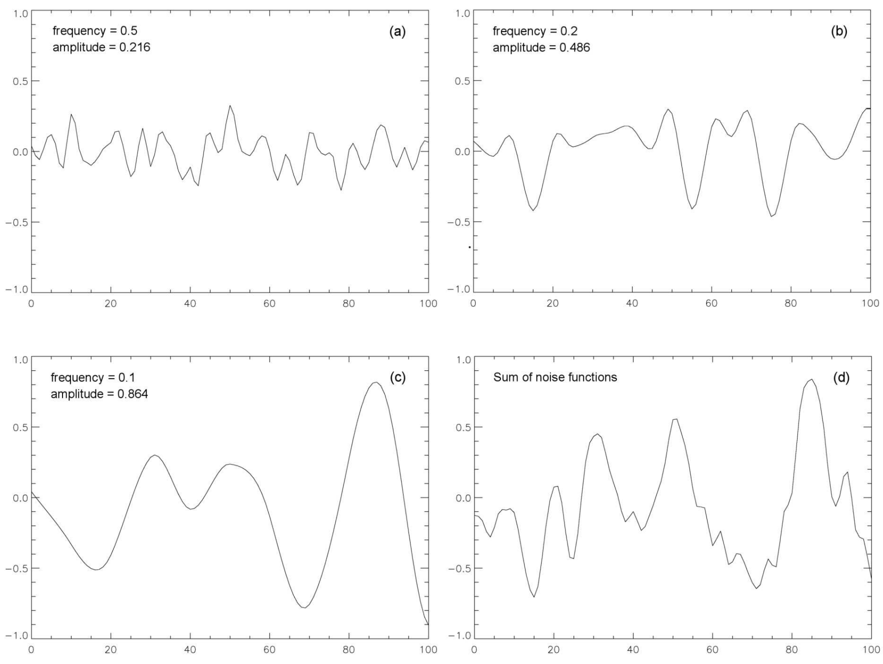

Figure 4.3: Panels a, b and c show pseudo-random noise functions with different frequencies and amplitudes. Panel d shows the sum of the 3 pseudo-random noise functions presented in Panels a, b and c. It is called the Perlin Noise Function. The amplitude (y-axis) is half the difference between the minimum and maximum values the noise could have here. The frequency is the inverse of the distance between random values defined along the dimension of the noise function (x-axis).

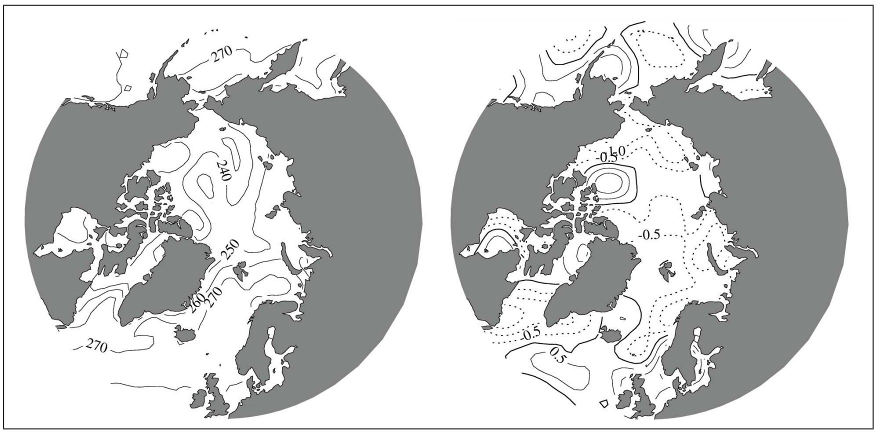

Figure 4.4: Surface air temperature forcing (left) and its corresponding noise (right) on the 1st of January 1984. Units are K. Contour intervals are 10 K for the air temperature forcing and 0.5 K for its corresponding noise.

4.5 Assimilation scheme

The assimilation scheme which is implemented in NEMO-LIM2 is based on the scheme implemented in the toy model (cfr. Section 3.4). Nevertheless, due to the larger degree of complexity of LIM2 and to coupling to an ocean model, additional attention is paid to the heat and mass conservations as well as to heat and mass exchanges between ice and ocean.

At each time step, an optimal interpolation scheme is used to assimilate ice concentration and ice velocity data into the model according to :

$$A_{ass} = A + k_A(A_{obs} - A) \tag{4.24}$$

$$\overrightarrow{u}_{ass} = \overrightarrow{u} + k_u(\overrightarrow{u}_{obs} - \overrightarrow{u}) \tag{4.25}$$

where the subscripts *ass* and *obs* stand for assimilated and observed data. While the ice velocity is updated at the end of the model velocity computation (before ice transport), the ice concentration update is done at the end of the model time step. k_A and k_u are the *weights* or *gains* for ice concentration and ice velocity data assimilation, respectively, and are usually determined through a least-squares minimization of the error variance of the assimilated value compared to a statistical true value (Meier *et al.*, 2000; Lindsay and Zhang, 2006). However, the present experimental design provides one observation per model grid cell with zero error. The weight should then be set to one, and TS data would directly be inserted into the model. Yet, analysis of the toy model results showed that a

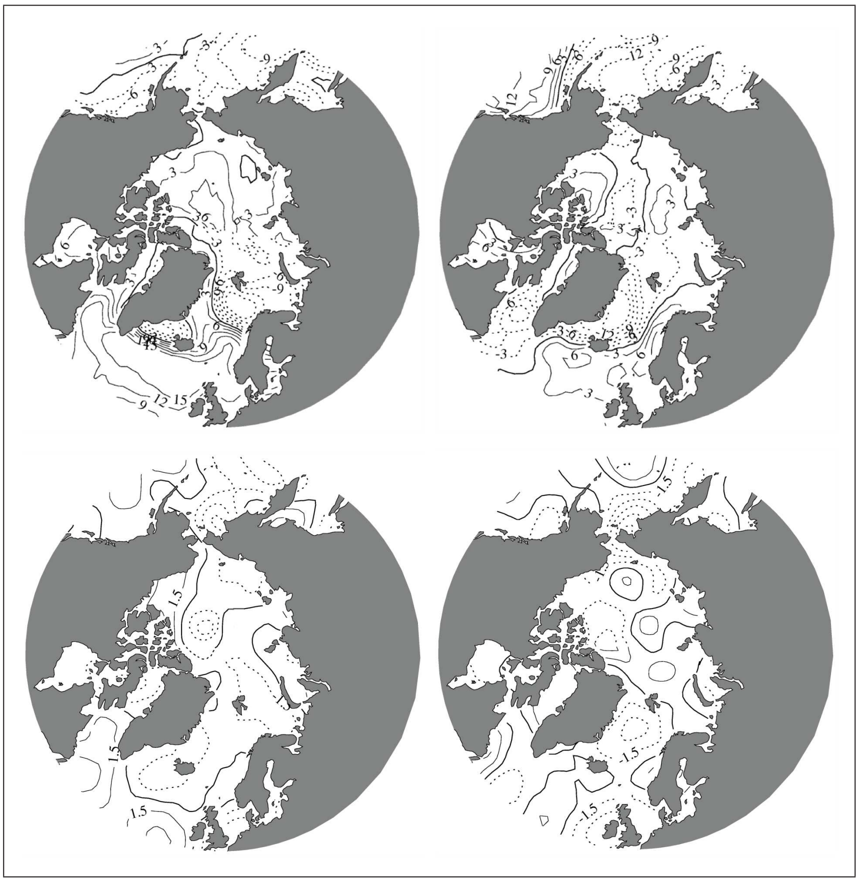

Figure 4.5: U- and V-components of the wind forcing (top right and left, respectively) and the corresponding noises (bottom) on the 1st of January 1984. Units are m/s and contour intervals are 3 m/s for the wind forcing and and 1.5 m/s for its corresponding noise.

weight equal to 1 does actually improve the assimilated variable but not systematically the other sea ice variables. In order to get the best results for the global sea ice state, k_A should then be lower than 0.15 value. Therefore, we here run experiments with $k_A = 0.1$. Note that, as mentioned in Section 3.4, our data assimilation scheme is not exactly an optimal interpolation scheme since we do not define the weights from statistical computations. In this study, we rather choose the weights on a physical basis in order to take into account the interactions between the different sea ice variables and to improve the global sea ice state. Nevertheless, for simplicity, we will still call this data assimilation scheme an *optimal interpolation* scheme.

Following the toy model data assimilation scheme, where the TS estimates zero ice cover, the scheme linearly interpolates the TS velocities of the 9 contingous grid cells with an inverse distance weighting function and assimilates the results into the model. This procedure avoids discontinuities in the assimilated velocity field at the edge between areas where ice velocity observations exist and areas where they don't (for more details, see Section 3.4). When the model estimates no ice where TS does, concentration data assimilation brings an ice block of thickness h_o = 0.3 *m* into the grid cell. If the temperature of the oceanic surface layer is equal to the freezing point, the ice remains. Otherwise, the ice block melts. Sometimes, ice melt provides enough energy loss to cool the ocean temperature to its freezing point so that some ice remains.

The data assimilation scheme conserves the snow volume and the heat contained in brine pockets. When the assimilation of concentration creates (melts) ice, we assume that no salt (freshwater) is rejected towards the ocean and that the temperature of the added (removed) ice block is the same as the one of the pre-existing ice. Such assumptions make the assimilation scheme fairly simple. Also, each of these assumptions is put to the test in Chapter 5.

This kind of assimilation technique already showed great ability in underlying a number of problems posed by the assimilation of ice concentration and/or velocity data in the previous chapter. In consequence, we assume this technique fully suitable to study the impact of assimilating data on the NEMO-LIM2 performance.

4.6 Results

4.6.1 Control run

Results of the control run which are detailed here are in general agreement with the ORCA2-LIM results described by Timmermann *et al.* (2005).

4.6.1.1 Sea ice extent

The average seasonal cycle of the ice extent simulated by the model is presented in Figure 4.6. It is in excellent agreement with observations derived from satellite passive microwave measurements except during the melt season. Compared to data, the summer minimum is delayed by about 2 weeks and its value is overestimated by about 28%. For some reasons which remain unclear, the simulated sea ice pack is generally too concentrated during the summertime, leading to too little ice melt.

Time series of the simulated sea ice extent (i.e. the area with ice concentrations greater than 15%) and volume are displayed in Figure 4.7. A pronounced interannual variability is visible. Over the 1979-2004 period, we find linear trends of $-15\ 730\ km^2yr^{-1}$ in the modeled sea ice extent and of $-38\ 830\ km^2yr^{-1}$ in the observations (Comiso, 1999). The model misses a significant part of the decreasing trend due to its underestimation of the summer melt. Indeed, the summer season encompasses for the strongest trend compared to other seasons (Walsh and Chapman, 2001). As shown in Figure 4.7b, the modeled ice volume is minimum in the early 80's due to too warm an air temperature forcing in years 1980 to 1981 (Tartinville *et al.*, 2001). We find a linear trend of $-180\ km^3yr^{-1}$ over the integration period, and of about $-8000\ km^3yr^{-1}$ over the last 4 years of integration.

Time series of monthly anomalies of ice extent (i.e. differences of monthly means from the average seasonal cycle; Figure 4.8) indicate that the model captures only part of the ice extent variability. Fluctuations of the Arctic ice extent occurring on time scales of a few months are at times inacurrately reproduced, sometimes not even with the correct sign. However, anomalies occurring on time scales from

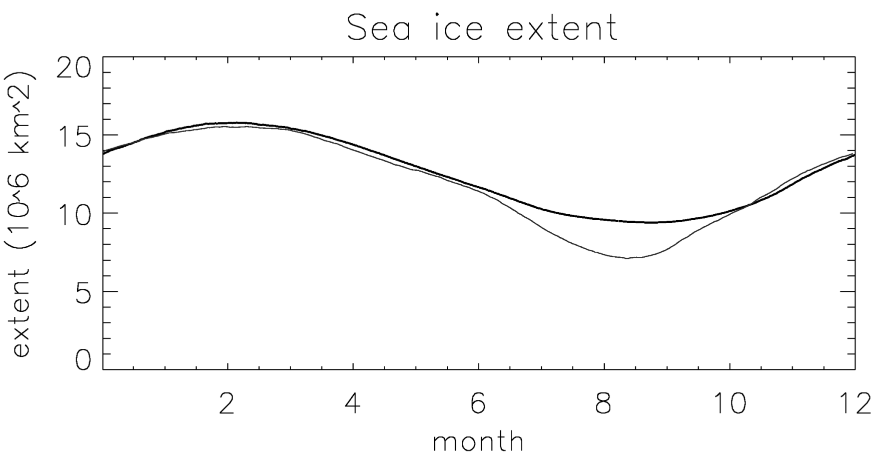

Figure 4.6: Average seasonal cycle of the Arctic sea ice extent ($10^6 km^2$) as simulated by NEMO-LIM2 (thick) and as derived from passive microwave measurements (thin; Comiso (1999)).

several months to one or two years, e.g. the increased ice extent in 1982-1983 or the negative trend in ice extent over the period 1993-1996, are correctly captured by the model. The correlation coefficient between the simulated and observed anomaly time series is 0.46.

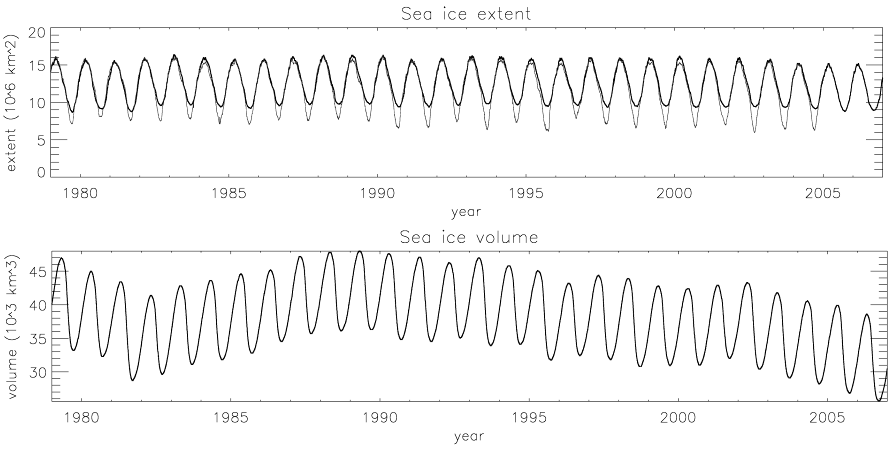

Figure 4.7: Time series of the Arctic sea ice extent (top) and volume (bottom) in the NEMO-LIM2 reference simulation (thick). The observed time series of ice extent (thin) is derived from the dataset of Comiso (1999). Units are given in $10^6 km^2$ and $10^3 km^3$, respectively.

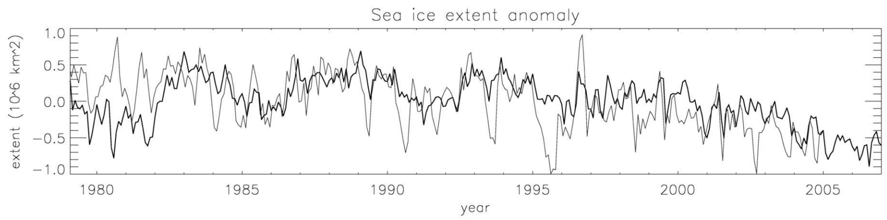

Figure 4.8: Time serie of monthly anomalies (i.e. differences of individual monthly means from the mean seasonal cycle) of sea ice extent ($10^6 km^2$) for the Arctic in the NEMO-LIM2 reference simulation (thick) and in observations (thin) derived from satellite passive microwave recordings (Comiso, 1999).

A comparison of the simulated averaged March sea ice concentrations in the Arctic (Figure 4.9) with observations derived from passive microwave data using the Bootstrap algorithm (Comiso, 1999) reveals a slight overestimation of sea ice extent in the Barents and Greenland Seas. Also, the model does not reproduce the Odden Ice Tongue visible in the remote sensing data. Furthermore, it overestimates the width of the ice stream along the east coast of Greenland and in the Denmark Strait, which leads to a spurious blocking of ice drift by the Iceland

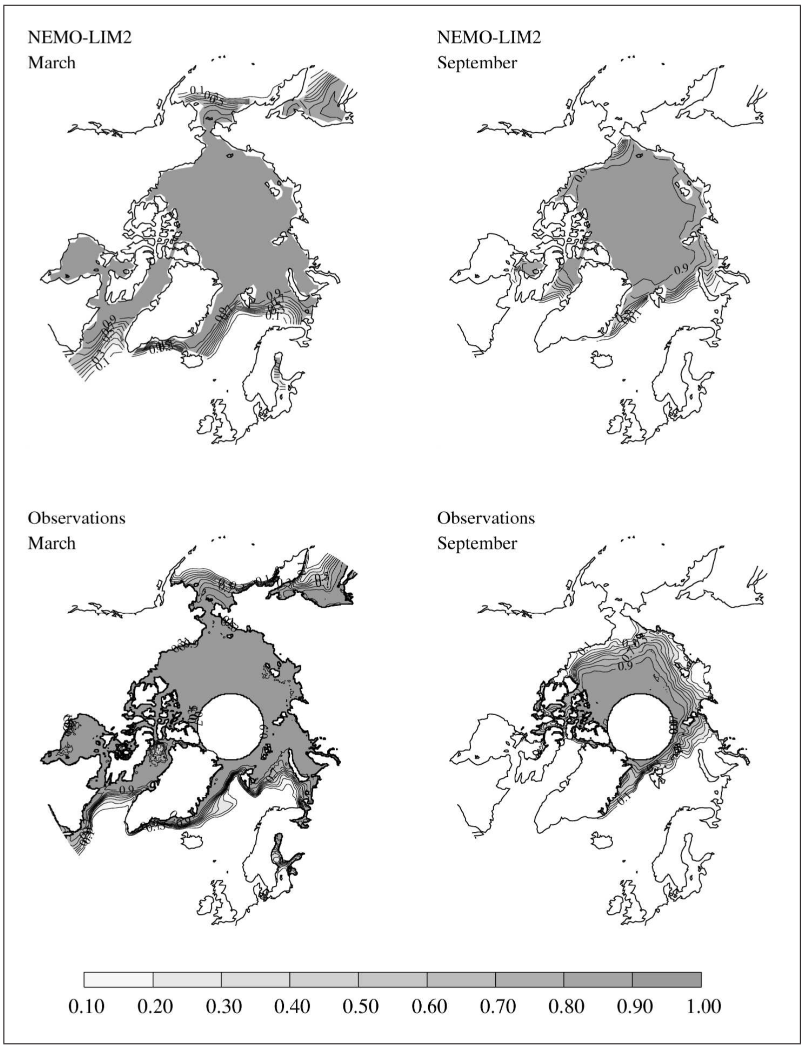

Figure 4.9: Simulated (top) and observed (bottom) March (left) and September (right) mean ice concentrations in the Arctic Ocean. Contour interval is 10%. Observed fields are derived from the dataset of Comiso (1999). The averaging period is 1979-2004 and was determined by the observations availability.

coast. Timmermann *et al.* (2005) attributes these deficiencies to the relatively coarse model resolution. In the model, the Denmark Strait is resolved by only three grid cells which clearly is not enough to capture a narrow ice stream. In summer, the model significantly overestimates the sea ice extent in the Kara Sea and in Baffin Bay. We also note that the percentage of open water over the Alaskan and Russian continental shelves is significantly underestimated.

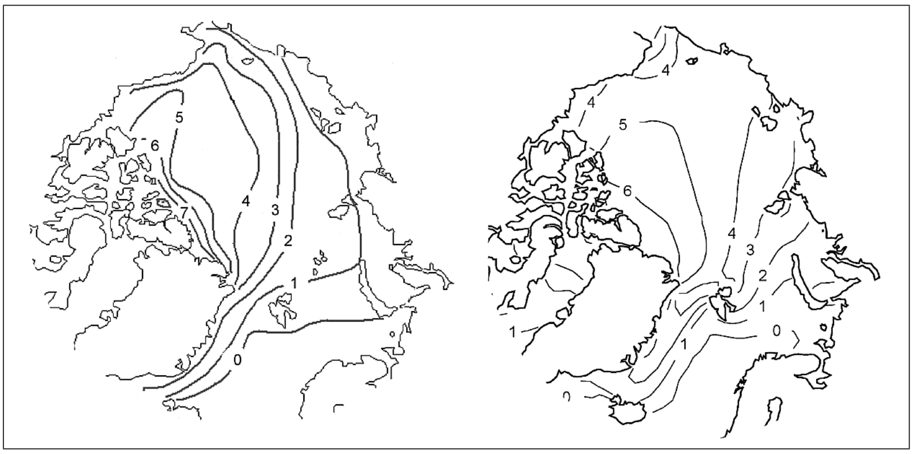

Figure 4.10: 1979-2006 mean winter ice thicknesses observed (left, Bourke and Garrett (1987)) and simulated by NEMO-LIM2 (right).

4.6.1.2 Sea ice thickness

As shown in Figure 4.10, the simulated sea ice thickness in the Arctic exhibits an ice thickness gradient from about 2-3 *m* over the western Siberian shelf Sea to 4-5 *m* at the North Pole and more than 6 *m* off the Canadian Archipelago. Figure 4.10 also shows a good agreement in the large-scale ice thickness distributions between the modeled data and data derived from measurements made by upward-looking sonars mounted on submarines (Bourke and Garrett, 1987; Bourke and McLaren, 1992). However, the model appears to overestimate ice thickness on the Siberian shelf by about 2 *m*. Also, the overestimation of ice extent in the Barents Sea (see previous section) is naturally connected to an overestimated ice thickness in this region. Finally, the spurious blocking of ice by Iceland coast causes an artificially too thick ice in that area.

4.6.1.3 Sea ice drift

The large-scale sea ice drift (Figure 4.11) reflects the general patterns of atmospheric and oceanic circulations. The ice drift field averaged over the 1979-2006 period features the Beaufort Gyre, the Transpolar Drift, and the ice export through Fram Strait. Velocities of about 1-2 *cm/s* in the Beaufort Gyre, 3-4 *cm/s* in the Transpolar Drift and about 10 *cm/s* in Fram Strait correspond well

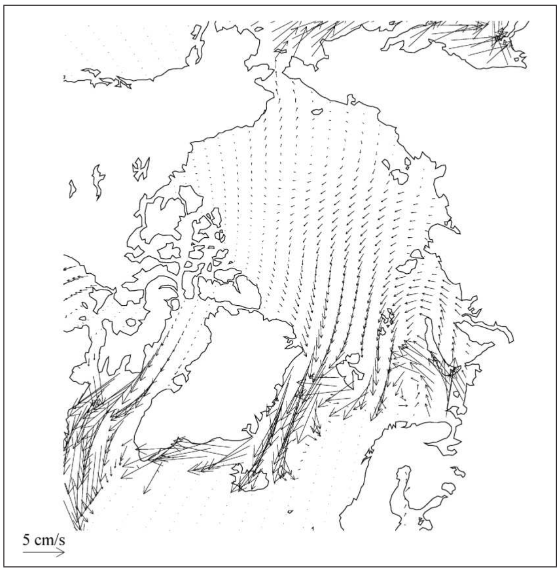

Figure 4.11: Simulated winter ice velocities in the Arctic (March) averaged over the 1979-2006 period.

with the mean ice motion derived from 85.5 *GHz* SSM/I data (Emery *et al.*, 1997).

4.6.1.4 conclusion

Although NEMO-LIM2 encounters some difficulties in representing the summer melt, the above discussion demonstrates good agreement between the model results and observations. The model features many aspects of the seasonal behavior of the Arctic sea ice cover and is therefore reliable to study the impact of the assimilation of ice concentration and/or velocity data. Owing to the best model ice estimation during the middle to late 80's, we will focus our twin experiments analysis on year 1984.

4.6.2 Thermodynamical perturbation

4.6.2.1 Velocity data assimilation

In this section, we assess the impact of the assimilation of ice velocities from the TS on the model performance when the model is thermodynamically perturbed (for detail, see Section 4.3). Several values of k_u have been tested. In Tables 4.3 and 4.4, we compare the area-averaged, annual mean results obtained without and with assimilation for the year 1984 to the TS.

According to Tables 4.3 and as expected, the larger k_u, the better the ice velocity estimation. However, Table 4.4 shows no significant improvement of the ice thicknesses and concentrations when velocity data are assimilated. Area-averaged, annual mean ice concentration and thickness biases as well as their error standard deviations are generally larger compared to the case with no assimilation. In fact, when a thermodynamical perturbation is applied to the model, thermodynamics seek an anomalous extreme in ice thickness. The model ice dy-

	Correlation		**Bias** ($10^{-4} m/s$)		**Error std** ($10^{-4} m/s$)	
	U	V	U	V	U	V
N_WA_T	0.998	0.998	-0.42	0.63	21.07	22.56
N_VA_T_0.3	0.999	0.999	-0.41	0.52	14.00	14.90
N_VA_T_0.5	1.000	1.000	-0.36	0.43	10.16	10.70
N_VA_T_0.9	1.000	1.000	-0.10	0.14	2.43	2.41
N_VA_T_1.0	1.000	1.000	0.00	0.00	0.00	0.00
N_CA_T_0.1(1)	0.999	0.999	-0.39	0.42	13.27	14.14
N_CA_T_0.1(2)	1.000	1.000	-0.19	0.36	9.95	10.63
N_CA_T_1.0(2)	1.000	1.000	-0.14	0.24	9.19	9.71
N_VCA_T_0.3_0.1(2)	1.000	1.000	-0.15	0.22	6.73	7.05
N_VCA_T_1.0_1.0(2)	1.000	1.000	0.00	0.00	0.00	0.00

Table 4.3: Area-averaged, 1984 annual mean correlations between the ice velocity components from experiments N_WA_T, N_VA_T_XX, N_CA_T_YY(y) and N_VCA_T_XX_YY(y) and the TS, and area-averaged, 1984 annual mean errors in the ice velocity components and standard deviations of these errors. y stands for concentration data assimilation scheme where either the ice volume (1) or ice thickness (2) is conserved. For the acronym definition, see Table 4.2.

	Correlation		Bias		Error std	
	h_i	A_i	h_i ($10^{-2}m$)	A_i (10^{-3})	h_i ($10^{-2}m$)	A_i (10^{-3})
N_WA_T	1.000	1.000	-2.14	-3.03	5.04	17.10
N_VA_T_0.3	1.000	1.000	-2.16	-2.98	5.48	16.82
N_VA_T_0.5	1.000	1.000	-2.19	-3.03	5.61	16.86
N_VA_T_0.9	1.000	1.000	-2.30	-3.24	6.17	17.41
N_VA_T_1.0	1.000	1.000	-2.23	-3.35	6.50	17.94
N_CA_T_0.1(1)	1.000	1.000	-2.20	-0.18	6.07	5.44
N_CA_T_0.1(2)	1.000	1.000	-1.39	-0.02	4.54	3.76
N_CA_T_1.0(2)	1.000	1.000	-1.25	0.00	4.47	0.00
N_VCA_T_0.3_0.1(2)	1.000	1.000	-1.45	-0.02	4.63	3.73
N_VCA_T_1.0_1.0(2)	1.000	1.000	-1.55	-0.02	4.80	3.69

Table 4.4: Area-averaged, 1984 annual mean correlations between the ice thickness and concentration from experiments N_WA_T, N_VA_T_XX, N_CA_T_YY(y) and N_VCA_T_XX_YY(y) and the TS, and area-averaged, 1984 annual mean errors in the ice thickness and concentration and standard deviations of these errors. y stands for concentration data assimilation scheme where either the ice volume (1) or ice thickness (2) is conserved. For the acronym definition, see Table 4.2.

namics act to reduce this anomaly, but data assimilation defeats this process. For instance, if the air temperature is too high, the excessive ice melt will affect the ice concentration and thickness and in turn, the ice velocity. Owing to this change in the ice geographical distribution, there is no evidence that restoring the modeled ice velocity towards the TS will correct the estimated ice distribution compared to the case with no assimilation. These results are consistent with the findings from the toy model (Section 3.5.2.1).

It is worth stressing that the NEMO-LIM2 results which are presented in Table 4.4 show no ice thinning nor concentration increase contrary to what was observed in the toy model results when velocity data were assimilated (see Section 3.5.2.1). We attribute this to the NEMO-LIM2 ice dynamics being smoother and more complex than the toy model ones. This result is important and will be further discussed in Section 4.6.3.1.

4.6.2.2 Concentration data assimilation

In this section, the perturbation which is applied to NEMO-LIM2 is thermodynamical and ice concentration data are assimilated.

As already discussed in Section 3.5.2.2, the ice concentration is tightly linked to the ice thickness and volume. When the ice concentration varies due to assimilation, one may either conserve ice volume or ice thickness. On one side, the toy model results exhibit an amplification of the ice thickness errors mainly around the ice edge when ice volume is conserved. This feature is also present with NEMO-LIM2. Indeed, even if concentration data assimilation decreases the averaged bias and error standard deviation of ice concentration compared to the TS (see N_CA_T_0.1(1) in Table 4.4), it also fails to improve the thickness and velocity estimations (cfr. Tables 4.4 and 4.3). On the other hand, experiments carried out with the toy model have shown that it is difficult to improve the model behavior when ice thickness is conserved and when large indirect dynamical errors are lasting for several days. This motivated us to implement an assimilation scheme which is a compromise between imposing the conservation of either ice volume or ice thickness. However, thanks to the better ice dynamics, NEMO-LIM2 does not reach situations where the dynamics would only permit the ice to move out of the grid cell (like due to the Kreyscher correction in the toy model). Therefore, the data assimilation scheme which conserves the ice thickness by adding or removing an ice block in the grid cell does not turn this grid cell into an important source of sea ice like in the toy model. Hence, we choose the ice thickness conservation scheme over the one that conserves the ice volume, and the compromise one.

Another important difference between NEMO-LIM2 and the toy model results is that, in opposition to the toy model, NEMO-LIM2 was found to be stable enough to handle k_A above $0.15 - 0.3$ values. The larger k_A, the better the improvement of the estimated ice concentration (Tables 4.3 and 4.4). However, improvements for experiments with $k_A = 0.1$ and $k_A = 1.0$ are very similar. This can be explained by the fairly slow variation in ice concentration (time scale of variation is about 10 days) compared to the frequency of data assimilation (namely 3 times a day, i.e. every time step). Hence, a light nudging of the modeled ice concentrations toward the observed ones is sufficient to significantly improve the global modeled ice estimation.

4.6.2.3 Concentration and velocity data assimilation

Simultaneous assimilation of ice velocities and concentrations from the TS can further improve the model performance. In Tables 4.3 and 4.4, we compare the annual mean results obtained without and with assimilation for the year 1984 to the TS for several sets of weights. For k_u = 0.3 and k_A = 0.1, the correlations between the estimated ice velocities, concentrations and thicknesses, and the TS ones are all at least similar, or larger in comparison to the respective correlations for the experiments where concentrations or velocities are separately assimilated (namely for N_CA_T_0.1(2) and N_VA_T_0.3 experiments). In the same way, the mean standard deviations of the errors in ice velocity, concentration and thickness are markedly reduced. Nevertheless, the simultaneous assimilation of velocities and concentrations slightly deteriorates the mean ice thickness compared to the case where concentrations alone are assimilated. The reason for this has already been explained in Section 4.6.2.1.

With larger gains, k_u and k_A, (see N_VCA_T_1.0_1.0(2) in Tables 4.3 and 4.4), the global ice estimation is further improved albeit the ice thicknesses are slightly deteriorated in comparison with N_VCA_T_0.3_0.1(2) ones. As described above, a larger k_A further improves the general model estimation, while a larger k_u further improves the ice velocity estimations but also slightly deteriorates the ice thickness and concentration estimations.

In summary, for a thermodynamical perturbation, the NEMO-LIM2 results are in good agreement with the toy model ones. Moreover, the present results are significantly better than the toy model ones, mostly due to the more complex and smoother ice dynamics included in the NEMO-LIM2 model. Furthermore, large gains are very usefull to improve the estimate of the variable which is assimilated into the model but this is sometimes on the detriment of other sea ice variables which require smaller gains. Also the assimilation gains (k_u and k_A) should be chosen with attention, regarding the prior improvements. Finally, the concentration data assimilation scheme should impose the ice thickness conservation.

4.6.3 Dynamical perturbation

4.6.3.1 Velocity data assimilation

In this section, the model is dynamically perturbed and ice velocities from the TS are assimilated in the NEMO-LIM2 model. Comparisons of the annual mean results obtained without and with assimilation for year 1984 to the TS are presented in Tables 4.5 and 4.6. Several values of k_u have been tested.

	Correlation		**Bias** ($10^{-4} m/s$)		**Error std** ($10^{-4} m/s$)	
	U	V	U	V	U	V
N_WA_D	0.903	0.908	2.03	-9.35	202.31	232.33
N_VA_D_0.3	0.957	0.959	2.30	-5.51	127.13	146.46
N_VA_D_0.5	0.979	0.980	1.89	-3.38	86.38	99.50
N_VA_D_0.9	0.999	0.999	0.46	-0.50	15.91	18.11
N_CA_D_0.1(1)	0.914	0.916	-0.15	-7.86	194.76	225.35
N_CA_D_0.1(2)	0.920	0.922	0.12	-9.79	186.40	217.13
N_VCA_D_0.9_0.1(2)	0.999	0.999	0.46	-0.51	15.90	18.05

Table 4.5: Area-averaged, 1984 annual mean correlations between the ice velocity components from experiments N_WA_D, N_VA_D_XX, N_CA_D_YY(y) and N_VCA_D_XX_YY(y) and the TS, and area-averaged, 1984 annual mean errors in the ice velocity components and standard deviations of these errors. y stands for concentration data assimilation scheme where either the ice volume (1) or ice thickness (2) is conserved. For the acronym definition, see Table 4.2.

Table 4.5 reveals a significant and expected improvement of the ice velocity estimations when TS velocities are assimilated into NEMO-LIM2. Furthermore, as seen in Table 4.6, velocity data assimilation also generally improves the ice thickness and concentration estimates. The larger the gain k_u, the larger the

	Correlation		Bias		Error std	
	h_i	A_i	h_i ($10^{-2}m$)	A_i (10^{-3})	h_i ($10^{-2}m$)	A_i (10^{-3})
N_WA_D	0.997	0.996	0.78	-1.89	21.22	56.98
N_VA_D_0.3	0.999	0.998	0.71	-0.20	14.35	42.59
N_VA_D_0.5	0.999	0.999	0.56	0.44	10.56	33.15
N_VA_D_0.9	1.000	1.000	0.09	0.64	2.62	10.24
N_CA_D_0.1(1)	0.992	1.000	-0.77	-0.51	36.73	17.26
N_CA_D_0.1(2)	0.998	1.000	5.39	-0.24	16.98	14.57
N_VCA_D_0.9_0.1(2)	1.000	1.000	0.26	0.03	1.56	1.70

Table 4.6: Area-averaged, 1984 annual mean correlations between the ice thicknesses and concentrations from experiments N_WA_D, N_VA_D_XX, N_CA_D_YY(y) and N_VCA_D_XX_YY(y) and the TS, and area-averaged, 1984 annual mean errors in the ice thickness and concentration and standard deviations of these errors. y stands for concentration data assimilation scheme where either the ice volume (1) or ice thickness (2) is conserved. For the acronym definition, see Table 4.2.

improvements. This is true for all statistical quantities of Tables 4.5 and 4.6, except the area-averaged annual concentration biases. Actually, these mean biases are not very representative of ice concentration errors. As displayed in Figure 4.12, the area-averaged monthly concentration biases point clearly towards significant concentration improvements as k_u increases. In summary, assimilating velocities into NEMO-LIM2 is a very suitable way to improve the simulation of the characteristics when the model is dynamically perturbed.

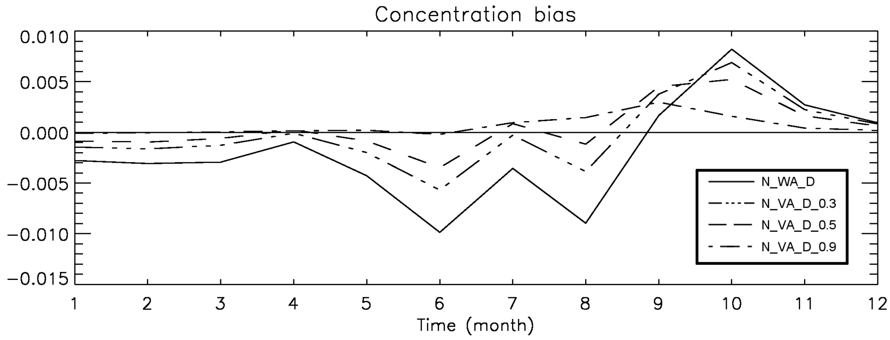

Figure 4.12: Area-averaged, 1984 monthly mean concentration biases between N_WA_D, N_VA_D_0.3, N_VA_D_0.5 and N_VA_D_0.9 experiments and the TS.

Moreover, in contrast to the toy model results (see Chapter 3), the NEMO-LIM2 results presented in Table 4.6 show no ice thinning nor concentration increase. We attribute this to the different model dynamics. Indeed, the toy model dynamics includes a threshold correction, namely the Kreyscher *et al.* (2000) correction, which leads to too disruptive an ice velocity field. When velocities are assimilated into the model, the velocity field is smoothed and the ice transport is lowered leading to ice thinning and concentration increase. In opposition, NEMO-LIM2 avoids such processes thanks to its more complex and smoother ice dynamics. This is seen in Figure 4.13 which displays the difference (in absolute value) in the ice thickness changes due to advection processes between the experiment without data assimilation (left) and the experiment with velocity data assimilation for $k_u = 0.5$ (right), and the TS during January 1984. Darker (lighter) areas show regions where less (more) ice is ridged in the perturbed model experiment than in the TS. In contrast to the toy model results (Figure 3.11), the two patterns are now similar, demonstrating no significant lowering in the amount of ice growth due to dynamical processes. This feature really stresses the importance of using appropriate dynamics, i.e. those that avoid thresholds.

One additional reason for the ice thinning and concentration increase when velocities were assimilated into the toy model could have been the use of too strong model perturbations (cfr. Chapter 3). Hence, a couple of one-year experiments have been carried out with NEMO-LIM2 using the same experimental configuration as for the toy model. Year 1995 of the control experiment was taken as TS, and the NEMO-LIM2 dynamical component was directly perturbed by using the wind forcing of year 1992 instead of year 1995. Area-averaged 1995, monthly mean ice thickness and concentration biases are presented in Figure 4.14. As can be seen from this figure, velocity data assimilation again does not cause ice thinning nor concentration increase compared to the no-assimilation case. Therefore, the problems encountered with the toy model may not be attributed, even partly, to the fairly strong model perturbations.

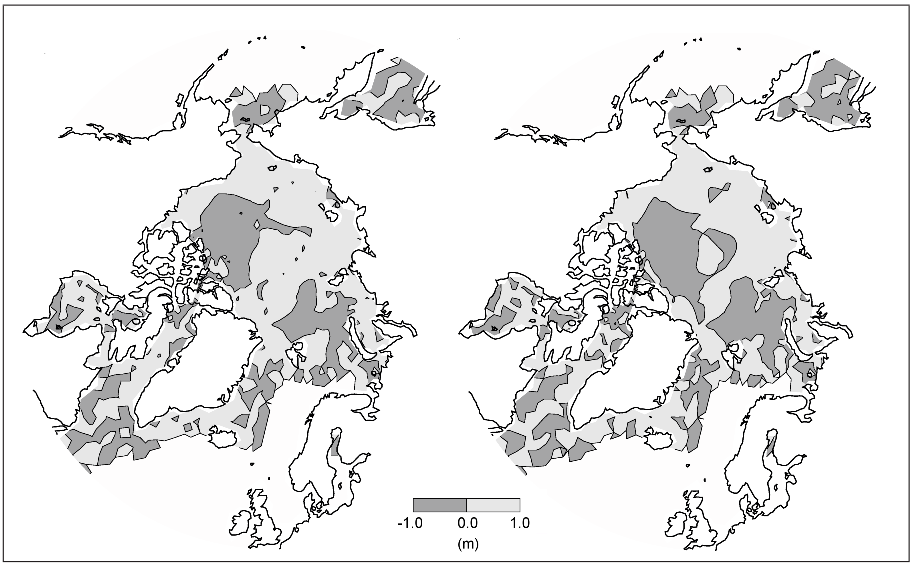

Figure 4.13: Differences (in absolute value) in the ice thickness growth through advection between the experiment without data assimilation (N_WA_D) and the control experiment (left) and between the experiment with data assimilation (N_VA_D_0.5) and the control experiment (right). Values are averaged over January 1984.

4.6.3.2 Concentration data assimilation

The perturbation is here dynamical and sea ice concentrations from the TS are assimilated into NEMO-LIM2. Tables 4.5 and 4.6 present area-averaged, yearly statistical quantities of ice velocity, thickness and concentration compared to TS.

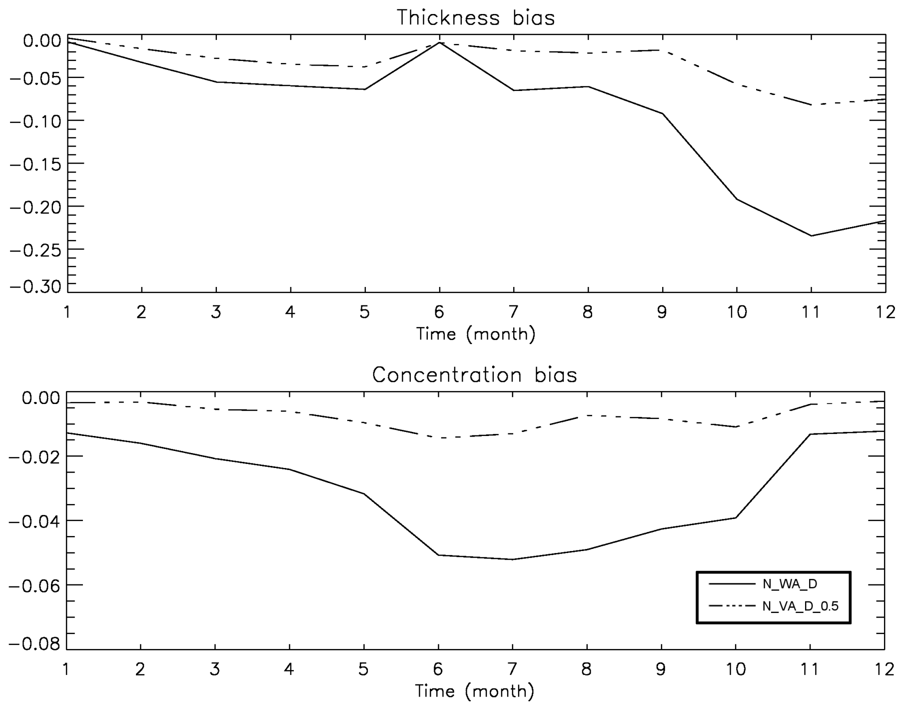

Figure 4.14: Area-averaged 1995 monthly mean ice thickness (top) and concentration (bottom) biases between N_WA_D and N_VA_D_0.5 experiments and the TS.

For the first case study, the ice volume is conserved after concentration data are assimilated into NEMO-LIM2 (N_CA_D_0.1(1) experiment). From Tables 4.5 and 4.6, it can be seen that the concentration and velocity data are better correlated to the TS with concentration data assimilation than without. Also, mean concentration and velocity errors compared to TS and their respective standard deviations are all reduced. However, the mean ice thickness errors compared to the TS and their standard deviation feature an overall deterioration. In fact, where the model dynamical perturbation modifies the ice pattern, the next time step ice transport and melt/growth rate may become very different from the TS, especially around the ice edges (Figure 4.15b). Therefore, concentration assimilation sometimes defeats to improve the ice thickness estimation. These results are very consistent with the toy model ones.

For the second case study, ice thickness is conserved when concentration data are assimilated. Tables 4.5 and 4.6 show an overall improvement of the ice concentration and velocity (N_CA_D_0.1(2) experiment). These improvements are

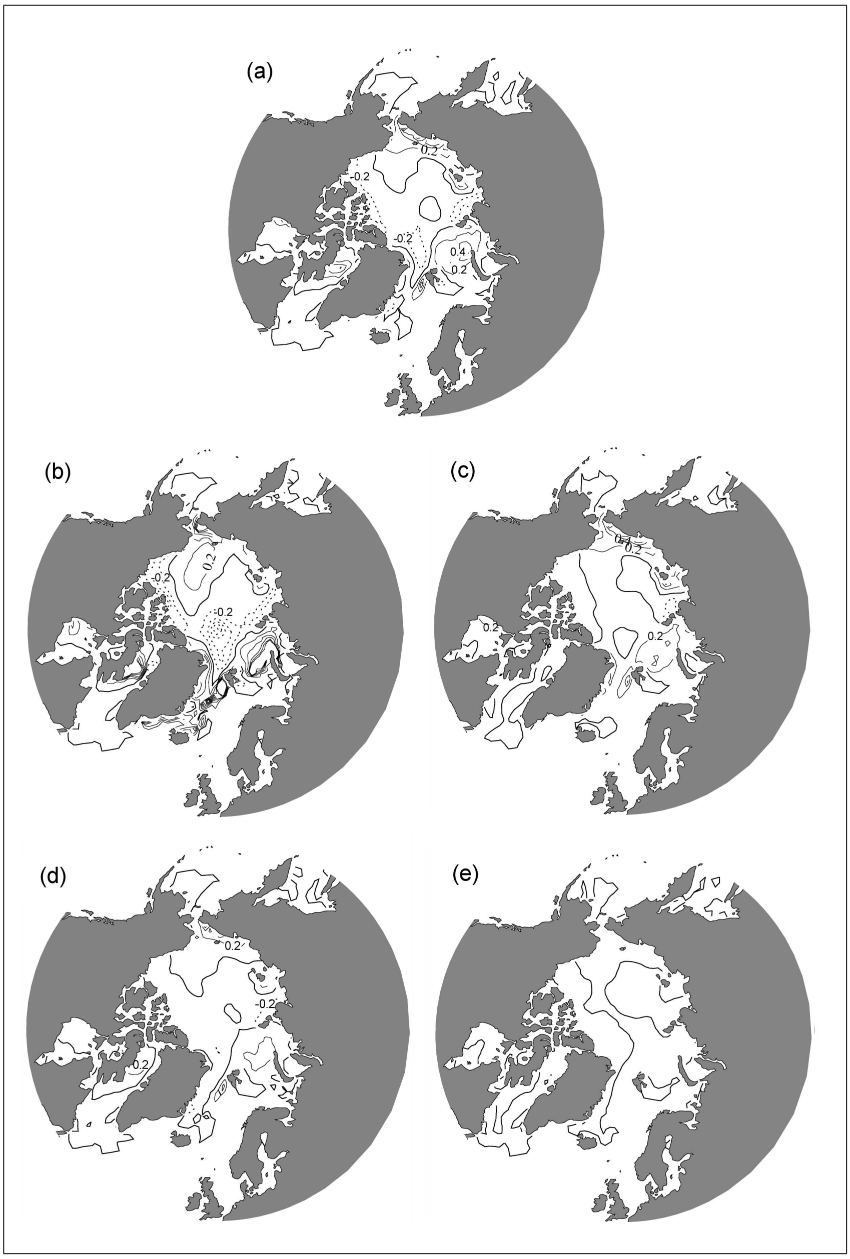

Figure 4.15: Geographical distributions of the 1984 annual mean ice thickness biases between N_WA_D (a), N_CA_D_0.1(1) (b), N_CA_D_0.1(2) (c), N_VA_D_0.3 (d) and N_VCA_D_0.3_0.1(2) (e) experiments and the TS. Contour interval is 0.2 m.

more significant than for the first case study. The area-averaged, 1984 annual mean ice thickness correlation is higher with than without data assimilation and the error standard deviation is lower. Despite the increase in the area-averaged, annual mean ice thickness bias, as presented in Table 4.6, most ice thicknesses are actually improved through the assimilation of ice concentration. This is demonstrated by Figure 4.15c, where the geographical distribution of the annual ice thickness bias is displayed.

For reminding, the data assimilation scheme implemented in the toy model could not improve the model estimation essentially where the ice thickened through advection processes (where $A_i > A_{max}$). Such remaining errors would weakly perturb the thermodynamic component of the model and in turn affect the dynamic one, leading to errors amplification. This process is also visible but less significantly in the NEMO-LIM2 results.

It is also worth noting that when k_A is larger than 0.1, the model does not present instabilities like it was the case with the toy model. Furthermore, improvements of the ice estimation brought with gains k_A larger than 0.1 are very similar to improvements brought with $k_A = 0.1$.

4.6.3.3 Concentration and velocity data assimilation

When ice concentrations and velocities from the TS are simultaneously assimilated into NEMO-LIM2, the global model behavior is further improved compared to no-assimilation case or to cases where ice concentrations and velocities are separately assimilated. As shown in Table 4.5, ice velocity estimates are then as good as estimates from the velocity-alone assimilation experiment using the same gain (k_u), while ice concentration estimations are better than any other concentration estimates from Table 4.6. Ice thicknesses are also improved by the simultaneous assimilation of concentration and velocity data. The area-averaged, mean ice thickness correlation coefficient to the TS is one of the largest of Table 4.6, and the error standard deviation is one of the lowest. The ice thickness bias is slightly larger than the bias from the velocity-alone data assimilation. However, like in Section 4.6.3.2, this increase in the area-averaged annual mean ice thickness bias is due to an artefact of the area average and is not representative. As seen in Figure 4.15, the geograpical distributions of the annual mean ice thickness errors compared to the TS, feature the lowest errors for the N_VCA_D_0.3_0.1(1) experiment in comparison with the N_VA_D_0.3 experiment (and other experiments as shown in this figure). Therefore, we can say that the ice thickness is significantly improved compared to the cases where concentration- and velocity-alone are assimilated into the model.

In summary, the assimilation of ice velocities is fully appropriate to improve the modeled ice characteristics in case of a dynamic perturbation. Concentration data assimilation may also improve the simulation, but attention should be paid to the ice thickness correction. The ice velocities assimilation is very complementary to the ice concentrations one and simultaneous assimilation of velocity and concentration data is certainly the best way to improve the ice characteristics when the model is dynamically perturbed. These results are in excellent agreement with the toy model findings. Nevertheless, due to its more complex and smooth ice dynamical component, NEMO-LIM2 was found to be more adapted to data assimilation than the toy model.

4.6.4 Initial conditions perturbation

In this section, we assess the impact of the assimilation of ice velocities and concentrations from the TS on the model performance when the model is badly initialized. Instead of initializing the model with the control experiment outputs to run year 1984, we use the control experiment outputs from next year and run year 1984.

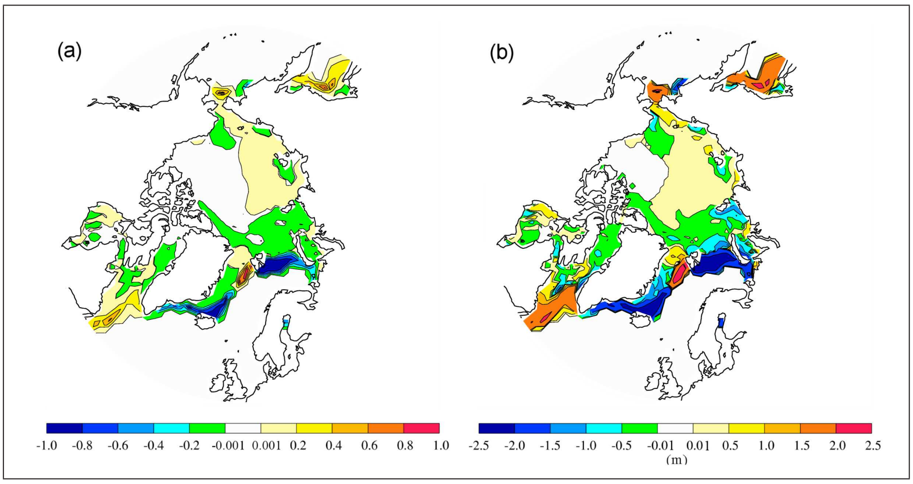

Figure 4.16: Initial conditions of ice concentration (a) and thickness (b) for year 1985 minus the respective initial conditions of year 1984, derived from control experiment outputs.

Figure 4.16a presents the differences between these two initial ice concentration data sets. Differences are lower than 1% in the Central Arctic and much larger along the ice edge, meaning that the ice edge pattern is quite different from one year to the other.

As displayed in Figure 4.16b, ice thickness discrepancies between the two initial ice thickness data sets remain generally lower than $0.5\ m$ in the Central Arctic and do not exceed $1.0\ m$ over the continental shelves. In some other regions, differences reach $2.5\ m$ like from the Greenland Sea down to the Denmark Strait and in the Labrador, Bering and Okhotsk Seas. These last ice thickness differences are strongly linked with the ice edge pattern ones. Nevertheless, the averaged correlation coefficient between the differences in ice concentration and thickness is fairly small (0.51).

4.6.4.1 Velocity data assimilation

As presented in Table 4.7 and as expected, the NEMO-LIM2 results show a significant improvement of the U- and V-components of the ice velocity estimation when ice velocities are assimilated into the model. This is true for all k_u values.

	Correlation		**Bias** ($10^{-4} m/s$)		**Error std** ($10^{-4} m/s$)	
	U	V	U	V	U	V
N_WA_IC	0.995	0.996	0.10	0.87	40.14	45.36
N_VA_IC_0.3	0.998	0.998	0.08	0.62	26.16	29.71
N_VA_IC_0.5	0.999	0.999	-0.02	0.49	19.25	21.81
N_VA_IC_0.9	1.000	1.000	-0.01	0.12	4.76	5.16
N_VA_IC_1.0	1.000	1.000	0.00	0.00	0.00	0.00
N_CA_IC_0.1(1)	0.959	0.968	-6.4	-7.47	110.20	123.86
N_CA_IC_0.1(2)	0.997	0.998	0.00	-0.08	27.22	31.18
N_VCA_IC_0.3_0.1(2)	0.999	0.999	0.06	-0.07	17.63	20.53

Table 4.7: Area-averaged, 1984 annual mean correlations between the ice velocity components from experiments N_WA_IC, N_VA_IC_XX, N_CA_IC_YY(y) and N_VCA_IC_XX_YY(y) and the TS, and area-averaged, 1984 annual mean errors in the ice thickness and concentration and standard deviations of these errors. y stands for concentration data assimilation scheme where either the ice volume (1) or ice thickness (2) is conserved. For the acronym definition, see Table 4.2.

The area-averaged, annual mean correlation coefficients are strongly increased for both velocity components. The mean biases and errors standard deviations are reduced. Moreover, the larger the gain (k_u), the better the estimations.

For $k_u = 0.3$, the velocity assimilation slightly improves the ice concentration estimation but not the ice thicknesses one (cfr. Table 4.8). For k_u larger than 0.3, data assimilation fails to improve both estimations. Indeed, the mean correlations between the estimated ice thicknesses and concentrations and the TS are slightly decreased. Also, the corresponding mean biases and error standard deviations are all globally increased. It is quite easy to understand that when TS velocities are combined with the TS ice pattern (i.e. ice thicknesses and ice concentrations), the model is able to estimate the TS ice pattern at the next time step. If initial conditions are changed, the ice velocities and the spatial distributions in the ice thickness and concentration are different. The model will then predict another ice pattern. When the model starts with the wrong ice distribution but with the TS velocities (for instance, with $k_u = 1$), there is no guarantee that the estimated ice pattern at the next time step will be better than the no-assimilation experiment one. This explains why restoring the estimated velocities towards the observed ones sometimes amplifies the ice pattern errors, failing to improve the ice estimation. This feature, which was already found in the toy model results,

	Correlation		**Bias**		**Error std**	
	h_i	A_i	h_i (m)	A_i (10^{-3})	h_i (m)	A_i (10^{-3})
N_WA_IC	0.998	0.998	0.117	-0.67	0.22	30.43
N_VA_IC_0.3	0.998	0.999	0.118	-0.63	0.23	30.37
N_VA_IC_0.5	0.998	0.999	0.118	-0.79	0.24	32.14
N_VA_IC_0.9	0.997	0.998	0.118	-1.62	0.26	38.84
N_VA_IC_1.0	0.997	0.998	0.118	-1.87	0.26	39.94
N_CA_IC_0.1(1)	0.994	0.999	0.092	-1.67	0.33	29.72
N_CA_IC_0.1(2)	0.998	1.000	0.109	0.05	0.22	5.53
N_VCA_IC_0.3_0.1(2)	0.998	1.000	0.113	0.04	0.23	5.27

Table 4.8: Area-averaged, 1984 annual mean correlations between the ice thickness and concentration from experiments N_WA_IC, N_VA_IC_XX, N_CA_IC_YY(y) and N_VCA_IC_XX_YY(y) and the TS, and area-averaged, 1984 annual mean errors in the ice thickness and concentration and standard deviations of these errors. y stands for concentration data assimilation scheme where either the ice volume (1) or ice thickness (2) is conserved. For the acronym definition, see Table 4.2.

is of lower significance in the NEMO-LIM2 ones, but it is still true that velocity data assimilation does not help to overcome spurious initial conditions.

4.6.4.2 Concentration data assimilation

Here, we determine the impact of assimilating ice concentration data on the global model behavior when the model is perturbed through its initial conditions.

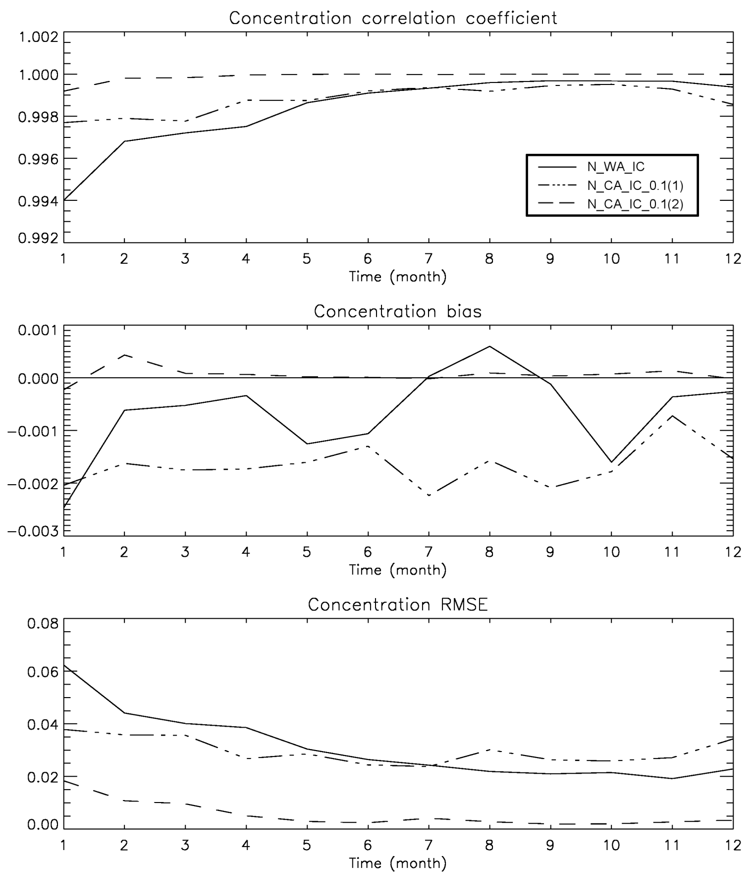

Figure 4.17: Area-averaged, 1984 monthly mean correlation coefficients, biases and error standard deviations between ice concentration estimations of N_WA_IC and N_CA_IC_0.1-experiments compared to the TS. N_CA_IC_0.1(1) stands for the experiment with concentration data assimilation where the ice volume conservation is imposed. N_CA_IC_0.1(2) represents the experiment with data assimilation where the ice thickness conservation is imposed.

As with the toy model, we have tested two different data assimilation schemes with NEMO-LIM2: the first one conserves the ice volume after concentrations are assimilated, while the second one conserves the ice thickness.

The first scheme which imposes ice volume conservation after assimilating concentrations slightly improves the estimation of the ice concentration during the first couple of months, compared to the no-assimilation case (cfr. the area-averaged, monthly statistical values presented in Figure 4.17). However, after

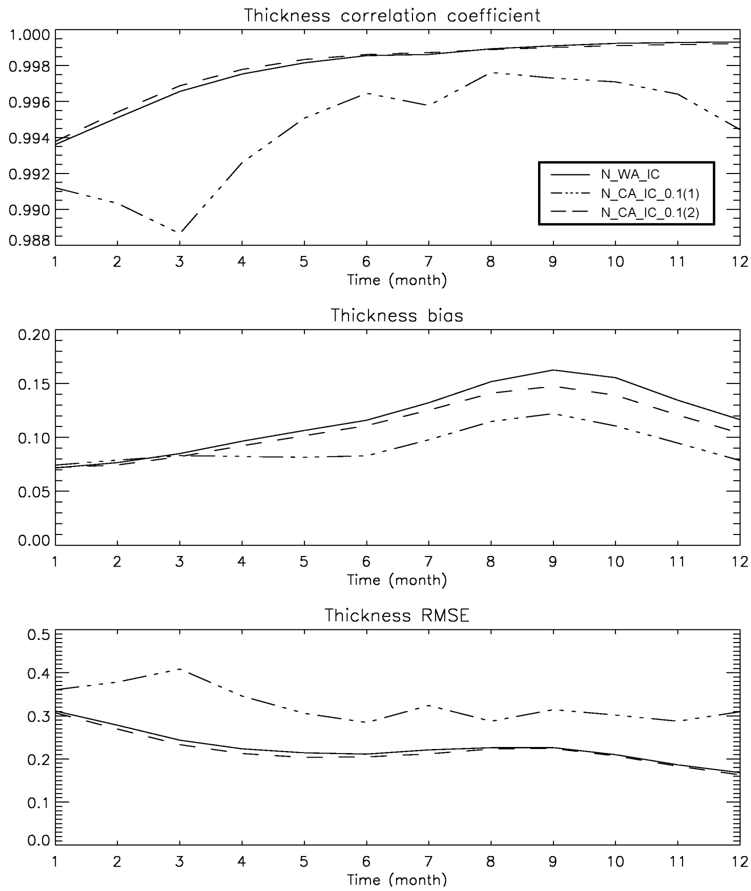

Figure 4.18: Area-averaged, 1984 monthly mean correlation coefficients, biases and error standard deviations between ice thickness estimations of N_WA_IC and N_CA_IC_0.1-experiments compared to the TS. N_CA_IC_0.1(1) stands for the experiment with concentration data assimilation where the ice volume conservation is imposed. N_CA_IC_0.1(2) represents the experiment with data assimilation where the ice thickness conservation is imposed.

about 5 months, the concentration improvement compared to the TS is not anymore true. Likewise, the data assimilation scheme is not able to improve the ice thickness estimate, as seen in Figure 4.18. When no data are assimilated, the model tends to naturally move away from its initial conditions and, in turn, this lowers the errors compared to TS. However, the assimilation of concentration data with ice volume conservation interferes with this process, leading to worse ice concentration and thickness estimation than the no-assimilation case. Indeed, close to the ice edge areas, errors in ice concentration and thickness are, most of the time, of the same sign even if the correlation between ice thickness and concentration errors are quite low. Hence, when the data assimilation scheme corrects the ice concentration by increasing (decreasing) it, it also decreases (increases) the ice thickness. Therefore, this process deteriorates the ice thickness estimation and in turn, it also deteriorates the ice velocities and concentrations as shown in Table 4.7 and in Figure 4.17.

When the ice volume varies in order to conserve the ice thickness after assimilation of ice concentrations into the model, ice concentrations are significantly improved. As displayed in Figure 4.17, the area-averaged, monthly mean correlations between the estimated concentrations and the TS are increased compared to the no-assimilation case. Furthermore, the mean concentration errors and their standard deviations are decreased. Likewise, the statistical values presented in Table 4.7 show a significant improvement if the ice velocity estimations. Unfortunately, the ice thickness improvement is less meaningfull.

The NEMO-LIM2 results are consistent with the toy model ones: assimilation of ice concentration data does not fully ameliorate the model simulation when wrong initial conditions are used. Nevertheless, the assimilation scheme which imposes the ice thickness conservation improves significantly the simulated ice concentration and velocity and, to a smaller degree, the ice thickness.

Also, when the data assimilation scheme conserves the ice thickness, the results from experiments with k_A larger than 0.1 are similar to the results from $k_A = 0.1$ experiments. This is in opposition with the toy model results where strong model instabilities were shown.

4.6.4.3 Concentration and velocity data assimilation

Here, we simultaneously assimilate ice velocities and concentrations from the TS. As mentioned in Section 4.6.4.1, when only ice velocities are assimilated, the best model results are obtained for a $k_u = 0.3$. Section 4.6.4.2 mentions that the concentration-alone assimilation scheme which imposes the ice thickness conservation already gives good results for $k_A = 0.1$. Therefore, we here discuss the results of N_VCA_IC_0.3_0.1(2) experiment as presented in Tables 4.7 and 4.8.

Simultaneously assimilating ice velocities and concentrations into the model significantly improves the ice characteristics estimation. Indeed, most of the statistical values are improved in comparison with the no-assimilation case or cases where ice concentrations and velocities are separately assimilated into the model using the same respective gains. However, the ice thicknesses estimation is slightly deteriorated compared to the N_CA_IC_0.1(2) one. Such deterioration, which becomes even larger as k_u increases, is due to the fact that TS ice velocities are often not capable of correcting the ice thickness pattern. This process has already been described in detail in Section 4.6.4.1. Finally, note that the mean bias of the velocity U-component is not representative and that most of the velocity U-components are actually further improved compared to any other experiments presented in Table 4.7.

Finally, the NEMO-LIM2 results, which are very consistent with the toy model ones, showed that the assimilation of ice velocity and/or concentration data is able to strongly attenuate the effect of the initial condition perturbation applied to the model. The model estimation of ice velocities and concentrations may be significantly improved, especially if the gains (k_u and k_A) are appropriately chosen. Nonetheless, since no coherent relation exists between the ice concentration and the ice thickness errors, the ice thickness model estimation is never significantly improved.

4.7 Summary

This chapter demonstrated the robustness of the conclusions of Chapter 3 by using a more realistic experimental design and a more complex sea ice model coupled to an ocean model. Twin experiments have been conducted with NEMO-LIM2 and the extent to what the assimilation of ice velocity and/or concentration data improves the model behavior and, in particular, the simulation of ice thickness has been determined. The major discrepancies between the NEMO-LIM2 and toy model results come from the difference in their sea ice dynamical component. In fact, the dynamics implemented in NEMO-LIM2 are more complex and smoother than in the toy model (which uses the Kreyscher *et al.* (2000) correction). Hence, no ice velocity smoothing occurred, and therefore no lowering in the ice growth through dynamical processes when velocity data are assimilated. This also avoids situations where concentration data are assimilated by imposing the ice thickness conservation and where grid cells would only accept movement of divergence. Finally, NEMO-LIM2 appears to be much more stable than the toy model when concentration data are assimilated and in turn, can handle larger assimilation weights.

- Like the toy model results, the NEMO-LIM2 results show that the assimilation of **ice concentration data** can lead to a deterioration of the model performance if it is not handled with care. This is mostly due to the strong connection between ice concentration and ice thickness. In opposition to the data assimilation scheme used in the toy model which needed to distinguish thermodynamical model errors from dynamical ones, the best way to estimate the sea ice state through concentration assimilation is here to add or remove an ice block of thickness equal to that of the pre-existing ice to better fit the observed ice concentration. This means that ice volume must not be conserved in the process. This scheme is very helpful to correct the ice state estimation in case of thermodynamic, dynamic or initial condition errors.

- Assimilation of **ice velocity data** is found to significantly improve the overall ice model estimation if the model dynamics are perturbed, especially when a large weight is utilized. When the model error is thermodynamic or when it comes from perturbation in initial conditions, the improvement brought by assimilation is not always as clear.

- The results obtained in the present study also reveal that the assimilation of ice velocity data and the assimilation of ice concentration data are very complementary. Indeed, assimilating simultaneously **ice velocity and ice**

concentration data into the model seems to be the best means to enhance the ability of the model to reproduce the observed features of the sea ice field.

In summary, this chapter confirmed that data assimilation is surely a suitable method for improving simulations of the sea ice pack made by sea ice models. Most of all, this chapter revealed some very important shortcomings brought by the use of too a simple sea ice model and highlighted the importance of using a suitable sea ice model to assimilate data.

Chapter 5

Solutions to specific issues in assimilating sea ice observations

5.1 Introduction

All along this work, many people showed a great interest in the particular approach used in our study to consider several issues that are brought when sea ice observations are assimilated into models. We have here selected a couple of those specific issues and try to solve them in the course of this chapter.

In the previous chapter, twin experiments demonstrated the ability of improving the simulation of the ice characteristics by implementing a data assimilation scheme which adds or removes an ice block of thickness equal to the one of the preexisting ice in order to better fit the ice concentration observations. This handling of the sea ice requires to make assumptions on variables which are linked to a change in the sea ice volume, namely here, the ice thickness, the freshwater (salt) flux toward the ocean, the ice and brine pocket heat contents as well as the snow thickness on the top of the ice. In the first part of this chapter, we discuss the impact of the assimilation of sea ice concentration data on each of these variables (except for the ice thickness, which was already considered in Chapter 4).

Another important issue when sea ice data are assimilated into models comes from errors in the observations (Weaver *et al.*, 2000). Many ways to observe sea ice exist. Each observational data set has its own advantages/disadvantages and is characterized by its proper spatial and temporal resolution. On one side, the temporal resolution of the different observation data sets are usually smaller than the model time steps. This might have an impact on the results when sea ice velocity data are assimilated into the model. Hence, this will be discussed in the course of this chapter. On the other side, the spatial resolution of the different observational data sets are most of the time larger than model ones. Therefore we assumed that effect on the data assimilation results is less significant. Nevertheless, it would be interesting to further study the impact of the gaps which are present in the observation data sets on the results (not done here).

Then, we discuss how the inaccuracy of the observed ice velocity data set affects the data assimilation results. Finally, we consider the effect of errors in the observed ice concentrations on the sea ice estimation improvement by the data assimilation scheme. We test this for three different data assimilation schemes.

5.2 Influence of rejecting salt and conserving the snow volume and the ice and brine pocket heat contents

In Chapter 4, the concentration data assimilation scheme was chosen in a way that it conserves the snow volume and the brine pocket heat content. It also assumed that no additional freshwater (nor salt) was rejected toward the ocean where an ice block was removed (or added) to better fit the observed ice concentration. Finally, the temperatures of the additional or removed ice block are assumed to be equal to the ones of the preexisting ice. Those assumptions, which made the assimilation scheme fairly simple, are now tested so as to answer the following questions:

- What happens when the snow volume changes in the same way that the sea ice volume does when concentration data are assimilated? In other words, what happens if the data assimilation scheme adds or removes an ice block which is uniformely covered with snow of thickness equal to that of the preexisting snow? (Figure 5.1a)

- What happens if freshwater (salt) is rejected toward the ocean when an ice block is removed (added) during data assimilation? (Figure 5.1b)
- What happens if, instead of adding (removing) an ice block free of brine pockets, we add (remove) an ice block with enclosed brine pockets with heat content proportional to the heat content of brine pockets enclosed in the preexisting ice block? (Figure 5.1c)
- What happens if the temperature of the ice block which is added is equal to the seawater freezing point and not to the temperature of the preexisting ice, like done in Chapter 4? (Figure 5.1d)

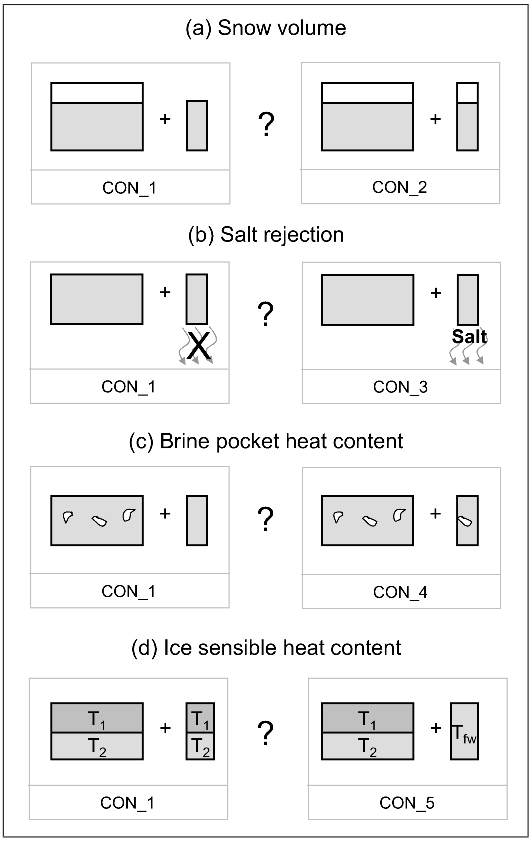

Figure 5.1: Illustration of the assumptions made in Chapter 4 (left) and the assumptions which are tested here (right) regarding the snow volume (a), the salt rejection (b), the brine pocket heat content (c) and the ice sensible heat content (d) when ice concentration data are assimilated into the model. The names of the corresponding experiments are given at the bottom of each panel.

Hence, we carried out a series of twin experiments with NEMO-LIM2 based on the experimental set up of Chapter 4. For each twin experiment, one of these assumptions is changed in comparison with the assumptions on which the data assimilation scheme of Chapter 4 is based. Then, we compare the results with and without concentration data assimilation to the TS and assess the impact of each assumption on the data assimilation results. Experiments are conducted for year 1984 (as in Chapter 4) while the model is thermodynamically perturbed. Many other twin experiments (not shown here) have been carried out using a stronger thermodynamical perturbation of the model or the dynamical and initial condition perturbations described in Chapter 4. Results remain generally the same, sup-

	snow volume conserv.	salt rejection	brine pocket heat content conserv.	constant ice temperature
N_WA_T	-	-	-	-
CON_1	yes	no	yes	yes
CON_2	***no***	no	yes	yes
CON_3	yes	***yes***	yes	yes
CON_4	yes	no	***no***	yes
CON_5	yes	no	yes	***no***

Table 5.1: Names of the twin experiments performed with NEMO-LIM2 and the assumptions on which their respective data assimilation scheme is based. The model is thermodynamically perturbed.

	Correlation		**Bias** ($10^{-4}m/s$)		**Error std** ($10^{-4}m/s$)	
	U	V	U	V	U	V
N_WA_T	0.9980	0.9977	-0.42	0.63	21.07	22.56
CON_1	0.9992	0.9995	-0.21	0.32	14.80	15.06
CON_2	0.9993	0.9995	-0.21	0.32	14.69	14.84
CON_3	0.9993	0.9995	-0.22	0.33	14.54	14.66
CON_4	0.9993	0.9995	-0.20	0.32	14.81	15.09
CON_5	0.9992	0.9995	-0.21	0.32	14.80	15.06

Table 5.2: Area-averaged, 1984 annual mean correlations between the ice velocity components from experiments N_WA_T, CON_1, CON_2, CON_3, CON_4 and CON_5 and the TS, and area-averaged, 1984 annual mean errors in the ice velocity components and standard deviations of these errors. For a brief description of the experiments, see Table 5.1.

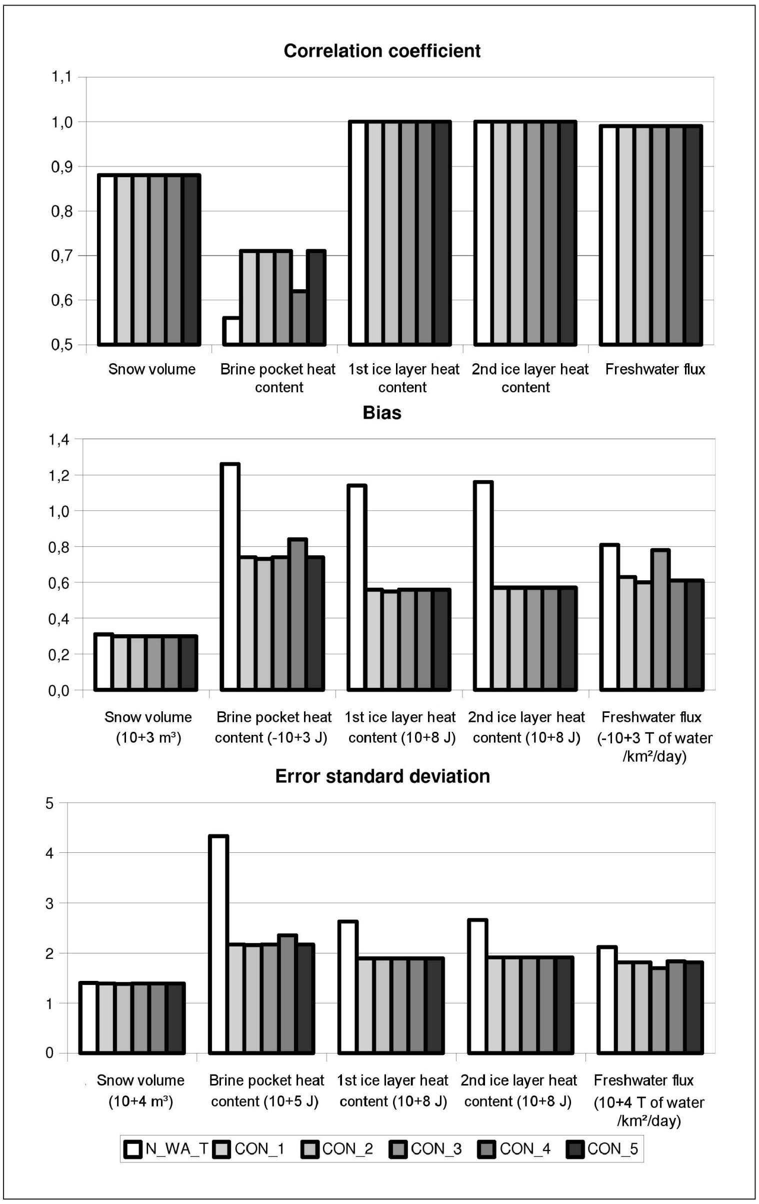

Figure 5.2: Area-averaged, 1984 annual mean correlations between several model variables (namely, the snow thickness, the brine pocket heat content, the first and second ice layer heat content and the freshwater/salt flux toward the ocean) from experiments presented in Table 5.1 and the TS, and area-averaged, 1984 annual mean errors in those model variables and standard deviations of these errors for experiments described in Table 5.1.

	Correlation		**Bias**		**Error std**	
	h_i	A_i	h_i $(10^{-2}m)$	A_i (10^{-3})	h_i $(10^{-2}m)$	A_i (10^{-3})
N_WA_T	0.9997	0.9994	-2.14	-3.03	5.04	22.56
CON_1	0.9999	0.9999	-1.39	-0.03	4.62	5.06
CON_2	0.9999	1.0000	-1.38	-0.03	4.62	5.08
CON_3	0.9999	0.9999	-1.39	-0.02	4.63	5.03
CON_4	0.9999	1.0000	-1.39	-0.03	4.63	5.07
CON_5	0.9999	1.0000	-1.39	-0.03	4.63	5.06

Table 5.3: Area-averaged, 1984 annual mean correlations between the ice thickness and concentration from experiments N_WA_T, CON_1, CON_2, CON_3, CON_4 and CON_5 and the TS, and area-averaged, 1984 annual mean errors in the ice thickness and concentration, and standard deviations of these errors. For a brief description of the experiments, see Table 5.1.

porting the results which are described below. The different experiments, which are presented here, and their respective assumptions are described in Table 5.1.

Figure 5.2 shows that, for any assumption, all experiments when concentration data are assimilated feature a tiny improvement in the snow thickness, and greater improvements in the ice and brine pocket heat contents as well as in the freshwater/salt flux in comparison to the no-assimilation case (note that we present results of ice heat contents instead of ice temperatures because we assume they are more appropriate to large-scale investigation). Furthermore, Figure 5.2 shows weak discrepancies in the snow volume, heat contents and freshwater/salt flux between experiments when concentration data are assimilated using the various assumptions (except maybe for the estimation of brine pocket heat content when this last variable is not conserved). In turn, these small differences only slightly affect the sea ice characteristics (namely the ice velocity, thickness and concentration). As seen in Tables 5.2 and 5.3, the area-averaged, annual mean correlation coefficients are all significantly larger for experiments with concentration data assimilation than without. Discrepancies between the experiments in which concentration data are assimilated are less significant. Likewise, the mean errors and their mean standard deviations are decreased when data are assimilated, but differences between data assimilation experiments are negligible.

In summary, the assumptions on which the data assimilation scheme of Chapter 4 is based are fully appropriate when concentration data are assimilated into the model. Their impact remains of low significance in all cases.

5.3 Impact of errors in the observed sea ice velocities

Several approaches have been used to observe sea ice motion: mainly in situ measurements and remote sensing observations. Each approach has yielded valuable insights into the polar regions. Nevertheless, none of these approaches can fully describe the Arctic processes at all scales.

- **In situ observations** come predominantly from buoys motions (Colony and Rigor, 1993). While accurate (error SD $\simeq$ 0.007 m/s), they are irregularly and sparsely distributed in the Arctic (about 10 to 30 buoys), and are very often available only for a short time period. This limits their use for data assimilation since sometimes only one observation, or none, may be available to represent large regions.
- **Satellite remote sensing** using visible and infrared advanced very high resolution radiometer (AVHRR) (Ninnis *et al.*, 1986; Emery *et al.*, 1991) and synthetic aperture radar (SAR) ERS-1 (Kwok *et al.*, 1990, 1995) sensors successfully tracked the ice motions over the past 20 years. They both use maximum cross-correlation methods (Emery *et al.*, 1991) which track a feature on a consistent grid over two succeeding images. However, these measurements tend to be incomplete and sparse. AVHRR provides multiple observations per day but is limited by clouds, which are persistent and widespread in polar regions. In contrast, SAR is not affected by clouds. However the narrow swath width of the sensor yields repeat coverages of approximatively 3 to 6 days.
- **Passive microwave imagery** from the Special Sensor Microwave Imager (SSM/I) overcomes some of the limitations in spatial and temporal coverage. Daily sea ice motions are computed from daily composite grids of brightness temperatures, using maximum cross-correlation methods. Error standard deviation is about 0.05 to 0.06 m/s (e.g. Kwok *et al.*, 1998; Lindsay and Zhang, 2006; Meier *et al.*, 2000; Zhang *et al.*, 2003). Data sets with lower temporal resolution and therefore reduced errors are also available. Nevertheless, summer ice motions are hard to obtain from SSM/I

mainly due to surface melt ponds which enhance the difficulty in differentiating ice surface from open water in passive microwave signals.

We assume that assimilating inappropriate sea ice velocities can cause the deterioration of the modeled ice estimation for several reasons. For instance, observed variables can be inadequate for assimilating them into the model if their temporal or spatial resolution are too different from the model one. Inadequacy might also be due to errors contained in the observed variables due to the way they are measured or derived from measurements.

Up to now, sea ice velocities derived from passive microwave measurements, combined with buoy observations, are the most commonly used drift estimates in sea ice data assimilation (e.g. Arbetter *et al.*, 2002; Dai *et al.*, 2006; Meier and Maslanik, 2003; Zhang *et al.*, 2003). This is due to both, their high temporal resolution and their large spatial coverage. Hence, we will focus on this data set and will discuss how the temporal resolution and the accuracy of these observed sea ice velocities can affect the data assimilation results. Finally, we will try to answer the question whether it is better to assimilate high temporal resolution velocity observations than observations with a lower temporal resolution but higher accuracy.

5.3.1 Temporal resolution of the observed sea ice velocities

Assimilating daily or weekly sea ice velocities into models might have an impact on the model ability to capture the sea ice short-term variability. In turn, this can affect the sea ice state in a more general way. To investigate the impact of the temporal resolution of the observed sea ice motions on the quality of the data assimilation, we run a series of twin experiments with NEMO-LIM2 using the same experimental design as in Chapter 4. We use year 1984 of the control experiment as true state (TS) and we assimilate data into the model which is perturbed. As seen in this previous chapter, assimilating sea ice velocities significantly improves the overall ice estimation of the model when its dynamical component is perturbed. When model errors come from its thermodynamics or its initial conditions, the improvement brought by the assimilation of sea ice velocity data remains sometimes unclear. Here, we focus on cases where assimilating sea ice motions might be of most use. Hence, we perturb the model dynamically. We then assimilate sea ice velocities which come from several idealized observation data sets with different temporal resolutions. For the VEL_1/3-experiment, sea

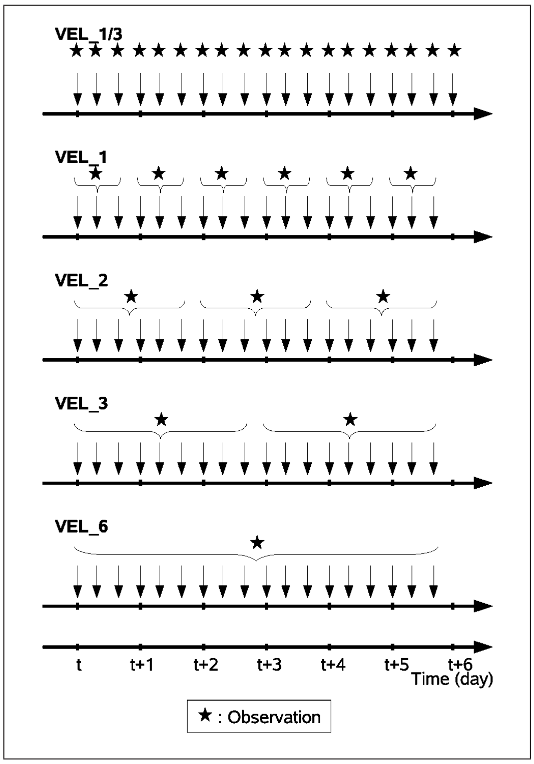

Figure 5.3: Illustration of the twin experiments carried out with the NEMO-LIM2 model. Data which are assimilated come from several idealized observation data sets with different temporal resolutions. For the VEL_1/3-experiment, sea ice velocity were available, and therefore assimilated, at each time step. For the VEL_1-experiment, only daily velocities were available and yet assimilated at each time step. In VEL_2, VEL_3 and VEL_6 experiments, sea ice velocities were available over 2, 3 and 6 days, respectively. Al data sets are built from model outputs and averaged to represent the mean ice displacement over 1, 2, 3 or 6 days.

ice velocities were available, and therefore assimilated, at each time step. For the VEL_1-experiment, only daily velocities were available and yet assimilated at each time step. In VEL_2, VEL_3 and VEL_6 experiments, sea ice velocities were available every 2, 3 and 6 days, respectively. All data sets are built from model outputs and averaged to represent the mean ice displacement over 1, 2, 3 or 6 days. Errors in the respective data sets are presented in Table 5.4. Each type of experiment is conducted for different values of k_u.

Figure 5.4 shows that, for any gain k_u, the velocity estimation is always the best for the VEL_1/3 experiment, namely when the temporal resolution of the

Experiment name	Observation temporal resolution	Observation Error SD (cm/s)		$k_{v,th}$	$k_{v,exp}$	Improvement (%)
		U	V			
VEL_1/3	3 obs. per day	0.00	0.00	1.00	~0.9	~100
VEL_1	1 obs. every 1 day	1.46	1.43	0.69	~0.9	~65
VEL_2	1 obs. every 2 days	3.13	3.49	0.30	~0.5	~30
VEL_3	1 obs. every 3 days	3.85	4.36	0.22	~0.3	~20
VEL_6	1 obs. every 6 days	4.99	5.81	0.14	~0.3	~15

Table 5.4: Names of experiments in which data sets of TS ice velocity of different temporal resolutions are assimilated into NEMO-LIM2. The table also shows the time resolution and area-averaged, annual mean error standard deviation (referred to as SD hereafter) for each velocity data set and the gains computed through the least-squares method ($k_{v,th}$, cfr 3.4 for detail) and determined experimentally ($k_{v,exp}$) by the maximum ice velocity improvement. The corresponding improvement, computed from the difference between the mean velocity error SD from the N_WA_D experiment minus the experiment with data assimilation and scaled by the N_WA_D mean velocity error SD, is also given. The area-averaged, annual mean error SD of the U- and V- sea ice velocity components from the N_WA_D experiment are equal to 2.02 and 2.32 cm/s. NEMO-LIM2 is dynamically perturbed.

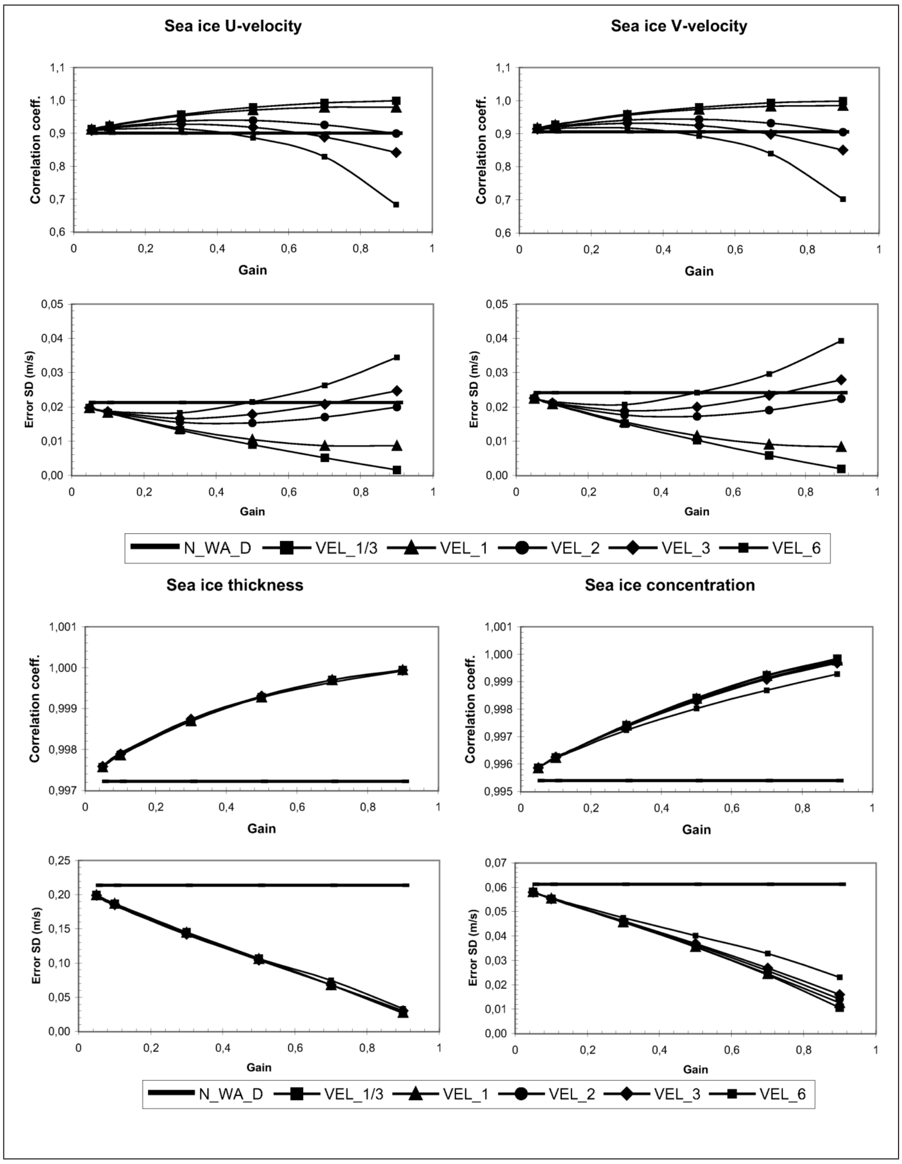

Figure 5.4: Area-averaged, 1984 annual mean correlations between the ice velocity components, thickness and concentration from experiments N_WA_D, VEL_1/3, VEL_1, VEL_2, VEL_3 and VEL_6 and the TS ones, and area-averaged, 1984 annual mean standard deviations of errors in the ice velocity components, thickness and concentration for experiments N_WA_D, VEL_1/3, VEL_1, VEL_2, VEL_3 and VEL_6. For the acronym definition, see Table 5.4

observation data set equals the model one. The area-averaged, annual mean correlation coefficients between the components of the sea ice velocity and the TS ones are the highest and the error standard deviations the lowest. The best model improvement occurs when $k_u = 0.9$. These results come from statistical computations for data sets with one modeled sea ice velocity per time step. Note that the same statistical values (not shown here) for 6-day averaged data sets have also been computed. They showed similar improvements of the 6-day averaged sea ice velocities, no matter the temporal resolution of the observational data set. Finally, note that the biases are not shown in this section for the reason that they are sometimes of positive and sometimes of negative signs, and that averaging them over the year and over the entire domain does not give a statistical value that is representative of the model behavior. However, mean correlations and error standard deviations do.

As the time resolution of the velocity data set moves away from the model temporal resolution, the ice velocity improvement becomes less significant. Moreover, the best improvement occurs for lower k_u in comparison with the VEL_1/3 experiment. These k_u values are larger than the ones computed from the least-squares method (Table 5.4). In fact, this method is not fully suitable here since the observation errors come from the discrepancies between the model time step and the temporal resolution of observations. With an appropriate weight (cfr. Table 5.5), the data assimilation of ice velocity improves the modeled ice velocity by 100% when the temporal resolution of the velocity data set equals the model time step, and by about 65, 30, 20 and 15% when velocities are given every 1, 2, 3 or 6 days, respectively.

A more interesting and somehow surprising result is that the temporal resolution of the ice velocity data set has barely no effect on the modeled ice thicknesses and ice concentrations. Indeed, these ice thickness and concentration estimates are clearly improved by the assimilation of ice velocities, and the larger the gain k_u, the better the estimates. However, this last statement is in opposition with the ice velocity results where a large gain deteriorates the ice velocities in comparison with the TS. Therefore, while assimilating 6-day averaged ice velocities fails to catch the daily ice velocity variability, it seems sufficient to account for most of the thermodynamical and dynamical changes in the sea ice concentration and thickness. Note that some studies found daily sea ice velocity variability important for the sea ice spatial distribution. Therefore, it would be interesting to further test our results with a different sea ice model in order to ensure that this result does not come from shortcomings in the NEMO-LIM2 model.

5.3.2 Uncertainties in the observed sea ice velocities

As mentioned above, sea ice velocity data contain errors due to the way they are measured or derived from measurements (Kwok, 2002). To test how this affects the data assimilation results, we build new idealized sea ice velocity data sets from TS velocities by adding pseudo-random noises and we assimilate them into the NEMO-LIM2 model which is dynamically perturbed (for the reasons which have already been described in the above section). The noises are generated as explained in Section 4.4, holding reasonable temporal and spatial frequencies of 1, 2 and 3 days, and 1, 2 and 3 grid cells, respectively. We have selected four noises of different amplitudes. The first noise has a standard deviation of 0.9 *cm/s*, which corresponds to half of the error SD in the modeled ice velocities when the model is dynamically perturbed. The SD of the second noise is close to the model error SD, while the third and fourth noises are larger (cfr. Table 5.5). We focus our attention on assimilating 2-day averaged sea ice velocities (one of the most commonly used data set in the assimilation of sea ice data).

Figure 5.5 shows that, as the noise increases, the velocity improvement decreases, and smaller gains should be used in order to optimize the data assimilation scheme. Nevertheless, even assimilating observations added to *noise 4* (which has mean error SD over 2 times larger than model one) still improves the model ice velocity estimation by about 4%. For *noises 1, 2* and *3*, this improvement reaches values of about 26, 16 and 12%, respectively.

For observation errors smaller than the model ones, $k_{u,exp}$, which is determined from looking at the best ice velocity model estimation, also improves the ice thickness. Unfortunately, for larger observation errors, the ice thickness is not anymore well corrected unless a smaller gain is used. This can be explained by the high sensitivity of the ice thickness to discontinuities in the ice velocity field. In fact, such discontinuities affect the ice transport, hence the ice ridging and the ice thickness. Smaller gains should be chosen in order to put less emphasis on the noisy observations of sea ice velocity.

Sea ice concentration is slightly less affected by the discontinuities in the ice velocity field. Hence, $k_{u,exp}$ is fully appropriate for improving this characteristic. This can be even further enhanced by using slightly larger gains (Figure 5.5).

In conclusion, assimilating 2-day averaged sea ice velocities is very convenient to improve the modeled ice velocities even if observations contain fairly large errors compared to the model. It is however important to choose an appropriate gain. A first approximation of the gain is given by the least-squares method. Nevertheless,

Experiment name	Observation temporal resolution	noise name	noise SD (cm/s)	Obs.+noise error SD (cm/s)		$k_{v,exp}$	Improvement (%)
				U	V		
VEL_1_n1	1 obs. every 1 day	noise 1	1.27	1.91	1.88	~0.7	~40
VEL_1_n2	1 obs. every 1 day	noise 2	2.70	3.07	3.03	~0.3	~17
VEL_1_n3	1 obs. every 1 day	noise 3	3.70	3.88	3.88	~0.3	~7
VEL_1_n4	1 obs. every 1 day	noise 4	6.65	6.57	6.50	~0.05	~1
VEL_2_n1	2 obs. every 1 day	noise 1	0.90	3.26	3.60	~0.3	~26
VEL_2_n2	2 obs. every 1 day	noise 2	2.00	3.73	4.02	~0.3	~15
VEL_2_n3	2 obs. every 1 day	noise 3	2.70	4.13	4.38	~0.3	~12
VEL_2_n4	2 obs. every 1 day	noise 4	4.70	5.64	5.81	~0.05	~4
VEL_6_n1	6 obs. every 1 day	noise 1	0.52	5.01	5.83	~0.3	~15
VEL_6_n2	6 obs. every 1 day	noise 2	1.15	5.09	5.90	~0.3	~15
VEL_6_n3	6 obs. every 1 day	noise 3	1.55	5.15	5.95	~0.1	~10
VEL_6_n4	6 obs. every 1 day	noise 4	2.70	5.55	6.25	~0.1	~10

Table 5.5: Names of experiments in which data sets of TS ice velocity with different temporal resolutions are assimilated into NEMO-LIM2. The table also shows the time resolution, the noise name and area-averaged, annual mean error standard deviation for each velocity data set, the corresponding k_u determined experimentally and the corresponding improvement, computed from the difference between the mean velocity error SD from the N_WA_D experiment minus the experiment with data assimilation and scaled by the N_WA_D mean velocity error SD. The area-averaged, annual mean error SD of the U- and V- sea ice velocity components from the N_WA_D experiment are equal to 2.02 and 2.32 cm/s. NEMO-LIM2 is dynamically perturbed.

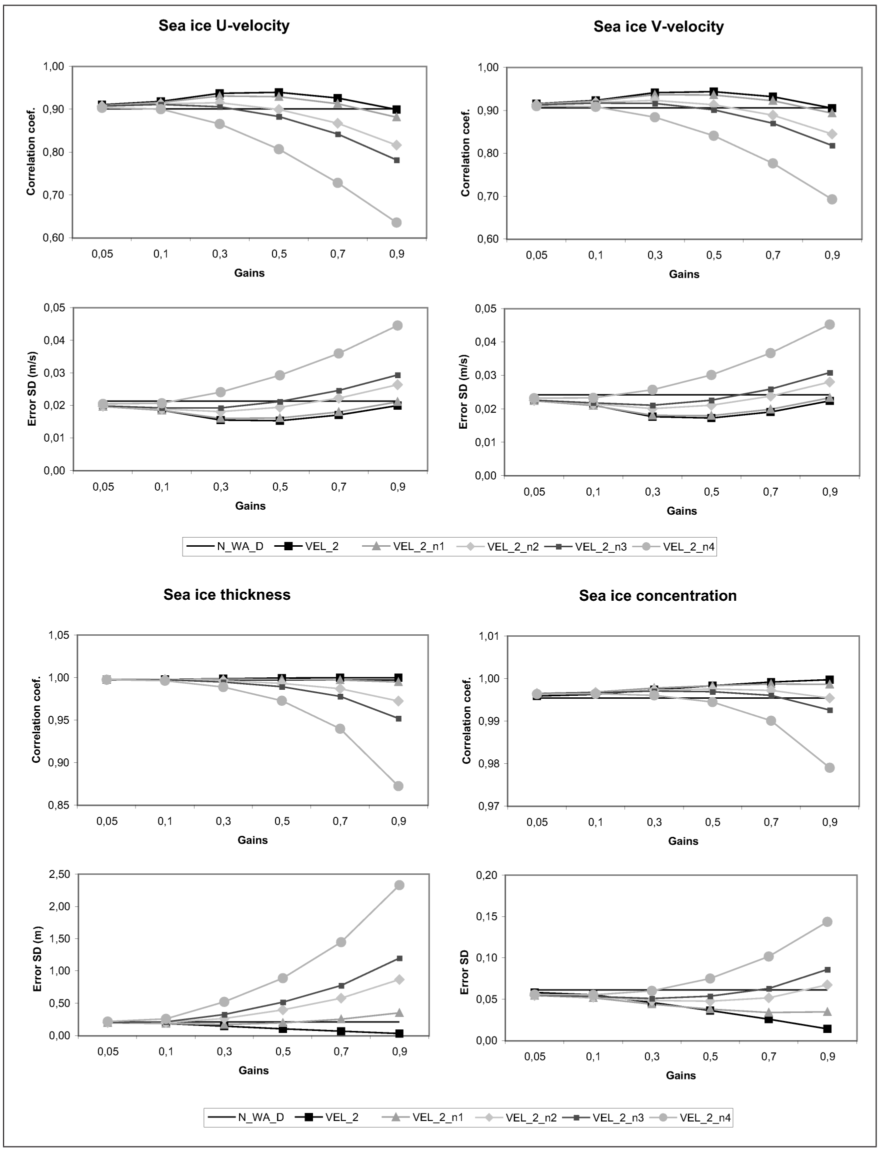

Figure 5.5: Area-averaged, 1984 annual mean correlations between the ice velocity components, thickness and concentration from experiments N_WA_D, VEL_2, VEL_2_n1, VEL_2_n2, VEL_2_n3 and VEL_2_n4 and the TS, and area-averaged, 1984 annual mean standard deviations of errors in the ice velocity components, thickness and concentration for experiments N_WA_D, VEL_2, VEL_2_n1, VEL_2_n2, VEL_2_n3 and VEL_2_n4. For the acronym definition, see Tables 5.4 and 5.5.

if errors in the observed ice velocities lead to too a discontinuous modeled velocity field and if emphasis is on the ice thickness, one should reduce the assimilation weight. On the other side, if the priority is given to the ice concentration, one should take a larger weight.

5.3.3 Which ice motion observations to choose?

The Jet Propulsion Laboratory (JPL) Remote Sensing Group provides both 1-day and 2-day SSM/I ice motion data sets derived from tracking a feature on a consistent grid over images taken every 1 or 2 days, respectively. Meier and Maslanik (2003) chose to assimilate daily motions to match as closely as possible the timescale of their model in order to simulate short-term variations in motion. At the same time, Zhang *et al.* (2003) chose to assimilate 2-day motions after finding that assimilating these motions generally reduce their model errors in ice motion and thickness more substantially than assimilating 1-day data.

According to Kwok *et al.* (1998), uncertainties in the ice motion derived from passive microwave measurements may be characterized as an unbiased additive Gaussian noise. Then, averaging would reduce the noise contribution to the estimates of mean motion; the decrease being proportional to $1/\sqrt{N}$, where N is the number of observations averaged in the mean displacement. Hence, a 2-day average of daily motions field would reduce the error standard deviation by a factor of 1.4. As a result of a discussion with Mark Drinkwater, we decided to investigate the effect of assimilating 6-day average of daily motions field. Indeed, a 6-day average would reduce the error standard deviation by a factor of 2.5 compared to daily motions and of 1.7 compared to 2-day averaged ice motions.

We run a series of twin experiments using the same experimental design as in the above section. Outputs from year 1984 of the control experiment are taken as TS, the model is dynamically perturbed and several data sets are assimilated. These data sets are built from averaging sea ice velocities from control experiment outputs over 1-, 2- and 6-day. Like in the above section, noises are added to these ice velocity data sets. The magnitude of the noises are computed in agreement with Kwok *et al.* (1998) who found a noise relation between different temporal resolution satellite derived data sets. Hence, *noise 1* has a standard deviation of 1.27 *cm/s* when it is added to the daily observed ice motions, and of 0.90 and 0.52 *cm/s* when added to the 2- and 6-day averaged ones, respectively (Table 5.5).

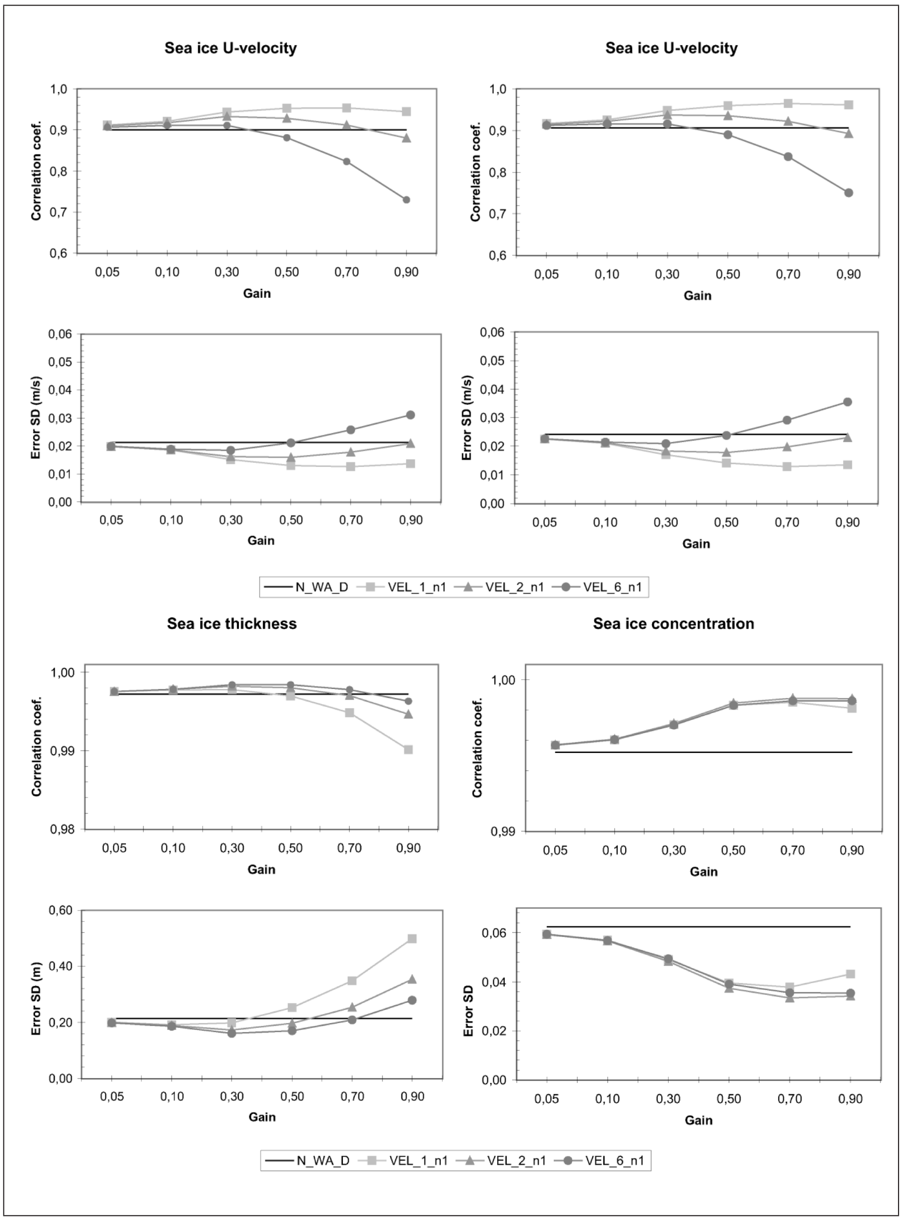

Figure 5.6: Area-averaged, 1984 annual mean correlations between the ice velocity components, thickness and concentration from experiments N_WA_D, VEL_1_n1, VEL_2_n1 and VEL_6_n1 and the TS, and area-averaged, 1984 annual mean standard deviations of these errors. For the acronym definition, see Table 5.5.

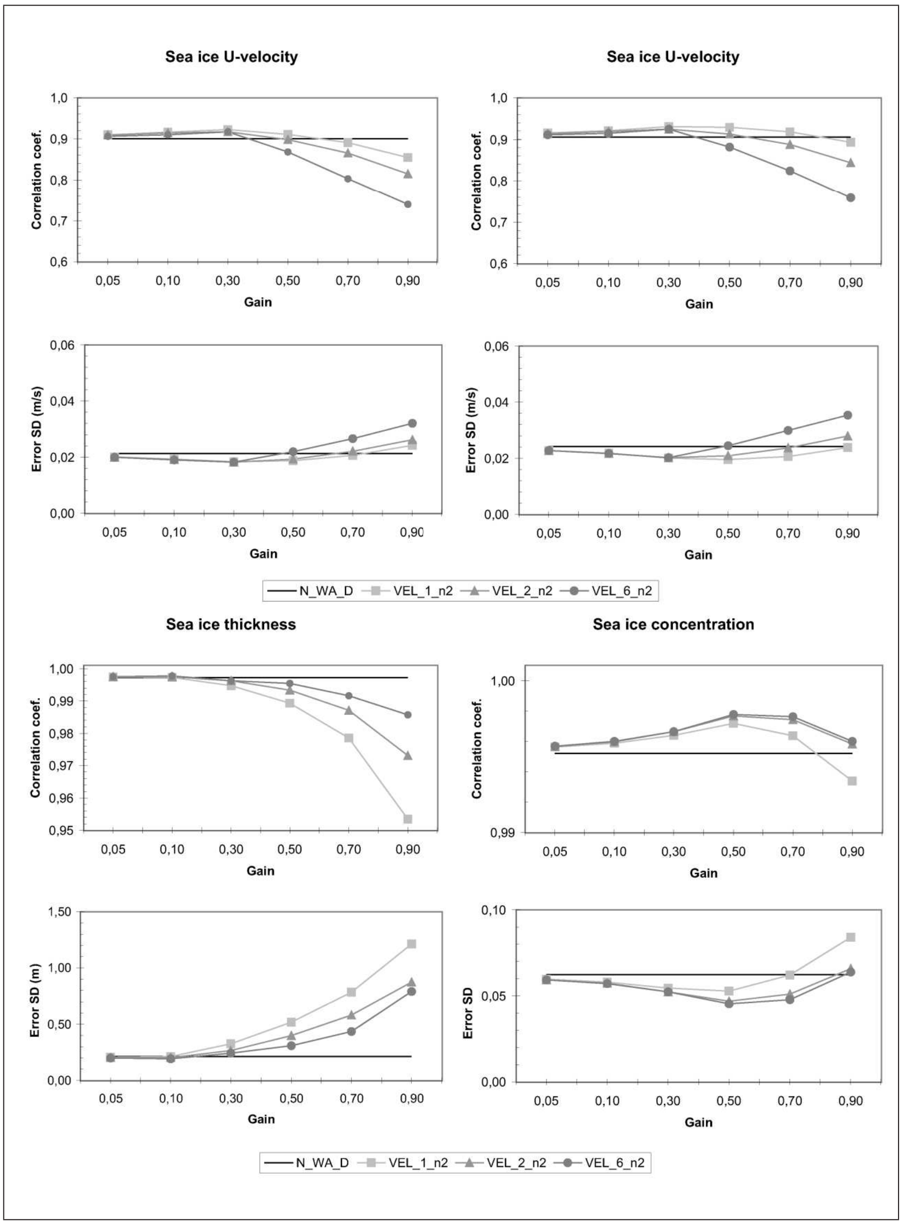

Figure 5.7: Area-averaged, 1984 annual mean correlations between the ice velocity components, thickness and concentration from experiments N_WA_D, VEL_1_n2, VEL_2_n2 and VEL_6_n2 and the TS, and area-averaged, 1984 annual mean standard deviations of these errors. For the acronym definition, see Table 5.5.

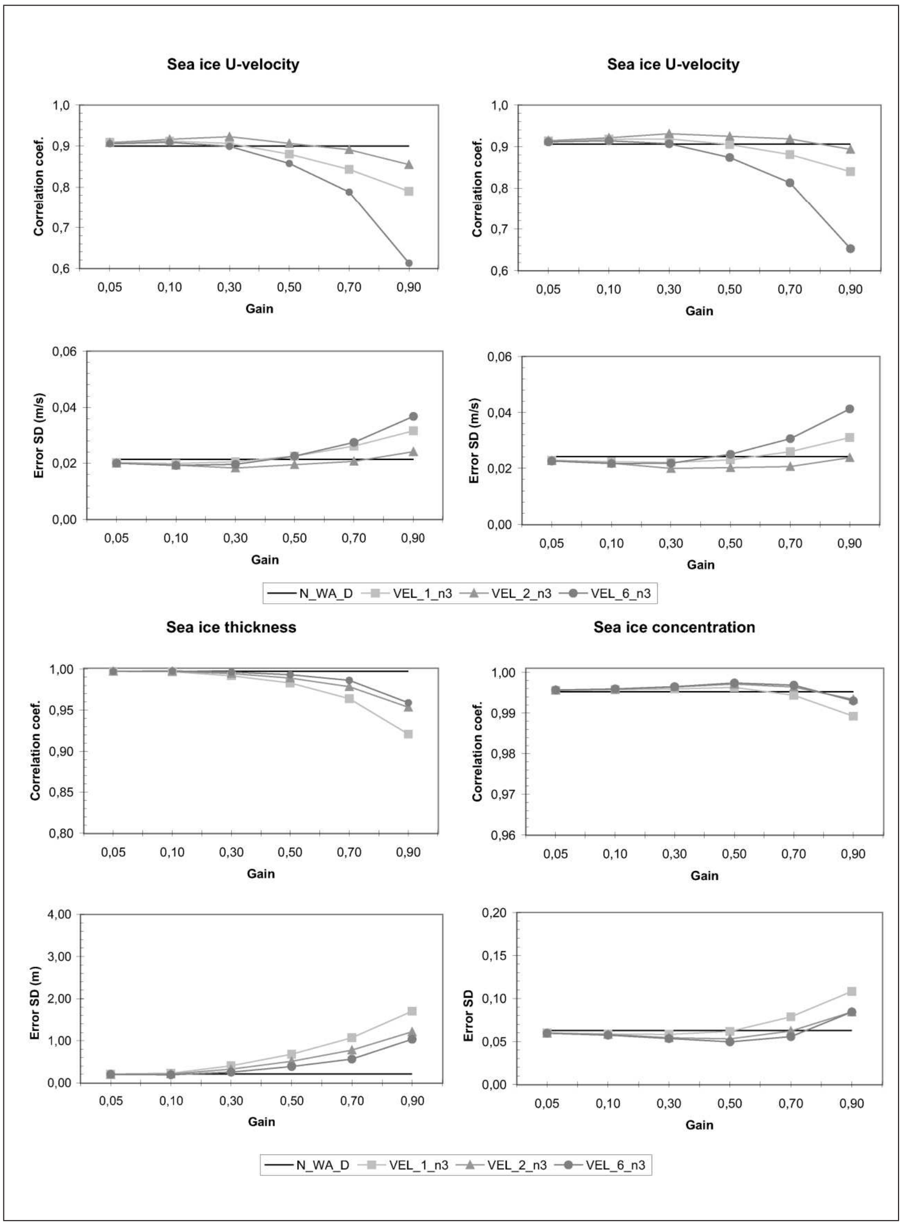

Figure 5.8: Area-averaged, 1984 annual mean correlations between the ice velocity components, thickness and concentration from experiments N_WA_D, VEL_1_n3, VEL_2_n3 and VEL_6_n3 and the TS, and area-averaged, 1984 annual mean standard deviations of these errors. For the acronym definition, see Table 5.5.

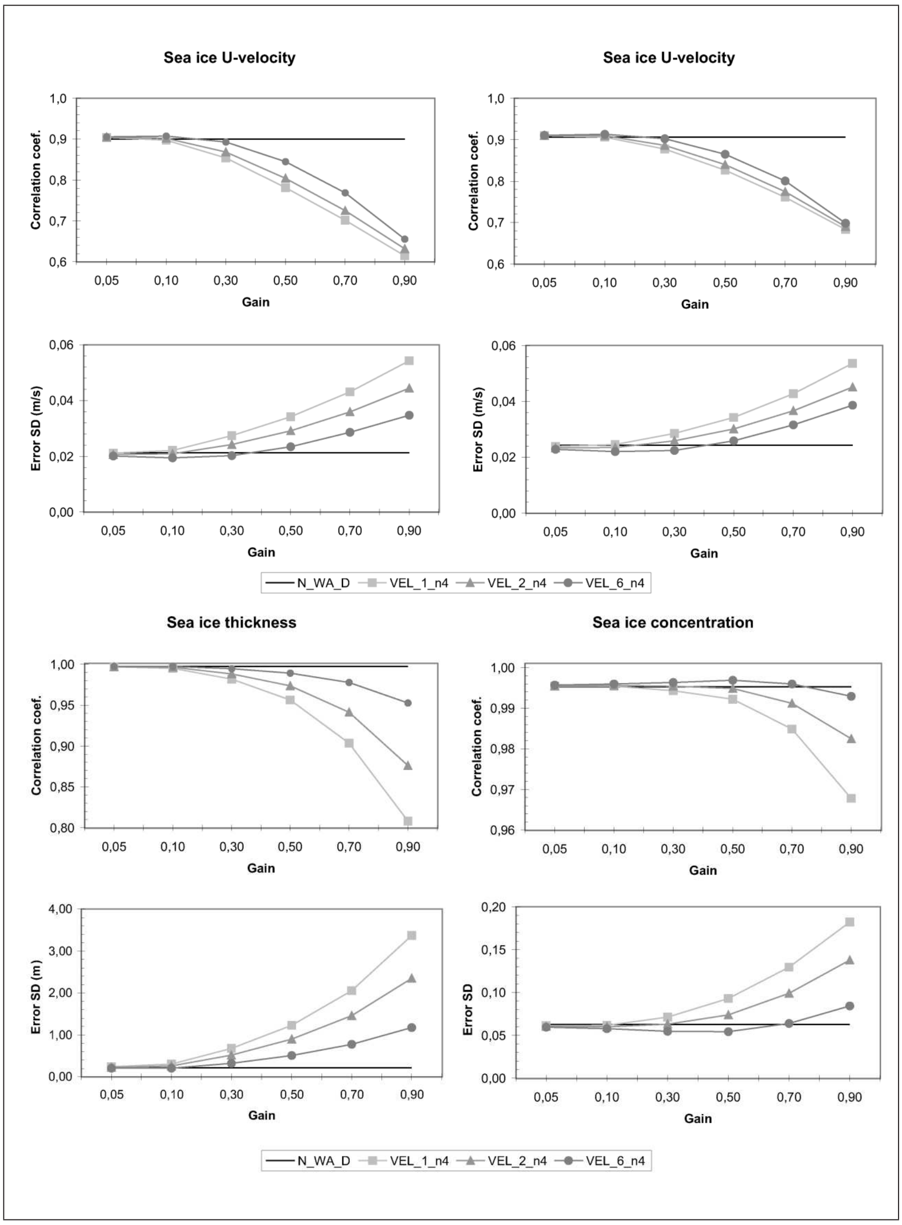

Figure 5.9: Area-averaged, 1984 annual mean correlations between the ice velocity components, thickness and concentration from experiments N_WA_D, VEL_1_n4, VEL_2_n4 and VEL_6_n4 and the TS, and area-averaged, 1984 annual mean standard deviations of these errors. For the acronym definition, see Table 5.5.

As discussed in Section 5.3.1, one should always prefer to assimilate data of temporal resolution close to the model one. When we compare the results of experiments in which several types of noisy observations are assimilated (see Figures 5.6, 5.7, 5.8 and 5.9), this statement is confirmed unless the SD of the noise in observations is greater than the model error SD by a factor of about 1.5. Hence, for noises smaller than this, assimilating daily data gives the best modeled ice velocities in comparison to the assimilation of 2- and 6-day averaged ice motions. This is confirmed by Table 5.5 which features the larger improvements (40 and 17%) for *noise 1* and *2* when daily motions are assimilated into the model. When the noise SD exceeds $2.70\ cm/s$ (about 3/2 of the model error SD), the use of a lower temporal resolution data set, which in turn has a reduced noise, is more helpful. In fact, the assimilation of 2-day (6-day) averaged ice velocities leads to the highest ice velocity improvement when *noise 3* (*noise 4*) is added to the observations. Note however that each data set is able to improve the model ice velocity estimation if the correct gain is chosen.

Previously, the ice thickness has been demonstrated to be very sensitive to discontinuities in noisy observed sea ice velocity field. In order to improve the sea ice thickness, it would therefore be more appropriate to assimilate the 6-day averaged ice velocity field. This is confirmed by Figures 5.6, 5.7, 5.8 and 5.9. This is an important result.

The ice concentration is less affected by discontinuities in noisy ice velocity field (cfr. Section 5.3.1). Yet, it is affected. This is the reason why assimilating 6-day averaged ice velocities gives the best ice concentration results for all noises except for *noise 1* where assimilating 2-day average data set seems sufficient. Also, note that the ice concentration can be further improved by the use of weights larger than $k_{u,exp}$.

5.4 Dealing with errors in the observed sea ice concentrations

Sea ice concentration is also observed in several ways. The most commonly assimilated data sets are derived from passive microwave measurements, like for ice velocity data. Sea ice concentration varies much slower in time than velocity does. Thus, there is no real need for studying the impact of the observation temporal resolution on the data assimilation results. There is however a need for studying the impact of their errors. Indeed, the optimal interpolation gain is usually computed through the least-squares method which assumes normally distributed unbiased errors. However, with a bounded quantity like concentration, the errors are not Gaussian and may be biased (Lindsay and Zhang, 2006). Moreover, the measurement of ice concentration by satellites is subject to errors (Kwok, 2002), especially during summertime when extensive melt ponds on the ice surface are easily confused with open water in passive microwave signals. Lindsay and Zhang (2006) believe that, at the ice margin, observations have a better signal-to-noise ratio and if there is a discrepancy between the model results and observations, here the observations should be weighted heavily. Hence, they used a new method based on restoring the model ice concentration A toward observed concentration A_{obs} in a manner that emphasizes the ice extent and minimizes the effect of observational errors in the interior of the pack. They chose a nudging weight $k_{A,L}$ which is a nonlinear function of the difference between the model and the observed ice concentration.

$$k_{A,L} = \frac{|A_{obs} - A|^{\alpha}}{|A_{obs} - A|^{\alpha} + R_{obs}^2} \tag{5.1}$$

where R_{obs}^2 is the error variance of the observations and the exponent α equals 6. They used a fixed value of $R_{obs} = 0.05$. This weighting factor $k_{A,L}$ ensures heavily weighted observations if the difference between the modeled and observed ice concentrations is above 0.5.

In addition, NEMO-LIM2 features well the ocean circulation (Timmermann *et al.*, 2005) and strong assimilation of the ice concentration along the ice edge could introduce errors in the ocean model, especially when ice errors persist. Therefore, we test another way to assimilate concentrations which consists of assimilating data exclusively within the ice pack (where a high fraction of the ocean is ice covered: e.g. 80-100%).

In this section, we conducted a couple of twin experiments as described in Chapter 4. We defined year 1984 from the control experiment as true state (TS), we perturb the model thermodynamically but we assume that the other ways to perturb the model would lead to the same type of results. We added a noise in the sea ice concentrations from control experiment outputs before they are assimilated into the model. This noise is produced as described in Section 4.4, holding temporal frequencies of 1, 2 and 3 days and space frequencies of 1, 2 and 3 grid cells. The standard deviation of this perturbation is about 0.010 except during the melting season in latitudes higher than 80^o N. There, it is set to 0.034. We chose this noise amplitude regarding model errors (0.015 during winter time and about 0.040 during melting season) as well as errors in observations derived from satellite measurements (about 0.06 for winter and 0.20 during melting season).

We tested and compared three different methods to assimilate concentration data : the simple optimal interpolation method (hereafter referred to as OI), the Lindsay and Zhang (2006) method (*Lin*) and the *ice pack* method (*Pack*) which assimilates data only for latitude higher than 80^o N. All methods correct the sea ice concentration by adding or removing an ice block of thickness equal to the thickness of the preexisting ice, like done in Chapter 4. The assimilation gains used by the OI and *ice pack* methods are computed from the least-squares method but have to be lowered to 0.01, which is about 10 times smaller than the weight used

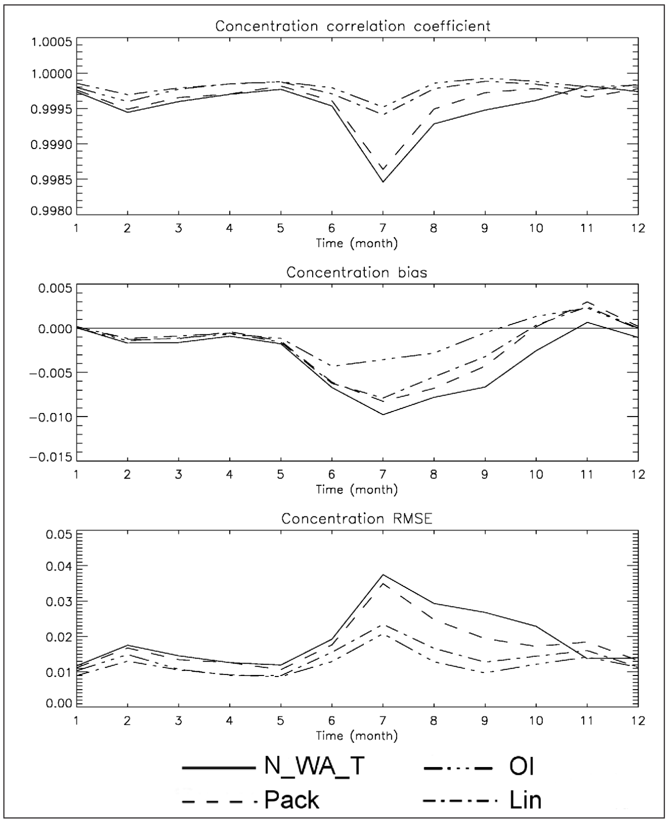

Figure 5.10: Area-averaged, 1984 monthly mean correlations between the ice concentration estimations of experiments without and with assimilation of concentration data compared to the TS, and area-averaged, 1984 monthly mean errors in the ice concentration and standard deviations of these errors for experiments without and with assimilation of concentration data. *N_ WA_ T* stands for the experiment with no data assimilation. *OI*, *Pack* and *Lin* are the experiments with assimilation of concentration data where the optimal interpolation, the *ice pack* and the Lindsay and Zhang (2006) data assimilation scheme are used, respectively.

to assimilate noiseless concentration data. The reason is that when the modeled ice concentrations are strongly nudged toward noisy observations, the noise can affect the modeled ice thickness, leading sometimes to model instabilities. This is avoided by using smaller gains. For the Lindsay and Zhang (2006) method, R_{obs} is set to 0.02.

As presented in Figures 5.10, 5.11, 5.12 and 5.13, area-averaged, monthly statistical values demonstrate a improved representation of the ice characteristics when concentration data are assimilated into NEMO-LIM2, no matter which data

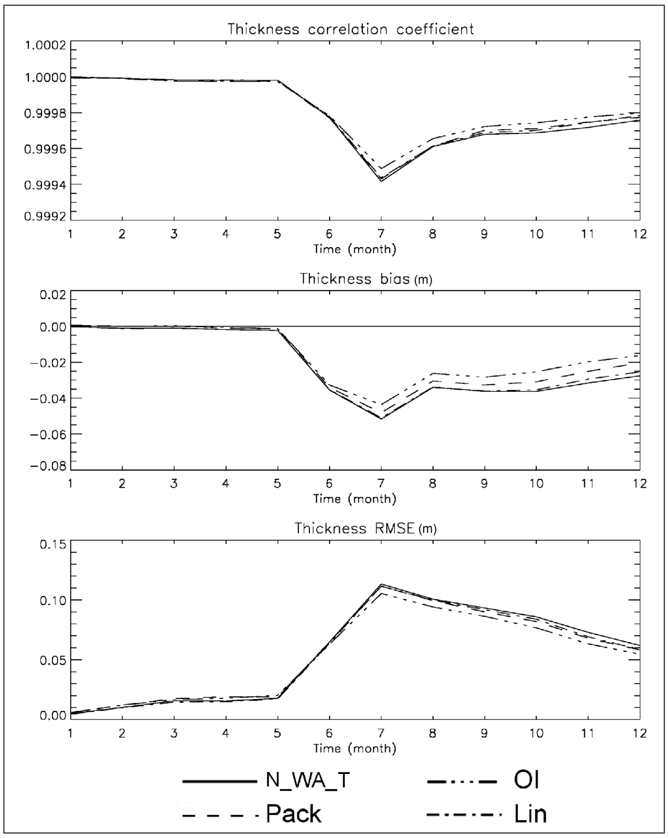

Figure 5.11: Area-averaged, 1984 monthly mean correlations between the ice thickness estimations of experiments without and with assimilation of concentration data compared to the TS, and area-averaged, 1984 monthly mean errors in the ice thickness and standard deviations of these errors for experiments without and with assimilation of concentration data. *N_ WA_ T* stands for the experiment with no data assimilation. *OI*, *Pack* and *Lin* are the experiments with assimilation of concentration data where the optimal interpolation, the *ice pack* and the Lindsay and Zhang (2006) data assimilation scheme are used, respectively.

assimilation scheme is used. Looking more carefully at the first couple of months in the ice concentration results, the best estimation is obtained with the Lindsay and Zhang (2006) scheme. During this period of time, the thermodynamical perturbation affects mainly the ice edge which is more sensitive to small temperature changes than the ice pack. Hence, a strong restoring of the modeled ice concentrations toward observed ones at the ice edge is very helpful to improve the location of the ice edge. Later, the classical OI scheme which corrects the ice concentration everywhere in the same manner gives the best estimation.

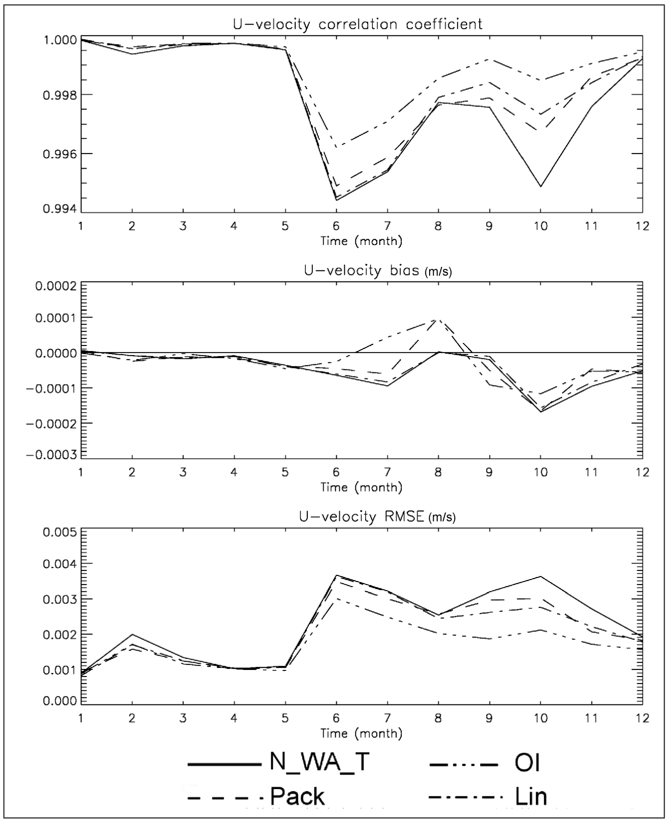

Figure 5.12: Area-averaged, 1984 monthly mean correlations between the U-component of the ice velocity estimations of experiments without and with assimilation of concentration data compared to the TS, and area-averaged, 1984 monthly mean errors in the U-component of the ice velocity and standard deviations of these errors for experiments without and with assimilation of concentration data. *N_ WA_ T* stands for the experiment with no data assimilation. *OI*, *Pack* and *Lin* are the experiments with assimilation of concentration data where the optimal interpolation, the *ice pack* and the Lindsay and Zhang (2006) data assimilation scheme are used, respectively.

Note also that the *ice pack* method ignores a lot of the usefull information carried by observations and therefore gives the lowest improvement of modeled ice concentration.

The ice thickness characteristics are slightly improved by assimilating data into the model (cfr. Figure 5.11). The best results are obtained with the OI scheme which is the only scheme out of the three able to improve simultaneously the ice

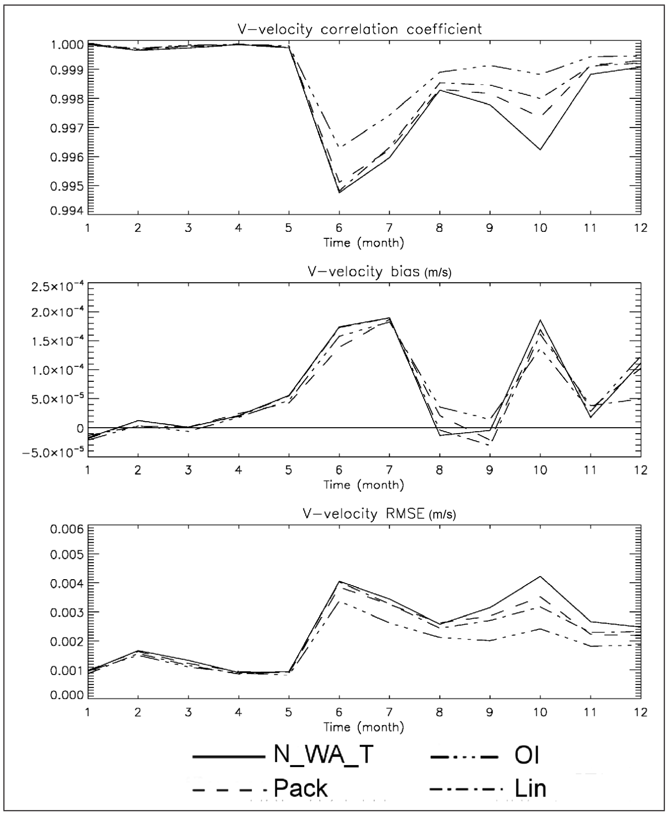

Figure 5.13: Area-averaged, 1984 monthly mean correlations between the V-component of the ice velocity estimations of experiments without and with assimilation of concentration data compared to the TS, and area-averaged, 1984 monthly mean errors in the V-component of the ice velocity and standard deviations of these errors for experiments without and with assimilation of concentration data. *N_ WA_ T* stands for the experiment with no data assimilation. *OI*, *Pack* and *Lin* are the experiments with assimilation of concentration data where the optimal interpolation, the *ice pack* and the Lindsay and Zhang (2006) data assimilation scheme are used, respectively.

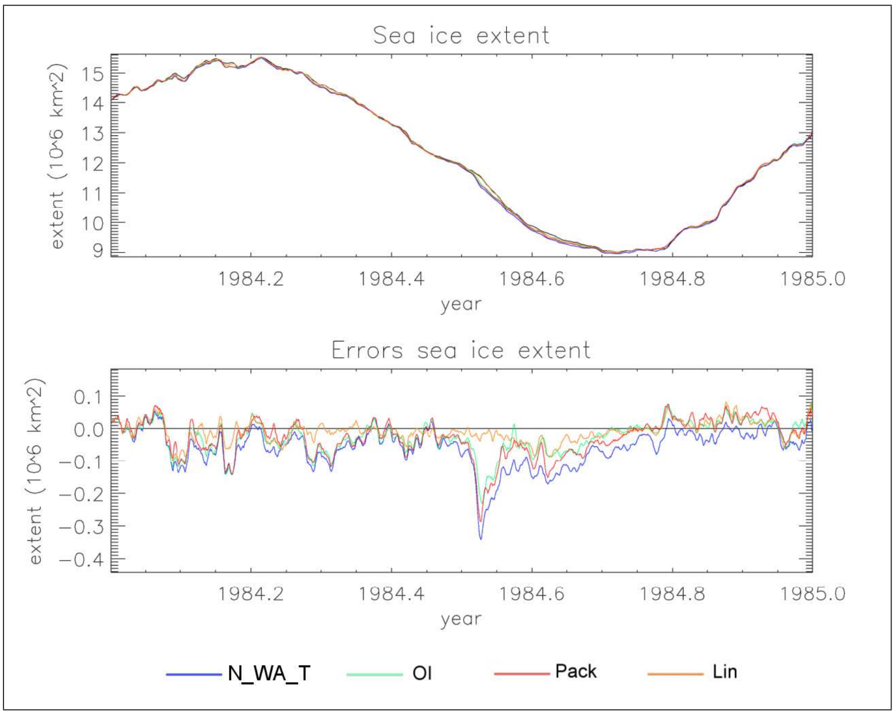

Figure 5.14: Seasonal cycle of the Arctic sea ice extent as simulated by NEMO-LIM2 in the N_WA_T, *OI*, *Pack* and *Lin* experiments (top) and their respective errors compared to the TS sea ice extent (bottom). N_WA_T stands for the experiment with no data assimilation and *OI*, *Pack* and *Lin* for the experiments when noisy sea ice concentration data are assimilated into the model through an optimal interpolation, *ice pack* and Lindsay and Zhang (2006) schemes, respectively. Units are $10^6 km^2$.

thickness in the ice pack and at the ice edge while the other schemes only correct the ice thickness in either of these regions.

The estimation of the two components of the ice velocity is best with the OI scheme, followed by the *Lin*, then the *ice pack* schemes. This is in agreement with the ice concentration and thickness estimations. Note that the errors predominantly appear with the melting period and remain afterwards, like for the ice concentrations and thicknesses.

Figure 5.14 shows the seasonal cycle of the Arctic sea ice extent as simulated by NEMO-LIM2 with and without concentration data assimilation for the three data assimilation schemes, and their respective errors in comparison with the TS. From January to June, the model which is thermodynamically perturbed globally underestimates the ice extent by about $0.05 \times 10^6 km^2$. In mid-July, the model strongly underestimates the ice-covered area in Davis Strait, leading to a global sea ice extent underestimation of about $0.32 \times 10^6 km^2$ which slowely decreases afterwards. While the improvements in the seasonal sea ice extent brought by the OI and the *ice pack* data assimilation schemes are visible, they remain smaller than the improvement due to the Lindsay and Zhang (2006) scheme.

In summary, we demonstrated that the classical optimal interpolation scheme is a safe way to assimilate sea ice concentration into large-scale sea ice models. Moreover, if the focus is put on the sea ice extent more than on the ice concentration, the Lindsay and Zhang (2006) scheme is the most appropriate assimilation scheme to use. Finally, assimilating sea ice concentration data in the ice pack and not around the ice edge certainly improves the knowledge of the sea ice state. However, this last scheme does not fully take advantage of the observed ice concentrations and would therefore be taken as our last choice. Finally, note that in the framework of this study, we have chosen constant weights (as well as a constant R_{obs}). However, model and observation errors strongly vary in time and space. It would thus be very interesting to study how weights which spatially and seasonally vary can further improve the data assimilation results.

5.5 Summary

In this chapter, we took advantage of our idealized experimental design to address a couple of specific issues brought by the assimilation of sea ice data.

First, we found that rejecting or not rejecting salt (freshwater) toward the ocean when sea ice concentration are assimilated into the model by adding (removing) an ice block of thickness equal to the one of preexisting ice has barely no effect on the data assimilation results. Same conclusions are drawn about conserving or not the snow volume and the heat contained in ice and brine pockets.

Then, we gave many features in sea ice data assimilation to help in the choice of the data sets to be assimilated. We investigated the impact of the temporal resolution of the observed ice velocities and we came to the conclusion that, if the noise in observations is negligible compared to model errors, the best assimilation results in order to improve the ice velocity are obtained for temporal resolutions which are as close as possible to the sea ice model time step. Noisy sea ice velocity observations are still suitable to improve the modeled ice velocities even if the noise magnitude is quite large compared to model errors. Yet, the best results are obtained with the smallest observation noise. According to Kwok *et al.* (1998), observation noise can be reduced if a lower temporal resolution is used. A reduction in the observation noise would improve the ice velocity estimation while a reduction in the observation temporal resolution would deteriorate it. Hence, we asked the question whether it is better to assimilate high temporal resolution sea ice velocities than sea ice velocities with a lower temporal resolution but a higher accuracy. We answered that the best sea ice velocity data assimilation results are obtained for the observed sea ice velocity data set which has the closest temporal resolution to the model time step and which accounts for a noise lower than the model error multiplied by a factor of 1.5. However, if the first goal is to improve the model ice volume, the observation noise should be as low as possible, privileging the assimilation of data set with small temporal resolution, but on the detriment of the daily variability of the sea ice velocity estimate.

In any case, the weight is crucial for the data assimilation results and should therefore be chosen very carefully. The least-squares method is a good way to estimate it. However, it assumes normally distributed unbiased errors and is not always adequate, as for instance, if errors come from an inappropriate temporal resolution in the observed data set. Moreover, the weight can be chosen in a way that it further improves one of the ice characteristics but, sometimes on the detriment of others.

Finally, we investigated several schemes to assimilate sea ice concentration data: the classical optimal interpolation scheme, the Lindsay and Zhang (2006) scheme (which heavily restores the modeled ice concentration toward the observed one if the difference between those two variables is above 0.5, as usually occurs along the ice edge) and another scheme that only assimilates data within the ice pack. We demonstrated that the classical optimal interpolation scheme is a safe way to improve the ice characteristics. Furthermore, if focus is put more on improving the sea ice extent than on the ice concentration, the Lindsay and Zhang (2006) scheme would be the scheme to use. Finally, we showed that assimilating sea ice concentrations only within the ice pack and not along the ice edge certainly improves the knowledge of the sea ice state with almost no change in the ocean, but it does not fully take advantage of the observed ice concentrations.

Chapter 6

Conclusions

All models give only estimates of the real state. Even the best models which account for complex physical processes are still subject to biases and errors. It is then essential to take benefit from information derived from actual observations to nudge the model state trajectory closer to the real one. This process is called *data assimilation* and has proven very useful in the atmospheric and oceanic modeling communities for many years. From reviewing the literature on data assimilation in sea ice modeling, we found that it holds a lot of promise in improving our knowledge of sea ice and polar climate. Some studies also suggested that the improvement brought by the assimilation is not straightforward. Yet, it has not been studied in details and the impact of data assimilation on the model behavior remains too little known. The aim of this work was to fill in these gaps and to find an appropriate way to assimilate sea ice concentration and velocity observations into large-scale sea ice-ocean models.

First, we have built a simplified model of the Arctic sea ice cover and we have conducted a series of twin experiments in which sea ice concentration and/or velocity data (from model outputs) were assimilated through an optimal interpolation scheme. To our knowledge, this is the very first time that such an experimental design has been used for sea ice while it has been, and still is, widely used in oceanic and atmospheric sciences. We have then tested the robustness of the results obtained with the toy model with NEMO-LIM2, a primitive equation ocean general circulation model coupled to LIM2 (the second generation of the Louvain-la-Neuve sea ice model), in a more realistic framework. We have shown the importance of choosing an appropriate model which should rather include smooth dynamics than discontinuous ones, like i.e. the *free drift* type dynamics combined with the Kreyscher *et al.* (2000) correction.

We have investigated several technical aspects of assimilating sea ice concentration and velocity data into large-scale sea ice models. We have demonstrated that assimilating sea ice concentration data can easily lead to deterioration of the model performance if no attention is paid. This is mostly explained by the strong link between ice concentration and ice thickness. For the smooth model dynamics, the best way to estimate the sea ice state through concentration data assimilation is to add or remove an ice block of thickness equal to that of the preexisting ice to better fit the observed ice concentration. The fact that this additional ice block is snow covered or not and that its temperature equals either the temperature of the preexisting ice or the seawater freezing temperature has barely no effect on the optimized sea ice distribution. We have also shown that the additional ice block should rather not contain heat within its brine pockets, eventhough the impact of this on the sea ice characteristics is small. Finally, rejecting salt (freshwater) toward the ocean is not necessary when the ice block is added (removed) to better fit the concentration observations. In the presently described process, the ice volume is not conserved. With dynamics similar to the toy model ones, one should preserve the ice volume when the model error is mainly dynamic.

We have examined three different schemes to assimilate sea ice concentration data: a classical scheme based on optimal interpolation, the Lindsay and Zhang (2006) scheme and another scheme that only assimilates data within the ice pack. We have shown that the classical optimal interpolation scheme is a reliable means to improve the model estimation of the ice characteristics. Moreover, if we rather want to improve the sea ice extent than the ice concentration, the Lindsay and Zhang (2006) scheme should be used. Finally, we have demonstrated that assimilating sea ice concentration data only within the ice pack and not along the ice edge certainly improves the model estimation of the sea ice state with almost no change in the ocean but it does not fully take advantage of the observations.

We have demonstrated that the assimilation of ice velocity data significantly improves the overall ice model estimation when the model dynamics are wrong. This is especially true if a large weight is used. When the model error is thermodynamic or when it comes from perturbation in initial conditions, the improvement brought by assimilation is not always as visible.

In the present study we have also demonstrated that the assimilation of ice velocity data and the assimilation of ice concentration data are very complementary.

Indeed, assimilating simultaneously ice velocity and ice concentration data into the model seems to be the best means to enhance the ability of the model to reproduce the observed features of the sea ice field. This was not obvious since sea ice is highly non-linear and since ice concentration is tightly bounded to ice thickness.

After investigating the effect of the temporal resolution of the observed ice motion, we concluded that, if the noise in observations is not significant in comparison with the model errors, the best sea ice velocity data assimilation results are obtained for observation temporal resolutions which are the nearest to the model time step. Noisy observations of sea ice velocity are still very handy to improve the sea ice velocity model performance even for large magnitudes of noise. Yet, the best model results are obtained with the smallest observation noises. According to Kwok *et al.* (1998), the observation noise might be reduced by lowering the observation temporal resolution. Nevertheless, if a reduction in the observation noise improves the sea ice velocity estimation, a reduction in the temporal resolution deteriorates it. Therefore, we have investigated whether it is better to assimilate high temporal resolution sea ice velocities than sea ice velocities with a lower temporal resolution but a higher accuracy. We have demonstrated that the best ice velocity data assimilation results are obtained for the observed sea ice velocity data set which has the closest temporal resolution to the model time step and which accounts for a noise lower than the model error multiplied by a factor of 1.5. Nevertheless, if the prior sea ice characteristic to improve is the ice volume, ice concentration or ice thickness, one should rather assimilate data with a lower temporal resolution, using a large weight. For instance, a temporal resolution of 6-day was found to be very appropriate for this last purpose.

In every instance, we have demonstrated that the weights are playing a crucial role in the data assimilation results. An appropriate weight enhances the model performance whereas an inappropriate one can deteriorate the model results. Moreover, the weight can be chosen in a manner that it further improves one of the ice characteristics, but sometimes on the detriment of others. This is often the case when weights are estimated through the least-squares method. Therefore, for a global improvement of the sea ice estimate, we found that choosing the weights on a physical more than on a statistical basis is generally more appropriate.

Now that we have a better understanding of how sea ice data can be assimilated into large-scale sea ice models, here are three main recommendations. Firstly, one should assimilate sea ice velocity and concentration data simultaneously. Secondly, if the ice concentration is modified due to the assimilation, one should conserve the ice thickness (not the ice volume). Thirdly, one should always look into the system carefully to make sure the assimilation is done properly. Most of all it is necessary to keep a close eye on the ice thickness bias and error standard deviation.

Finally, along this PhD thesis, we always kept in mind the needs of the sea ice modeling community. We hope this work will find its place among it, helping the assimilation of real sea ice observations which we assume has a nice future ahead.

Appendix A

Statistical quantities

To assess model errors as well as model benefits from several data assimilation schemes, we use different statistical quantities. Here, we describe the most often used quantities, namely the bias, the error standard deviation and the correlation coefficient. For this study, those quantities are in general averaged yearly or monthly over the model domain.

A.1 Bias

The bias, sometimes simply called "error", is defined as the observation value y subtracted from the modeled one x.

$$\epsilon_i = x_i - y_i \tag{A.1}$$

A.2 Error standard deviation

The standard deviation of errors is a statistic that tells you how tightly the model estimations are clustered around the observed values. It is computed by the following equation :

$$\sigma_\epsilon = [\frac{\sum_{i=1}^{n}(x_i - y_i)^2}{n}]^{1/2} \tag{A.2}$$

A small error standard deviation means that model estimations are tightly bunched together with the observations while a relatively large error standard deviation tells that model estimations are spread apart from the observations. The squared in the computation of the error standard deviation prevents the errors of opposite signs from canceling each other (in opposition to the bias computation). Likewise, this equation weights heavily large errors and is therefore a great alarm bell to inform, for instance, that a data assimilation scheme has made simulation worse.

A.3 covariance

The extent to which 2 variables, x and y, vary together can be measured by their covariance :

$$cov(x,y) = \frac{\sum_{i=1}^{n}[(x_i - \overline{x}).(y_i - \overline{y})]}{n} \tag{A.3}$$

where the overbars represent the mean of the values. If this product is positive, the values of x and y vary together in the same direction from their means. If the product is negative, they vary in opposite directions. The larger the magnitude of the product, the stronger the strength of the relationship. The covariance is defined as the mean value of this product, calculated using each pair of data points x_i and y_i. If the covariance is zero, then the cases in which the product is positive are offset by those in which it is negative, and there is no linear relationship between the 2 variables.

Because the number representing covariance depends on the units of the data, it is difficult to compare covariances among data sets having different scales. A value that might represent a strong linear relationship for one data set, might represent a very weak one for another data set. The correlation coefficient addresses this issue by normalizing the covariance to the product of the standard deviations of the variables. This creates a dimensionless quantity that facilitates the comparison of different data sets.

A.4 correlation coefficient

Another way to measure the degree to which 2 variables vary together or oppositely is by computing their correlation coefficient :

$$\rho(x,y) = \frac{cov(x,y)}{\sigma_x.\sigma_y} \tag{A.4}$$

The maximum positive correlation is 1 and means that there is a complete dependence between the two variables. A zero or near zero-correlation means that the two variables vary separately. That is, when the magnitudes of one variable are high, the other's magnitudes are sometimes high, and sometimes low. They are independent.

List of abbreviations

AVHRR	Advanced Very High Resolution Radiometer
CA	sea ice Concentration data Assimilation
CE	Control Experiment
DA	Data Assimilation
IC	Initial Conditions
IPCC	Intergovernmental Panel on Climate Change
LIM2	Louvain-la-neuve Ice Model, second generation
NCAR	National Center for Atmospheric Research (US)
NCEP	National Center for Environmental Prediction (US)
RGPD	RADARSAT Geophysical Processor System
SAR	Synthetic Aperture Radar
SD	Standard Deviation
SMMR	Scanning Multichannel Microwave Radiometer
SSM/I	Special Sensor Microwave/Imager
TS	True State
VA	sea ice Velocity data Assimilation
VCA	sea ice Velocity and Concentration data Assimilation

Bibliography

Arbetter, T., Lynch, A., Maslanik, J., and Meier, W. 2002. Effects of data assimilation of ice motion in a basin-scale sea ice model. Ice in the Environment: Proceedings of the 16th IAHR International Symposium on Ice. Dunedin, New Zealand, 2nd-6th December 2002. International Association of Hydraulic Engineering and Research, V. Squire and P. Langhore, 3:186–193.

Bamber, J. and Payne, A. 2004. *Mass Balance of the Cryosphere: Observations and Modelling of Contemporary and Future Changes*. Cambridge University Press. 644 pp.

Barnier, B., Madec, G., Penduff, T., Molines, J.-M., Treguier, A.-M., Le Sommer, J., Beckmann, A., Biatoch, A., Böning, C., Dengg, J., Derval, C., Durand, E., Gulev, S., Remy, E., Talandier, C., Theetten, S., Maltrud, M., McClean, J., and De Cuevas, B. 2006. Impact of partial steps and momentum advection schemes in a global ocean circulation model at eddy permitting resolution. Ocean dynamics, 4. Doi: 10.1007/s10236-006-0082-1.

Baumgartner, A. and Reichel, E. 1975. *The world water balance*. Elsevier, Amsterdam and New York. 179 p. + 31 maps.

Beckmann, A. and Döscher, R. 1997. A method for improved representation of dense water spreading over topography in geopotential-coordinate models. Journal of Physical Oceanography, 27(4):581–591.

Bergthorsson, P. and Döös, B. 1955. Numerical weather map analysis. Tellus, 7:329–340.

Berliand, M. and Strokina, T. 1980. *Global distribution of the total amount of clouds*. Hydrometeorological, Leningrad, Russia. 71 pp.

Bitz, C. and Lipscomb, W. 1999. An energy-conserving thermodynamic model of sea ice. Journal of Geophysical Research, 104(C7):15669–15678.

Bjørgo, E., Johannessen, O., and Miles, M. 1997. Analysis of merged SMMR/SSMI time series of Arctic and Antarctic sea ice parameters. Geophysical Research Letters, 24(4):413–416.

Blanke, B. and Delecluse, P. 1993. Low frequency variability of the tropical Atlantic ocean simulated by a general circulation model with mixed layer physics. Journal of Physical Oceanography, 23(7):1363–1388.

Bougeault, P. and Lacarrère, P. 1989. Parameterization of orography-induced turbulence in a mesobeta-scale model. Monthly Weather Review, 117:1872–1890.

Bourke, R. and Garrett, R. 1987. Sea ice thickness distribution in the Arctic Ocean. Cold Regions Science and Technology, 13:259–280.

Bourke, R. and McLaren, A. 1992. Contour mapping of Arctic Basin ice draft and roughness parameters. Journal of Geophysical Research, 97(C11):17715–17728.

Brandt, R., Warren, S., Worby, A., and Grenfell, T. 2005. Surface albedo of the Antarctic sea ice zone. Journal of Climate, 18:3606–3622.

Cavalieri, D., Gloersen, P., Parkinson, J., Comiso, J., and Zwally, H. 1997. Observed hemispheric assymetry in global sea ice changes. Science, 278:1104–1106.

Cavalieri, D., Parkinson, C., and Vinnikov, K. 2003. 30-Year satellite record reveals contrasting Arctic and Antarctic decadal sea ice variability. Geophysical Research Letters, 30(18). Doi:10.1029/2003GL018031.

Colony, R. and Rigor, I. 1993. International Arctic Ocean Buoy Program data report for 1 January 1992-31 December 1992. Technical report, APL-UW TM 29-93, 215 pp., Applied Physics Laboratory, University of Washington, Seattle, USA.

Comiso, J. 1999. Bootstrap sea ice concentrations for NIMBUS-7 SMMR and DMSP SSM/I. Boulder, CO, USA : National Snow and Ice Data Center. Digital media.

Comiso, J. 2002. A rapidly declining perennial sea ice cover in the Arctic. Geophysical Research Letters, 20(20):1956, doi:10.1029/2002GL015650.

Comiso, J. 2006. Abrupt decline in the arctic winter sea ice cover. Geophysical Research Letters, 33(L18504). Doi: 10.1029/2006GL027341.

Comiso, J. and Steffen, J. 2001. Studies of Antarctic sea ice concentrations from satellite data and their applications. Journal of Geophysical Research, 106(C12):31361–31385.

Cressman, G. 1959. An operational objective analysis system. Monthly Weather Review, 87:367–374.

Dai, M., Arbetter, T., and Meier, W. 2006. Data assimilation of sea-ice motion vectors: Sensitivity to the parameterization of sea-ice strength. Annals of Glaciology, 44:357–360.

Drecourt, J., Haines, K., and Martin, M. 2006. Influence of systematic error correction on the temporal behavior of an ocean model. Journal of Geophysical Research, 111, C11020. Doi: 10.1029/2006JC003513.

Dulière, V. 2002. *ORCA2-LIM, un nouveau modèle couplé océan-glace de mer*. Master's thesis, Université catholique de Louvain, Louvain-la-Neuve, Belgium.

Ebert, D., Musgrave, F., Peachey, D., Perlin, K., and Worley, S. 1998. *Texturing and Modeling: A Procedural Approach, Second Edition*. AP Professional, Cambridge. 350 pp.

Ebert, E. and Curry, J. 1993. An intermediate one-dimensional thermodynamic sea ice model for investigation ice-atmosphere interactions. Journal of Geophysical Research, 98(10):10085–10109.

Eicken, H., Grenfell, T., Perovich, D., Richter-Menge, J., and Frey, K. 2004. Hydraulic control of summer Arctic pack ice albedo. Journal of Geophysical Research, 109(C8). Doi:10.1029/2003JC001989.

Emery, W., Fowler, J., Hawkins, J., and Preller, R. 1991. Fram Strait satellite image derived ice motions. Journal of Geophysical Research, 96(C5):4751–4768.

Emery, W., Fowler, C., and Maslanik, J. 1997. Satellite-derived maps of Arctic and Antarctic sea ice motion: 1988 to 1994. Geophysical Research Letters, 24(8):897–900.

Evensen, G. 2003. The Ensemble Kalman filter : theoretical formulation and practical implementation. Ocean Dynamics, 53:343–367.

Ferry, N., Rémy, E., Brasseur, P., and Maes, C. 2007. The Mercator global ocean operational analysis system: Assessment and validation of an 11-year reanalysis. Journal of Marine Systems, 65(1-4):540–560.

Fichefet, T. and Morales Maqueda, M. 1997. Sensitivity of a global sea ice model to the treatment of ice thermodynamics and dynamics. Journal of Geophysical Research, 102(C6):12609–12646.

Fichefet, T. and Morales Maqueda, M. 1999. Modelling the influence of snow accumulation and snow-ice formation on the seasonal cycle of the Antarctic sea-ice cover. Climate dynamics, 15(4):251–268.

Fichefet, T., Tartinville, B., and Goosse, H. 2003. Antarctic sea ice variability during 1958-1999: A simulation with a global ice-ocean model. Journal of Geophysical Research, 108(C3). Doi:10.1029/2001JC001148.

Foreman, S., Alves, J., Bell, M., Brookes, N., Cooper, A., Forbes, R., and Sherlock, C. 1996. FOAM - the forecasting model. Journal of Defense Science, 1:439–445.

Fowler, C., Emery, W., and Maslanik, J. 2004. Satellite-derived evolution of Arctic sea ice ages: October 1978 to March 2003. IEEE Geoscience and Remote Sensor Letters, 1(2):71–74.

Fox, A., Haines, K., de Cuevas, B., and Webb, D. 2000. Altimeter assimilation in the OCCAM global model, Part I : A twin experiment. Journal of Marine Systems, 26:303–320.

Gaspar, P., Grégoris, Y., and Lefevre, J.-M. 1990. A simple eddy-kinetic-energy model for simulations of the oceanic vertical mixing : tests at Station Papa and Long-Term Upper Ocean Study Site. Journal of Geophysical Research, 95(C9):16179–16193.

Gent, P. and McWilliams, J. 1990. Isopycnal mixing in ocean circulation models. Journal of Physical Oceanography, 20(1):150–155.

Ghil, M. and Malanotte-Rizzoli, P. 1991. Data assimilation in meteorology and oceanography. Advances in Geophysics, 33:141–266.

Goosse, H. 1997. *Modelling the large-scale behaviour of the coupled ocean-sea ice system*. Ph.D. thesis, Université catholique de Louvain, Louvain-la-Neuve, Belgium. 208 pp.

Goosse, H. and Fichefet, T. 1999. Importance of ice-ocean interactions for the global ocean circulation : A model study. Journal of Geophysical Research, 104(C6):23337–23355.

GRDC. 2000. Observed historical discharge data from major rivers for climate model validation. Technical report, Max Planck Institute. Report first published in 1993, updated in 2000. Report and data available from www.mpimet.mpg.de/deutsch/Sonst/Reports/HTMLReports and www.bafg.de/grdc.htm.

Grenfell, T. and Maykut, G. 1977. The optical propreties of ice and snow in the Arctic Basin. Journal of Glaciology, 18(80):445–463.

Hibler. 1979. A dynamic thermodynamic sea ice model. Journal of Physical Oceanography, 9(4):815–846.

Hollingsworth, A. and Lönnberg, P. 1986. The statistical structure of short range forecast errors as determined from radiosonde data. Part I. The wind field. Tellus, 38A:111–136.

Holloway, G. and Sou, T. 2002. Has Arctic sea ice rapidly thinned? Journal of Climate, 15(13):1691–1701.

Houghton, J., Ding, Y., Griggs, P., D.and Noguer, van der Linden, P., Dai, X., Maskell, K., and Jonhson, C. 2001. *IPCC: Climate Change 2001: The Scientific Basis. Contribution of Working Group I to the Third Assessment Report of the Intergovernmental Panel on Climate Change*. Cambridge University Press, Cambridge, United Kingdom and New York, NY, USA. 881 pp.

Jackett, D. and McDougall, T. 1995. Stabilization of hydrographic data. Journal of Atmospheric and Oceanic Technology, 12(2):381–389.

Kalnay, E., Kanamitsu, M., Kistler, R., Collins, W., Deaven, D., Gandin, L., Iredell, M., Saha, S., White, G., Woollen, J., Zhu, Y., Chelliah, M., Ebisuzaki, W., Higgins, W., Janowiak, J., Mo, K., Ropelewski, C., Wang, J., Leetmaa, A., Reynolds, R., Jenne, R., and Joseph, D. 1996. The NCEP/NCAR 40-year reanalysis project. Bulletin of the American Meteorological Society, 77(3):437–471.

Köberle, C. and Gerdes, R. 2003. Mechanisms determining the variability of the Arctic sea ice conditions and export. Journal of Climate, 16(17):2843–2858.

Kreyscher, M., Harder, M., Lemke, P., and Flato, G. 2000. Results of the Sea Ice Model Intercomparison Project : Evaluation of sea ice rheology schemes for use in climate simulations. Journal of Geophysical Research, 105(C5):11299–11320.

Kwok, R. 2002. Sea ice concentration from passive microwave radiometry and openings from SAR ice motion. Geophysical Research Letter, 29(14). Art. No. 1705. Doi:10.1029/2002GLO14787.

Kwok, R., Curlander, J., McConnell, R., and Pang, S. 1990. An ice-motion tracking system at the Alaska SAR Facility. IEEE Journal Oceanic Engineering, 15:1–44.

Kwok, R., Rothtock, D., Stern, H., and Cunningham, G. 1995. Determination of the age distribution of sea ice from Lagrangian observations of ice motion. IEEE Transactions on Geosicence and Remote Sensing, 33:392–100.

Kwok, R., Scheiger, D., Rothrock, D., Pang, S., and Kottmeier, C. 1998. Sea ice motion from satellite passive microwave imagery assessed with ERS SAR and buoy motions. Journal of Geophysical Research, 103(C4):8191–8214.

Kwok, R., Zwally, H., and Yi, D. 2004. ICEsat observations of Arctic sea ice : a first look. Geophysical Research Letters, 31(L16401). Doi:10.1029/2004GL020309.

Large, W. and Yeager, S. 2004. Diurnal to decadal global forcing for ocean and sea-ice models: the data sets and flux climatologies. NCAR Technical Note NCAR/TN-460+STR. 111 pp.

Laxon, S., Peacock, N., and Smith, D. 2003. High interannual variability of sea ice thickness in the Arctic region. Nature, 425:947–950.

Lin, C.-L., Chai, T., and Sun, J. 2001. Retrieval of flow structures in a convective boundary layer using an adjoint model : identical twin experiments. Journal of Atmospheric Sciences, 58(13):1767–1783.

Lindsay, R. and Zhang, J. 2005. The thinning of Arctic sea ice, 1988-2003: have we passed a tipping point? Journal of Climate, 18(22):4879–4894. Doi:10.1175/JCLI3587.1.

Lindsay, R. and Zhang, J. 2006. Assimilation of ice concentration in an ice-ocean model. Journal of Atmospheric and Oceanic Technologies, 23(5):742–749.

Lindsay, R., Zhang, J., and Rothrock, D. 2003. Sea ice deformation rates from measurements and in a model. Atmosphere-Oceans, 40:35–47.

Lisaeter, K., Rosanova, J., and Evensen, G. 2003. Assimilation of ice concentration in a coupled ice-ocean model, using the Ensemble Kalman Filter. Ocean Dynamics, 53(4):368–388. Doi:10.1007/s10236-003-0049-4.

Lorenc, A. 1981. A global three-dimensional multivariate statistical interpolation scheme. Monthly Weather Review, 109:701–721.

Madec, G., Delecluse, P., Imbard, M., and Levy, C. 1999. *OPA 8.1 Ocean General Circulation Model reference manual*. Notes du Pôle de modélisation, Institut Pierre-Simon Laplace (IPSL), France. 99 p.

Maslowski, W., Newton, B., Schlosser, P., Semtner, A., and Martinson, D. 2000. Modeling recent climate variability in the Arctic Ocean. Geophysical Research Letters, 27(22):3743–3746.

Maykut, G. and Untersteiner, N. 1971. Some results from a time-depedent thermodynamic model of sea ice. Journal of Geophysical Research, 76(6):1550–1575.

McPhee, M. 1980. An analysis of pack ice drift in summer. In Sea Ice Processes and Models, R.S. Pritchard ed., University of Washington Press, Seattle, USA, pages 62–75.

McPhee, M. 1992. Turbulent heat flux in the upper ocean under sea ice. Journal of Geophysical Research, 97(C4):5365–5379.

Meier, W. and Maslanik, J. 2001a. Improved sea ice parcel trajectories in the Arctic via data assimilation. Marine Pollution Bulletin, 42(7):506–512.

Meier, W. and Maslanik, J. 2001b. Synoptic-scale ice-motion case-studies using assimilated motion fields. Annals of Glaciology, 33(C5):145–150.

Meier, W. and Maslanik, J. 2003. Effect of environmental conditions on observed, modeled, and assimilated sea ice motion errors. Journal of Geophysical Research, 108:21.1–21.11. Doi:10.1029/2002JC001333.

Meier, W., Maslanik, J., and Fowler, C. 2000. Error analysis and assimilation of remotely sensed ice motion within an Arctic sea ice model. Journal of Geophysical Research, 105(C2):3339–3356. Doi:10.1029/1999JC900268.

Mellor, G. and Kantha, L. 1989. An ice-ocean coupled model. Journal of Geophysical Research, 94(C8):10937–10954.

Merryfield, W., Holloway, G., and Gargett, A. 1999. A global ocean model with double-diffusive mixing. Journal of Physical Oceanography, 29(6):1124–1142.

Ninnis, R., Emery, W., and Collins, M. 1986. Automated extraction of pack ice motion from advanced very high resolution radiometer imagery. Journal of Geophysical Research, 91:10725–10734.

Pacanowski, R. and Gnanadesikan, A. 1998. Response in a z-level ocean model that resolves topography with partial-cells. Monthly Weather Review, 126(12):3248–3270.

Parkinson, C. and Washington, W. 1979. A large-scale numerical model of sea ice. Journal of Geophysical Research, 84(C1):311–337.

Parkinson, C., Cavalieri, D., Gloersen, P., Zwally, H., and Comiso, J. 1999. Arctic sea ice extents, areas, and trends, 1978-1996. Journal of Geophysical Research, 104(C9):20837–20856.

Perovich, D., Grenfell, T., Light, B., and Hobbs, P. 2002. Seasonal evolution of the albedo of multiyear Arctic sea ice. Journal of Geophysical Research, 107(C10):8044.

Perovich, D., Grenfell, T., Richter-Menge, J., Light, B., Tucker III, W., and Eicken, H. 2003. Thin and thinner : sea ice mass balance measurements during SHEBA. Journal of Geophysical Research, 108(C3):8050, doi: 10.1029/2001JC001079.

Pringle, D., Trodahl, H., and Haskell, T. 2006. Direct measurement of sea ice thermal conductivity : No surface reduction. Journal of Geophysical Research, 111(C5). Doi:10.1029/2005JC002990.

Rigor, I. and Wallace, J. 2004. Variations in the age of Arctic sea-ice and summer sea-ice extent. Geophysical Research Letters, 31:L09401, doi: 10.1029/2004GL019492.

Rothrock, D. and Zhang, J. 2005. Arctic Ocean sea ice volume: What explains its recent depletion? Journal of Geophysical Research, 110(C01002). Doi:10.1029/2004JC002282.

Rothrock, D., Yu, Y., and Maykut, G. 1999. Thinning of the arctic sea-ice cover. Geophysical Research Letters, 26(23):3469–3472.

Rothrock, D., Zhang, J., and Yu, Y. 2003. The Arctic ice thickness anomaly of the 1990s: A consistent view from observations and models. Journal of Geophysical Research, 108(C3):3083, doi: 10.1029/2001JC001208.

Semtner, A. 1976. A model of the thermodynamic growth of sea ice in numerical investigations of climate. Journal of Physical Oceanography, 6(3):379–389.

Smolarkiewicz, P. 1983. A simple positive definite advection scheme with small implicit diffusion. Monthly Weather Review, 111(3):479–486.

Steele, M., Morley, R., and Ermold, W. 2001. PHC: A global ocean hydrography with a high quality Arctic Ocean. Journal of Climate, 14(9):2079–2087.

Tartinville, B., Cavanié, A., Ezraty, R., and Fichefet, T. 2001. Arctic multiyear ice coverage: A model study. Technical report, Université catholique de Louvain, Louvain-la-Neuve, Belgium.

Thomas, D. and Rothrock, D. 1989. Blending Sequential Scanning Multichannel Microwave Radiometer and buoy data into a sea ice model. Journal of Geophysical Research, 94(C8):10907–10920.

Thomas, D. and Rothrock, D. 1993. The Arctic ocean ice balance : a Kalman smoother estimate. Journal of Geophysical Research, 98(C6):10053–10067.

Thomas, D., Martin, S., Rothrock, D., and Steele, M. 1996. Assimilating satellite concentration data into an Arctic sea ice mass balance model. Journal of Geophysical Research, 101(C9):20849–20868.

Thorndike, A. 1986. *Kinematics of sea ice*, volume 146 of *B : Physics*. Plenum Press, New York, USA.

Timmermann, R., Goosse, H., Madec, G., Fichefet, T., Ethe, C., and Dulière, V. 2005. On the representation of high latitude processes in the ORCALIM global coupled sea ice-ocean model. Ocean Modelling, 8(1-2):175–201.

Trenberth, K., Olson, J., and Large, W. 1989. A global ocean wind stress climatology based on the ECMWF analyses. Technical report, National Center for Atmospheric Research, Boulder, USA. 93 pp.

Tucker, W., Weatherly, J., Eppler, D., Farmer, D., and Bentley, D. 2001. Evidence for rapid thinning of sea ice in the western Arctic Ocean at the end of the 1980s. Geophysical Research Letters, 28(9):2851–2854.

Wadhams, P. and Davis, N. 2000. Further evidence of ice thinning in the Arctic Ocean. Geophysical Research Letters, 27(4):3973–3975.

Walsh, J. and Chapman, W. 2001. Twentieth-century sea ice variations from observational data. Annals of Glaciology, 33:444–448.

Weaver, R., Steffen, K., Heinrichs, J., Maslanik, J., and Flato, G. 2000. Data assimilation in sea-ice monitoring. Annals of Glaciology, 31:327–332.

Winsor, P. 2001. Arctic sea ice thickness remained constant during the 1990s. Geophysical Research Letters, 28(6):1039–1041.

WMO. 1970. WMO sea ice nomenclature, terminology, codes and illustrated glossary. World Meteorological Organization, Geneva, WMO/OMM/BMO 259, TP 145.

Yu, Y. and Lindsay, R. 2003. Comparisons of thin ice fractions estimated from RGPS and AVHRR. Journal of Geophysical Research, 108(C12). Doi:10.1029/2002JC001319.

Yu, Y., Maykut, G., and Rothrock, D. 2004. Changes in the thickness distribution of the Arctic sea ice between 1958-1970 and 1993-1997. Journal of Geophysical Research, 109:C08004, doi: 10.1029/2003JC001982.

Zhang, J., Thomas, D., Rothrock, D., Lindsay, R., Yu, Y., and Kwok, R. 2003. Assimilation of ice motion observations and comparisons with submarine ice thickness data. Journal of Geophysical Research, 108(C6):1–18. Doi:10.1029/2001JC001041.